UNIVERSIDAD DE MÁLAGA

PROGRAMA DE DOCTORADO EN INGENIERÍA MECÁNICA Y EFICIENCIA ENERGÉTICA

ESCUELA DE INGENIERÍAS INDUSTRIALES

Propagation of nonlinear waves on graphene superlattices

D.ª FRANCISCA MARTÍN VERGARA

PhD Thesis

ADVISORS:
Dr. D. FRANCISCO RUS MANSILLA
Dr. D. FRANCISCO R. VILLATORO MACHUCA

UNIVERSIDAD DE MÁLAGA

Marzo 2023

AUTORA: Francisca Martín Vergara

https://orcid.org/0000-0003-1478-8444

EDITA: Publicaciones y Divulgación Científica. Universidad de Málaga

DECLARACIÓN DE AUTORÍA Y ORIGINALIDAD DE LA TESIS PRESENTADA PARA OBTENER EL TÍTULO DE DOCTOR

D./Dña FRANCISCA MARTÍN VERGARA
Estudiante del programa de doctorado INGENIERIA MECÁNICA Y EFICIENCIA ENERGÉTICA de la Universidad de Málaga, autora de la tesis, presentada para la obtención del título de doctor por la Universidad de Málaga, titulada: PROPAGATION OF NONLINEAR WAVES ON GRAPHENE SUPERLATTICES

Realizada bajo la tutorización de FRANCISCO R. VILLATORO y dirección de FRANCISCO RUS MANSILLA Y FRANCISCO R. VILLATORO

DECLARO QUE:

La tesis presentada es una obra original que no infringe los derechos de propiedad intelectual ni los derechos de propiedad industrial u otros, conforme al ordenamiento jurídico vigente (Real Decreto Legislativo 1/1996, de 12 de abril, por el que se aprueba el texto refundido de la Ley de Propiedad Intelectual, regularizando, aclarando y armonizando las disposiciones legales vigentes sobre la materia), modificado por la Ley 2/2019, de 1 de marzo.

Igualmente asumo, ante a la Universidad de Málaga y ante cualquier otra instancia, la responsabilidad que pudiera derivarse en caso de plagio de contenidos en la tesis presentada, conforme al ordenamiento jurídico vigente.

En Málaga, a 20 de marzo de 2023

Fdo.: FRANCISCA MARTÍN VERGARA Doctorando/a	Fdo.: FRANCISCO R. VILLATORO Tutor/a
Fdo.: FRANCISCO RUS MANSILLA	FRANCISCO R. VILLATORO

Edificio Pabellón de Gobierno. Campus El Ejido. 29071
Tel.: 952 13 10 28 / 952 13 14 61 / 952 13 71 10
E-mail: doctorado@uma.es

Dr. D. **Francisco Román Villatoro Machuca** y Dr. D. **Francisco de Asís Rus Mansilla**, Profesores Titulares de Universidad del Departamento de Lenguajes y Ciencias de la Computación de la Universidad de Málaga.

Certifican:

Que D.ª **Francisca Martín-Vergara**, Ingeniera en Informática por la Universidad de Málaga, ha realizado en el programa de doctorado Ingeniería Mecánica y Eficiencia Energética, bajo nuestra dirección, el trabajo de investigación correspondiente a su Tesis Doctoral titulada:

Propagation of nonlinear waves on graphene superlattices

Revisado el presente trabajo, estimamos que puede ser presentado al Tribunal que ha de juzgarlo. Y para que constate a efectos de lo establecido en el artículo octavo del Real Decreto 99/2011, autorizamos la presentación de este trabajo en la Universidad de Málaga.

Málaga, a 20 de marzo de 2023

Firmado:
Dr. D. Francisco Román Villatoro Machuca y Dr. D. Francisco de Asís Rus Mansilla
Profesores Titulares de Universidad

Dedicada a María y Nacho

Agradecimientos

Esta tesis no hubiera podido llevarse a cabo sin el apoyo de varias personas e instituciones a las que quiero mostrar mi más sincero agradecimiento.

En primer lugar, a mi tutor y director, el doctor Francisco Villatoro no solo por haberme sabido transmitir parte de su gran conocimiento sobre la materia, sino también por su comprensión, su infinita paciencia y empatía sin las cuales este trabajo no hubiera sido posible. A mi segundo director, el doctor Francisco Rus por su apoyo y sus consejos. La combinación de orientación y libertad que ambos me han proporcionado durante esta investigación creo que ha ayudado de manera significativa a la mejora de mis habilidades.

Agradezco también a la Fundación IMFAHE a través del Vicerrectorado de Empresa, Territorio y Transformación Digital de la Universidad de Málaga, por su apoyo económico haciendo posible la realización de la estancia internacional en Massachusetts (USA). Allí tuve la oportunidad de trabajar con los doctores Panos Kevrekidis y Jesús Cuevas. Fue un período muy constructivo en el que aprendí nuevas metodologías de trabajo y me puso en contacto con otras culturas.

A Juan Ignacio por darme su más sincera visión y hacerlo más fácil dentro de la dificultad que ha supuesto para mí este camino. A todos mis compañeros de la Escuela de Ingenierías, gracias por las horas compartidas y las historias vividas.

A mis padres por estar siempre ahí y por haberme brindado la oportunidad de estudiar. A Jose por su apoyo e incondicional ayuda con los peques.

En definitiva, a todos aquellos que de una forma u otra han contribuido con sus enseñanzas, apoyos y consejos a que esta tesis sea hoy una realidad.

GRACIAS.

Contents

Resumen **III**

Abstract **V**

Resumen en español **VII**

1 Introduction **1**
1.1 Motivation 1
1.2 Objectives 2
1.3 Methodology 3
1.4 Papers and contributions 4
1.4.1 ISI JCR Indexed Journals 4
1.4.2 Book chapter 5
1.4.3 International conferences 6
1.5 Brief summary of the papers 7
1.6 Thesis contents 9

2 Graphene superlattice equation **11**
2.1 Solitons in the nonlinear Klein–Gordon equation 11
2.2 Ratnikov's graphene superlattice 14
2.3 Graphene superlattice equation 15
2.4 Solitary waves 18

3 Numerical schemes **21**
3.1 Numerical schemes for the sine–Gordon equation 21
3.2 Padé schemes based on Strauss–Vázquez method 23
3.3 Numerical results 28
3.3.1 Kink–antikink and breather exact solutions 28
3.3.2 Results without Richardson's extrapolation 29
3.3.3 Results with Richardson's extrapolation 32
3.4 Selection of the method for the GSLeq 33

4 Results for the graphene superlattice equation **35**
4.1 Initial conditions 35
4.1.1 Collision of a kink and an antikink 35
4.1.2 Perturbation of the null solution 37

4.2 Kink–antikink interaction 39
4.3 Quasi-breather search 48

5 Conclusions **57**
5.1 Concluding remarks 57
5.2 Future research 59

Bibliography **61**

Appendices **71**

A Solitary waves on graphene superlattices **73**

B Padé numerical schemes for the sine-Gordon equation **75**

C Padé schemes with Richardson extrapolation for the sine-Gordon equation **77**

D Fractal structure of the soliton scattering for the graphene superlattice equation **79**

E Numerical search for the stationary quasi-breather of the graphene superlattice equation **81**

Resumen

Se ha estudiado mediante métodos numéricos la propagación de ondas electromagnéticas no lineales en un dispositivo optoelectrónico llamado superred de grafeno de Ratnikov. Este dispositivo está compuesto de una hoja de grafeno sobre una estructura formada por franjas alternas de un dieléctrico y un semiconductor. Las ondas electromagnéticas en la superred de grafeno se modelan mediante una ecuación de onda no lineal de tipo Klein–Gordon en 1+1 dimensiones, una versión modificada de la ecuación del seno-Gordon (sGeq), bautizada como ecuación de la superred de grafeno (GSLeq, del inglés *graphene superlattice equation*). Sus soluciones son ondas solitarias de tipo topológico, *kinks* y *antikinks*. Se han estudiado numéricamente las colisiones de un *kink* contra un *antikink* y la generación de soluciones oscilatorias en tiempo localizadas en espacio de tipo *quasi-breather*.

Para seleccionar el mejor método numérico para la GSLeq se ha usado la sGeq como modelo, una ecuación integrable con soluciones exactas de tipo *kink* y *breather*. Se han estudiado dos familias de métodos de tipo Padé, una familia tipo Strauss–Vázquez (1978) y otra tipo Guo *et al.* (1986), cuyo tratamiento de la no linealidad asegura una buena conservación de la energía. En cada familia se incluyen cinco métodos, el original de segundo orden en espacio, dos de cuarto orden, uno de sexto orden y otro de octavo orden; todos ellos integrados a segundo orden en tiempo. Dado que los métodos de la segunda familia son más robustos, se ha usado extrapolación de Richardson en ellos para alcanzar cuarto orden en tiempo. La comparación entre sí de los quince métodos desarrollados para la sGeq en cuanto a error, invariantes, estabilidad y coste computacional indica que la mayor eficiencia computacional la alcanza un método de la segunda familia con cuarto orden en espacio y segundo orden en tiempo (sin extrapolación de Richardson).

El método numérico seleccionado se ha aplicado a la GSLeq para estudiar las colisiones simétricas *kink–antikink*. Como se ha observado en otras ecuaciones de tipo Klein–Gordon, por debajo de cierta velocidad crítica ambos se aniquilan mutuamente generando una solución de tipo *pseudo-breather* que decae en radiación, salvo en unas ventanas de resonancia, donde escapan hasta infinito tras acoplarse en un estado ligado con cierta frecuencia de resonancia. Se ha caracterizado la estructura fractal de estas ventanas por debajo de la velocidad crítica y se ha introducido una notación específica multiíndice para formalizarla. Se ha aplicado la teoría de intercambio de energía resonante desarrollada por Campbell *et al.* (1986) obteniéndose un buen acuerdo con los resultados numéricos para la posición de las ventanas de resonancia y para la frecuencia de resonancia.

Las colisiones *kink–antikink* fuera de la ventana de resonancia conducen a la

aparición de estados oscilatorios transitorios tipo *pseudo-breather* que a ciertas velocidades se asemejan a un *quasi-breather* de larga vida. Se ha realizado una búsqueda numérica sistemática de soluciones de tipo *quasi-breather*. Para ello se ha introducido una nueva condición inicial caracterizada por una frecuencia de oscilación obtenida perturbando la solución nula de la GSLeq. Los resultados numéricos muestran que por debajo de una frecuencia crítica aparece un par *kink–antikink*, pero por encima se observan soluciones de tipo *pseudo-breather*, que para una frecuencia muy superior son de tipo *quasi-breather* de larga vida. La gran robustez de estos *quasi-breathers* de alta frecuencia sugiere que su búsqueda experimental en superredes de grafeno en laboratorio puede ser exitosa.

Abstract

The propagation of non-linear electromagnetic waves in an optoelectronic device called the Ratnikov's graphene superlattice has been studied using numerical methods. This device is composed by a sheet of graphene on a structure formed by alternating layers of a dielectric and a semiconductor. Electromagnetic waves in the graphene superlattice can be modeled with a Klein-Gordon nonlinear wave equation in 1+1 dimensions, a modified version of the sine–Gordon equation (sGeq), referred to as graphene superlattice equation (GSLeq). Its solutions are solitary waves of topological type, kinks and antikinks. Kink–antikink collisions and the generation of quasi-breathers, oscillatory solutions in time which are localized in space, have been numerically studied.

Numerical methods for the sGeq have been developed to select the best numerical method for the GSLeq. The sGeq is integrable and presents exact kink, antikink, and breather solutions, which makes it easy to compare these methods in terms of error, invariants, stability, and computational cost. Specifically, two families of Padé methods have been studied, one family based on Strauss-Vázquez (1978) and another one on Guo *et al.* (1986), both with the same non-linearity treatment which ensures good conservation of energy. Five methods are included in each family, the original second-order method in space, two fourth-order methods, one sixth-order method, and one eighth-order method; all of them integrated with second order in time. Since the methods of the second family are more robust, Richardson's extrapolation has been used in them to reach the fourth order in time. The comparison among themselves of the fifteen methods developed for the sGeq indicates that the highest computational efficiency (least error at the lowest cost) is achieved with a method of the second family of fourth order in space and second order in time (without Richardson's extrapolation).

The selected numerical method has been applied to the GSLeq to study the collision of a kink against an antikink, both with equal but opposite speeds. According to other Klein–Gordon equations, below a certain critical velocity the kink and the antikink annihilate, bounding in a pseudo-breather solution that decays in radiation; except in certain regions (called resonance windows), in which they manage to escape to infinity after coupling in a bound state with a resonant frequency. The fractal structure of the resonance windows below the critical velocity has been characterised; a new multi-index notation has been introduced to formalize a conjecture on its fractal structure *ad infinitum*. The resonant energy exchange theory developed by Campbell *et al.* (1986) has been applied, showing a good agreement with the numerical results for both the position of the resonance windows and the resonance

frequency.

The kink–antikink collisions outside the resonance windows lead to pseudo-breather transient oscillatory states that at certain speeds resemble a long-lived quasi-breather. A systematic numerical search for quasi-breather solutions has been carried out. For this purpose, a new initial condition has been introduced, characterised by an oscillation frequency obtained by a perturbation of the null solution of the GSLeq. The numerical results show that a kink–antikink pair appears below a critical frequency, but pseudo-breather and quasi-breather solutions are observed above that frequency. The quasi-breather is robust and has a long life for a frequency much higher than the critical one. The numerical robustness of these high-frequency quasi-breathers suggests that their experimental search for graphene superlattices in the laboratory may be successful.

Resumen en español

Motivación y objetivos

El grafeno es un alótropo del carbono aislado en 2004 por el grupo de Andre K. Geim y Konstantin S. Novoselov [1], lo que les valió el premio Nobel de Física en 2010. Este extraordinario material tiene notables propiedades mecánicas, de conducción de calor y de conducción eléctrica llegando a considerarse como el futuro de la industria electrónica y optoelectrónica del silicio. Los dispositivos actuales se basan en semiconductores, materiales con una banda prohibida, pero el grafeno es un semimetal. Se puede no obstante inducir una banda prohibida en el grafeno colocándolo encima de un sustrato adecuado [2], lo que permite desarrollar transistores y otros dispositivos optoelectrónicos.

En el régimen de los terahercios (THz) los dispositivos optoelectrónicos basados en grafeno más prometedores son las superredes de grafeno. Esta estructura está formada por una lámina de grafeno depositada sobre franjas paralelas que alternan un material que no afecta a la estructura de bandas del grafeno y otro que introduce una banda prohibida. Cuando la radiación electromagnética transversal incide sobre este dispositivo se propaga una onda en las franjas del dieléctrico que están acopladas con los portadores (electrones y huecos) en la hoja de grafeno. La respuesta electrodinámica del dispositivo para una irradiación intensa está descrita por una ecuación de ondas no lineal. Dicha ecuación, para la amplitud de la componente transversal del potencial vectorial del campo electromagnético es una ecuación de Klein–Gordon (KGeq), en concreto, una modificación de la ecuación del seno-Gordon (sGeq) bautizada como ecuación de la superred de grafeno (GSLeq). Esta ecuación propaga ondas solitarias de tipo topológico, *kinks* y *antikinks*, cuyas interacciones mutuas conducen a la generación de armónicos superiores que pueden tener interés tanto en la detección como en la generación de señales de THz.

El principal objetivo de esta tesis doctoral es el estudio de las soluciones de la ecuación de la superred de grafeno y sus interacciones. Para lograr este objetivo se han planteado tres subobjetivos parciales. El primero es la implementación de un método numérico eficiente y de bajo coste para la resolución de la ecuación GSLeq; para seleccionarlo se han comparado métodos numéricos para la sGeq, ya que sus soluciones exactas facilitan la búsqueda del mejor método en cuanto a coste y error. El segundo es el estudio de las colisiones de un *kink* contra un *antikink*, determinando la región de parámetros para los que estas colisiones se comportan de forma casi elástica o decaen de forma inelástica. Y el tercero es realizar una

búsqueda de la posible existencia de ondas periódicas robustas similares a las soluciones de tipo *breather* de la sGeq; caracterizando las regiones de parámetros en las que se observan soluciones de tipo *pseudo-* y *quasi-breather*.

Artículos publicados

A continuación se presenta un breve resumen de cada uno de los artículos publicados en revistas científicas y en un capítulo de libro. No se resumen otras publicaciones, como comunicaciones orales y pósteres en congresos internacionales, porque presentan contribuciones preliminares o parciales que se incluyen en estos artículos.

Artículo 1. *Ondas solitarias en superredes de grafeno* [3]. Este artículo de revisión resume la derivación de la GSLeq y presenta un primer análisis numérico de sus soluciones. Se describe la estructura de bandas electrónicas del grafeno y cómo determina las propiedades electrónicas de la superred de grafeno de Ratnikov. Se repasan los resultados ya obtenidos con dos métodos diferentes, el de transferencia de matrices usado por Ratnikov (2009) [4] y el basado en el modelo de Kronig–Penny de Maksimova *et al.* (2012) [5], que conducen a resultados equivalentes. Bajo la incidencia de ondas electromagnéticas de gran intensidad se propagan en este dispositivo ondas no lineales regidas por una ecuación para la componente transversal del vector potencial derivada por Kryuchkov y Kukhar' (2013) [6]; bautizada como GSLeq es una modificación de la sGeq que presenta ondas solitarias topológicas de tipo *kink* y *antikink*. La GSLeq no es una ecuación integrable, pero sus solitones se pueden aproximar analíticamente usando métodos asintóticos; se presentan dos aproximaciones basadas en dos *ansatz*. Como primer estudio de sus interacciones mutuas, se implementa el método numérico conservativo para la energía de Strauss–Vázquez [7] y se presentan resultados que indican que las colisiones *kink–antikink* de la GSLeq son casi elásticas cuando dicha ecuación es una perturbación pequeña de la sGeq.

Artículo 2. *Métodos numéricos de Padé para la ecuación del seno–Gordon* [8]. La ecuación del seno–Gordon aparece en múltiples problemas científicos y de ingeniería; aunque sea integrable, en la mayoría de las aplicaciones prácticas se requiere su simulación numérica. Para esta ecuación se han desarrollado cinco métodos implícitos de diferencias finitas de orden $(q+s)$ en espacio basados en aproximaciones de tipo Padé (q,s), con un operador en diferencias finitas que es un cociente de polinomios de grado q en el numerador y s en el denominador; todos comparten el mismo tratamiento para la no linealidad y método de integración en tiempo. El primer método es el usado en el artículo 1, que se interpreta como un método de Padé $(2,0)$; este método se ha comparado con cuatro nuevos métodos de Padé $(4,0)$, $(2,2)$, $(4,2)$ y $(4,4)$ en términos de error global, coste computacional

y conservación de la energía, tanto para las soluciones tipo *kink–antikink* como *breather* de la sGeq. El estudio de la relación coste-error indica que el método más eficiente para errores pequeños es el método de tipo Padé $(4,0)$ y para errores muy pequeños es el $(4,2)$. Además, en simulaciones de largo tiempo de integración, los resultados muestran que el orden espacial de consistencia es más importante para la eficiencia del método que la conservación de la energía.

Artículo 3. *Métodos de Padé con extrapolación de Richardson para la ecuación del seno–Gordon* [9]. Para una comparación más exhaustiva de métodos numéricos para la sGeq, se han desarrollado otros cinco métodos implícitos de diferencias finitas de orden $(q+s)$ en espacio basados en aproximaciones de tipo Padé (q,s), pero con otro método de integración en tiempo basado en el esquema de Guo *et al.* [10]; este último se interpreta como un método tipo Padé $(2,0)$ que conserva un equivalente discreto de la energía; además, se han desarrollado cuatro nuevos métodos de Padé $(4,0)$, $(2,2)$, $(4,2)$ y $(4,4)$. La estabilidad lineal de todos estos métodos es incondicional. Para incrementar el orden en tiempo se ha usado la extrapolación de Richardson, dando lugar a otros cinco métodos de cuarto orden en tiempo. Estos diez métodos se han comparado en cuanto a error global, coste computacional y conservación de la energía tanto para las soluciones de tipo *kink–antikink* como *breather* de la sGeq. Los resultados muestran que los métodos con extrapolación de Richardson son más costosos que los métodos sin ella a la hora de alcanzar cierta cota de error mínimo. Entre estos últimos, el método más eficiente para errores pequeños es el método de tipo Padé $(4,0)$ y para errores muy pequeños es el $(4,4)$. La comparación entre los quince métodos estudiados en los artículos 2 y 3 muestra que el método más efectivo para errores pequeños es el método de Padé $(4,0)$ del artículo 3, que será usado para simular la ecuación GSLeq en los siguientes artículos.

Artículo 4. *Estructura fractal en las colisiones de solitones de la ecuación de la superred de grafeno* [11]. La ecuación de la superred de grafeno tiene una solución tipo *kink* sin una expresión analítica explícita, por lo que es necesario calcularla usando métodos de integración numérica. Usando el método numérico seleccionado en los artículos 2 y 3 se estudia, por primera vez, la colisión inelástica de un *kink* contra un *antikink*, ambos con velocidades iguales pero de sentido opuesto. Tras su interacción, ambos escapan hacia el infinito cuando su velocidad común es mayor que un valor crítico; por debajo, forman un estado oscilatorio similar al de un *breather* que decae lentamente al irradiar energía, salvo cuando están dentro de una serie de intervalos en velocidad. En estos intervalos, llamados ventanas de resonancia, el *kink* y el *antikink* se acoplan en un estado resonante del que escapan hacia el infinito tras cierto tiempo. Estas ventanas de resonancia muestra una estructura fractal; para describirla se desarrolla una nueva notación de índices múltiples que permite conjeturar una estructura válida *ad infinitum*. Se

ha usado la teoría del intercambio de energía resonante de Campbell *et al.* [12, 13] para describir las principales características de esta estructura fractal; se observa un buen acuerdo entre las predicciones teóricas y las simulaciones numéricas. Nuestros hallazgos pueden interpretarse como una nueva evidencia que respalda esta teoría en ecuaciones que sean una modificación de la sGeq.

Artículo 5. *Búsqueda numérica del* quasi-breather *estacionario en la ecuación de la superred de grafeno* [14]. Las colisiones *kink–antikink* estudiadas en el artículo 4 sugieren la posibilidad de que exista una solución de tipo *quasi-breather* en la GSLeq. La búsqueda numérica del *quasi-breather* estático se lleva a cabo utilizando una nueva condición inicial derivada de una perturbación regular de la solución nula de la GSLeq caracterizada por una frecuencia. Los resultados muestran una frecuencia crítica mínima para la observación de una solución periódica; para valores superiores pero próximos a dicha frecuencia esta solución se comporta como un *pseudo-breather* que decae en radiación tras presentar oscilaciones irregulares. Sin embargo, para valores superiores de la frecuencia se observa un *quasi-breather* robusto capaz de sobrevivir miles de períodos. Por supuesto, la GSLeq no tiene una solución de tipo *breather* como la sGeq, por lo que a medida que pasa el tiempo, la amplitud y la energía del *quasi-breather* disminuyen, mientras su frecuencia se incrementa. Este nuevo *quasi-breather* de gran robustez, junto con la contribución del artículo 4, respalda la búsqueda experimental de ondas no lineales en dispositivos de superredes de grafeno.

Mi contribución a estos cinco artículos ha sido la implementación y desarrollo del software, la ejecución de la metodología, el análisis de los resultados, la escritura de los manuscritos y la edición y revisión de los mismos. Los otros dos autores, Francisco Rus y Francisco R. Villatoro, son responsables de la conceptualización, el diseño de la metodología, el análisis de los resultados, la escritura de los manuscritos y la edición y revisión de los mismos.

Solitones

Las ecuaciones de evolución que presentan ondas solitarias son modelos ideales para la propagación de ondas en sistemas físicos; aunque siempre bajo condiciones adecuadas, y cuando se incorporan términos disipativos, dispersivos y no lineales de mayor orden, estas ondas describen muchas observaciones experimentales. Entre las ecuaciones con ondas solitarias destacan las ecuaciones integrables que presentan solitones, término acuñado por Zabusky y Kruskal [15] para las soluciones de la ecuación de Korteweg–de Vries [16]; los solitones son ondas solitarias robustas y localizadas que se comportan como partículas manteniendo su amplitud, forma y velocidad, incluso tras interacciones mutuas. Las colisiones entre solitones son

perfectamente elásticas, sin generar ningún tipo de radiación, salvo por un cambio de fase en el punto de colisión. Las ecuaciones de evolución no integrables presentan ondas solitarias que no son solitones, en sentido estricto, porque sus interacciones son inelásticas; sin embargo, a veces se usa el término solitón, en sentido amplio, para referirse a dichas soluciones.

Los solitones se han encontrado en muchas ecuaciones de evolución no lineales [17–20]. Gracias a ello su estudio abarca todos los campos de la matemática aplicada y de la física matemática, desde el estudio de ondas en fluidos, como los tsunamis [21], a las ondas en sistemas biológicos, como en las moléculas de ADN [22], o incluso, el movimiento de seres vivos [23]. Sin embargo, las aplicaciones más relevantes de los solitones se encuentran en los medios unidimensionales, como la fibra óptica [24] y las líneas de transmisión no lineales [25].

La ecuación integrable con solitones más relevante para nuestra investigación es la ecuación del seno-Gordon [26] descubierta en el estudio de superficies de cuadratura negativa constante por Bour en 1862. Fue redescubierta como modelo continuo para las ondas en una serie de péndulos acoplados que permiten estudiar las dislocaciones en cristales por Frenkel y Kontorova en 1939. Tras el descubrimiento de su integrabilidad a principios de los años 70 se multiplicaron sus aplicaciones, abarcando desde el modelado de uniones superconductoras de Josephson a la propagación de pulsos ultracortos en fibras ópticas, entre otras [27, 28]. La sGeq es de tipo Klein–Gordon, por lo que es una ecuación invariante relativista y tiene aplicaciones como modelo clásico en teoría cuántica de campos [29].

Los solitones de la sGeq se llaman *kinks* (rizos, en español), porque conectan dos estados constantes diferentes en infinito; cuando estos estados se interpretan como dos vacíos, se denominan solitones topológicos y están caracterizados por una carga que tiene valores descritos (de ahí el adjetivo topológico). Como la sGeq es una ecuación de ondas de segundo orden, junto a los *kinks* presenta *antikinks*, que tienen la misma velocidad pero de signo opuesto y que se obtienen aplicando una reflexión especular en el espacio. La integrabilidad de la sGeq permite escribir soluciones exactas con múltiples solitones en interacción; la más sencilla es la solución con un kink y un antikink, en la que se aproximan desde infinito, colisionan de forma elástica y se separan dirigiéndose hacia infinito. Otra solución muy relevante es el *breather* (respirador, en español), una solución localizada en espacio y oscilatoria en el tiempo que corresponde a un estado ligado de un *kink* y un *antikink* caracterizado por una frecuencia; los *breathers* pueden ser estáticos o pueden moverse a una velocidad constante (se obtienen tras aplicarles una transformación de Lorentz a los estáticos).

Ecuación de la superred de grafeno

La superred de grafeno de Ratnikov (GSL) está compuesta por una hoja de grafeno monocapa sobre una superred formada por franjas alternas de un material que no altera la estructura de bandas del grafeno, normalmente un dieléctrico como la sílice, SiO_2, y otro material que introduce un salto de banda (*band gap*), como el nitruro de boro hexagonal, h-BN, o el carburo de silicio, SiC. Como resultado se introduce una modulación periódica del salto de banda en el grafeno que afecta a la propagación de los portadores (electrones y huecos) como demostró Ratnikov en 2009 [4]. Además del salto de banda en la GSL también se modula la velocidad de Fermi, a la que se propagan dichos portadores [30].

La GSL se comporta como un dispositivo optoelectrónico en el que se pueden propagar ondas electromagnéticas en el dieléctrico transparente inducidas por una irradiación transversal; gracias a ello, las ondas en la GSL se comportan como plasmones y polaritones superficiales (*surface plasmons polaritons*) [31]. Bajo ciertas hipótesis razonables, entre las que destaca que la frecuencia de la onda incidente sea mayor que la llamada frecuencia de plasma del dispositivo, Kryuchkov y Kukhar' en 2012 [32] derivaron una ecuación de onda no lineal de tipo d'Alembert para las ondas electromagnéticas en la GSL que coincide con la sGeq. Además, conforme la frecuencia de la irradiación crece se describen de forma más adecuada con una ecuación del seno–Gordon doble (dsGeq) [33] y con una nueva ecuación, que hemos bautizado como ecuación de la superred de grafeno [34]; esta última es el objeto de estudio de esta tesis doctoral.

En el artículo 1 se revisa la derivación en detalle de la GSLeq realizada por Kryuchkov y Kukhar' para la componente a lo largo del eje de la GSL del vector potencial del campo electromagnético que se propaga por una franja del dieléctrico. Esta ecuación no lineal está dada por

$$\frac{\partial^2 \alpha}{\partial t^2} - c^2 \frac{\partial^2 \alpha}{\partial y^2} + \frac{\omega_{pl}^2 b^2 \sin\alpha}{\sqrt{1+b^2(1-\cos\alpha)}} = 0\,, \tag{1}$$

donde α es dicha componente del potencial vector normalizada, b es un parámetro geométrico asociado a la superred, c es la velocidad de propagación de la onda electromagnética, ω_{pl} es la frecuencia de plasma del dispositivo, y es la dirección longitudinal de la franja de dieléctrico y t es el tiempo.

Para estudiar las soluciones de la GSLeq (2) usando métodos numéricos y asintóticos es conveniente adimensionalizarla. Usaremos el cambio de variables $t' = \omega_{pl}\, b\, t$, $x' = \omega_{pl}\, b\, y/c$, y $u = \alpha$, para obtener la ecuación de Klein–Gordon (2) dada por

$$\frac{\partial^2 u}{\partial t^2} - \frac{\partial^2 u}{\partial x^2} + \frac{dF(u)}{du} = 0, \tag{2}$$

donde se han eliminado los apóstrofos y

$$\frac{dF(u)}{du} = \frac{\sin u}{\sqrt{1+b^2\,(1-\cos u)}}, \qquad F(u) = \frac{2\,(1-\cos u)}{1+\sqrt{1+b^2\,(1-\cos u)}}.$$

Nótese que el potencial no lineal se reduce al de la sGeq para $b = 0$, es decir, $F(u) = 1-\cos u$.

Las ondas solitarias de la GSLeq (2) con velocidad v, dadas por $u(x,t) = u((x-vt)/\sqrt{1-v^2})$ (donde se ha aplicado una transformación de Lorentz a la solución estacionaria $u(x)$) cumplen que

$$\frac{d^2u}{dx^2} = \frac{dF(u)}{du}, \qquad \frac{1}{2}\left(\frac{du}{dx}\right)^2 = F(u).$$

Como el potencial periódico $F(u)$ tiene infinitos ceros en $u_n^* = 2\,n\,\pi$, para $n \in \mathbb{Z}$, la onda solitaria estática $u(x)$ conecta dos ceros consecutivos; llamamos a una solución *n-kink* cuando conecta los valores asintóticos u_n^* y u_{n+1}^*, y *n-antikink* cuando conecta a u_{n+1}^* y u_n^*. Por tanto, el 0-*kink* estático, $u_{k,0}(x)$, está dado por

$$\int_{\pi}^{u_{k,0}} \frac{d\tilde{u}}{\sqrt{2\,F(\tilde{u})}} = \int_{x_0}^{x} d\tilde{x}, \qquad 0 < u_{k,0} < 2\,\pi, \tag{3}$$

donde x_0 es el centro del 0-*kink*, es decir, la posición del máximo de su derivada espacial. En general, el *n-kink* se puede escribir como $u_{k,n}(x) = 2\,\pi\,n + u_{k,0}(x)$, y el *n-antikink* como $u_{ak,n}(x) = 2\,\pi\,(n+1) - u_{k,0}(x)$. En concreto, para la GSLeq (3) con $u_{k,0}(x)$ se tiene

$$\int_{\pi}^{u_{k,0}} \frac{\sqrt{1+\sqrt{1+b^2\,(1-\cos\tilde{u})}}}{2\sqrt{1-\cos\tilde{u}}}\,d\tilde{u} = x - x_0, \tag{4}$$

cuya integración da como resultado una complicada expresión implícita escrita en términos de integrales elípticas. No se puede obtener una expresión analítica explícita. Además, como la expresión implícita tiene una formulación complicada, en la práctica se prefiere la evaluación mediante integración numérica.

Como la GSLeq no es integrable, entre otras cosas porque no cumple con la propiedad de Painlevé [35], sus soluciones de tipo *kink* y *antikink* no son solitones en sentido estricto, sino ondas solitarias [36]. Además, tampoco presenta soluciones exactas de tipo *kink-antikink* y *breather* como la sGeq; a pesar de ello, para un valor pequeño del parámetro geométrico b se pueden usar métodos asintóticos o perturbativos para obtener una solución aproximada similar a un par *kink-antikink* o a un *breather*. En esta tesis, la GSLeq se simulará mediante métodos numéricos que utilizarán este tipo de aproximaciones como condiciones iniciales.

Métodos numéricos

Dado que la ecuación GSLeq se puede considerar una modificación de la sGeq, a la hora de seleccionar el mejor método numérico para su estudio parece razonable realizar una comparación de métodos numéricos para la sGeq. Los primeros dos métodos numéricos para la ecuación del seno–Gordon fueron un método de características y un método en diferencias finitas tipo *leapfrog* (salto de la rana, en español) ambos desarrollados por Perring y Skyrme (PS) [37]. Ablowitz, Kruskal y Ladik (AKL) propusieron un método *staggered-leapfrog* (de salto de la rana escalonado, en español) que estabiliza el método *leapfrog* de PS [38]. Strauss y Vázquez (SV) desarrollaron un método de diferencias finitas implícito de tipo *leapfrog* que conserva un análogo discreto de la energía para la KGeq [7], que fue usado para la sGeq en [39]. Guo, Pascual, Rodríguez y Vázquez (GPRV) [10] desarrollaron una variante del método SV para la KGeq, que conserva otro análogo discreto de la energía y que en sus simulaciones es más robusto en simulaciones de largo tiempo de integración. Jiménez y Vázquez [40] compararon cuatro métodos tipo *leapfrog*, en concreto, PS, AKL, SV y un nuevo método totalmente explícito, mostrando que en integraciones de largo tiempo el mejor es el método SV. Desde entonces se han publicado varias generalizaciones del método SV, que también conservan la energía, manteniendo su segundo orden en espacio y en tiempo [41–44]. Se han desarrollado procedimientos generales para desarrollar métodos que conservan la energía cuando el término no lineal se discretiza como en el método SV [45] y que permiten forzar la conservación de un análogo discreto concreto de la energía [46]. Sin embargo, una comparación entre métodos conservativos y no conservativos muestra que la propiedad clave para la robustez a largo plazo es que el método sea implícito, en lugar de que conserve un análogo discreto de la energía [47].

También se han usado métodos en diferencias finitas basados en aproximaciones de Padé (q,s) (un operador en diferencias que es un cociente de polinomios de grado q para el numerador y s para el denominador), de orden $(q+s)$ en espacio, también conocidos como métodos de operadores compactos. Bratsos y Twizell [48] desarrollaron esquemas de Padé $(2,0)$, $(1,1)$, y $(2,1)$ para la sGeq, y Duncan [49] presenta un esquema de Padé $(2,2)$, que es aplicado a la sGeq por Bratsos [50]; y Sari y Güarslan [51] proponen un esquema de Padé $(4,2)$. Una comparación de algunos de los métodos de Padé con los esquemas PS, AKL, y SV muestra que para obtener errores pequeños los métodos de alto orden son más eficientes [48,49]. Algunos de estos esquemas de Padé se han usado también para la sGeq en dos dimensiones espaciales [52–54]. Debemos destacar que en todos estos métodos de Padé se ha usado un tratamiento para la no linealidad de la sGeq similar al usado en el esquema PS. En esta tesis hemos centrado nuestra atención en métodos de Padé para la sGeq con los tratamientos para la no linealidad de SV y GPRV.

El número y tipo de métodos numéricos usados para la sGeq es muy vasto, tanto que no se ha realizado ninguna comparación exhaustiva entre todos ellos. Se han usado métodos pseudoespectrales, como el esquema de Fourier de paso dividido (*split-step Fourier*) [55–57]. Y también métodos espectrales como un esquema de Fourier que conserva la energía [58], un método basado en ondículas (*wavelets*) [59, 60], un método de ondículas de Legendre de tipo análisis de multiresolución [61], y un método de elementos espectrales de tipo Legendre [62]. También se han usado métodos de elementos finitos basados en un esquema de Petrov–Galerkin [63], en un esquema de colocación usando puntos de Legendre–Gauss–Lobatto [64], *B-splines* (esplines básicas, en español) cúbicas [65], métodos de Galerkin discontinuos localmente [66, 67], y métodos de elementos de contorno [68]. Más aún, aprovechando la estructura hamiltoniana de la sGeq se han desarrollado métodos multisimplécticos [69, 70], incluso un procedimiento sistemático para lograr que dichos métodos conserven exactamente la energía [58, 71]. Además, para la sGeq se han desarrollado métodos sin malla (*meshless*) [72, 73] y basados en funciones de base radial [74, 75]. También podemos destacar los métodos basados en *exponential-fitting* (ajuste por exponenciales, en español), por aproximación analítica a trozos (*piecewise analytical*) [76], y las implementaciones discretas de la transformada espectral inversa [77, 78]. Finalmente, hay que tener en cuenta que la mayoría de estos métodos han sido extendidos a dos y a tres dimensiones espaciales [79].

Para la integración numérica de la GSLeq (2) hay que especificar las condiciones iniciales y de contorno; usaremos las condiciones iniciales

$$u(x,0) = u_0(x), \quad \frac{\partial u}{\partial t}(x,0) = u_1(x), \qquad x \in (-L/2, L/2],$$

y las condiciones de contorno periódicas dadas por

$$u(x,t) = u(x+L,t), \quad \frac{\partial u}{\partial x}(x,t) = \frac{\partial u}{\partial x}(x+L,t), \qquad x \in (-L/2, L/2], \quad t \in [0,T],$$

donde L es el período espacial y T es el intervalo de integración en tiempo. Discretizaremos el espacio usando $x_m = -L/2 + m\Delta x$, $m = 1, 2, \ldots, M$, con el tamaño de malla es $\Delta x = L/M$ (nótese que $u(x_0,t) \equiv u(x_M,t)$), y el tiempo $t^n = n\Delta t$, $n = 0, 1, \ldots, N$, con el paso de tiempo $\Delta t = T/N$. Para obtener la solución numérica de la GSLeq, $U_m^n \approx u(x_m,t^n) = u_m^n$, usamos dos familias de métodos de Padé, una basada en el método SV [7], dada por

$$\mathscr{A}_i(\mathrm{E})\,\frac{U_m^{n+1} - 2U_m^n + U_m^{n-1}}{\Delta t^2} - \mathscr{B}_i(\mathrm{E})\,U_m^n + \mathscr{A}_i(\mathrm{E})\,H(U_m^{n+1}) = 0, \tag{5}$$

y otra basada en el método GPRV [10] dada por

$$\mathscr{A}_i(\mathrm{E})\,\frac{U_m^{n+1}-2\,U_m^n+U_m^{n-1}}{\Delta t^2}-\mathscr{B}_i(\mathrm{E})\,\frac{(U_m^{n+1}+U_m^{n-1})}{2}+\mathscr{A}_i(\mathrm{E})\,H(U_m^{n+1})=0, \quad (6)$$

usando en ambos casos para el término no lineal la expresión

$$H(U_m^{n+1})\equiv\frac{F(U_m^{n+1})-F(U_m^{n-1})}{U_m^{n+1}-U_m^{n-1}}, \quad (7)$$

donde $\mathscr{A}_i^{-1}(\mathrm{E})\,\mathscr{B}_i(\mathrm{E})\,u_m^n$ es una aproximación de Padé (q,s) de orden $(q+s)$ para la segunda derivada espacial de $u(x_m,t^n)$, siendo E el operador de desplazamiento tal que $\mathrm{E}\,U_m^n=U_{m+1}^n$. La evaluación numérica de la expresión (7) puede presentar diferencias cancelativas catastróficas; se ha implementado una técnica para evitarlas que aprovecha propiedades elementales de las funciones trigonométricas.

Hemos estudiado cinco métodos de ambas familias cuyos operadores en diferencias $\mathscr{A}_i$ y $\mathscr{B}_i$ se muestran en la Tabla 1; los cinco métodos numéricos (5) se denominan métodos 1–5 y los otros cinco (6) como métodos 6–10 (como se indica en dicha tabla). El método 1 es el método de Strauss–Vázquez [7], interpretado como un método numérico de Padé (2,0) de segundo orden en espacio. El método 2 es un método de Padé (4,0) de cuarto orden en espacio. El método 3 es un método de cuarto orden es espacio interpretado como un método de Padé (2,2) desarrollado por Duncan [49] y Bratsos [50]. Un esquema de sexto orden de Padé (4,2) y otro de octavo orden (4,4) son los métodos 4 y 5, respectivamente. El método 6 es el método GPRV [10] interpretado como un método de Padé (2,0). El método 7 es un método de Padé (4,0) y el método 8 una aproximación de Padé (2,2). El método 9 y el método 10 son métodos de Padé (4,2) y (4,4), respectivamente. Los términos de error de truncado local para todos los métodos se han calculado utilizando la expansión por series de Taylor. Para la estabilidad lineal de estos esquemas se ha realizado un análisis de von Neumann que demuestra que son incondicionalmente estables. Los cinco esquemas de la segunda familia son más robustos que los de la primera, por ello se les ha aplicado un nivel de extrapolación de Richardson en tiempo para alcanzar cuarto orden en tiempo.

Se han estudiado los diez métodos tanto para la solución tipo *kink–antikink* como para la tipo *breather*. Para los métodos 1–5 de la familia SV (5), nuestros resultados indican que, para integraciones de corto tiempo, el método 2 es el que logra una cota máxima de error a menor coste para errores pequeños y que, para errores muy pequeños, lo logra el método 4; para integraciones de largo tiempo, los métodos 2 y 5 con un número impar de puntos en espacio son los mejores, siendo el método 2 mejor que el método 3, a pesar de que ambos tienen cuarto orden, y el método 5 mejor que el método 4. Para los métodos 6–10 de la familia

GPRV (6) con y sin extrapolación de Richardson, nuestros resultados muestran que a la hora de lograr cierto error máximo, los métodos con extrapolación son más costosos que los que no la tienen; de los métodos sin extrapolación, tanto para la solución tipo *kink–antikink* como para la tipo *breather*, logran un error máximo a menor costo el método 7 para errores pequeños y el método 10 para errores muy pequeños. La comparación entre los quince métodos estudiados muestra que el método 10 con extrapolación de Richardson es el que menor error ofrece para un Δt y un Δx dados, pero su costo es tan elevado que no puede competir con los métodos sin extrapolación; en nuestras simulaciones el mejor método en cuanto a relación coste-error es el método 7.

En definitiva, el método seleccionado para usarlo con la GSLeq en el estudio de las colisiones *kink–antikink* y para la búsqueda de *quasi-breather* es el método 7, un esquema de segundo orden en tiempo y cuarto orden en espacio basado en GPRV [10] sin extrapolación de Richardson.

Colisiones *kink–antikink*

Para estudiar la colisión entre un *kink* y un *antikink* mediante métodos numéricos para la GSLeq se va a usar como condición inicial un *ansatz* para su suma [80] dado por

$$\tilde{u}_{kak}(x,t) = u_k\left(\frac{x+x_0-vt}{\sqrt{1-v^2}}\right) + u_{ak}\left(\frac{x-x_0+vt}{\sqrt{1-v^2}}\right), \tag{8}$$

donde el *kink* está localizado en x_0 y el *antikink* en $-x_0$, teniendo ambos la misma velocidad pero en sentido opuesto. En las simulaciones numéricas, se han utilizado condiciones de contorno periódicas, pero la ecuación (8) no es una solución periódica de la ecuación (2), teniendo derivadas no contínuas en el contorno. Para

Método	Padé	Operador $\mathscr{A}_i$	Operador $\mathscr{B}_i$
1, 6	(2,0)	$\mathscr{I}$	$\frac{E^{-1}-2+E^{1}}{\Delta x^2}$
2, 7	(4,0)	$\mathscr{I}$	$\frac{-E^{-2}+16E^{-1}-30+16E^{1}-E^{2}}{12\Delta x^2}$
3, 8	(2,2)	$\frac{E^{-1}+10+E^{1}}{12}$	$\frac{E^{-1}-2+E^{1}}{\Delta x^2}$
4, 9	(4,2)	$\frac{2E^{-1}+11+2E^{1}}{3}$	$\frac{E^{-2}+16E^{-1}-34+16E^{1}+E^{2}}{4\Delta x^2}$
5, 10	(4,4)	$\frac{23E^{-2}+688E^{-1}+2358+688E^{1}+23E^{2}}{15}$	$\frac{31E^{-2}+128E^{-1}-318+128E^{1}+31E^{2}}{\Delta x^2}$

Table 1: Operadores en diferencias $\mathscr{A}_i$ y $\mathscr{B}_i$ en los métodos de Padé (5) y (6). El símbolo $\mathscr{I}$ es el operador identidad.

solventar este problema se puede utilizar una serie de solitones imbricados [81, 82]. La imbricación para la solución $\tilde{u}_{kak}(x,t)$ es muy sencilla y basta con utilizar la siguiente suma

$$u_{kak}(x,t) = \sum_{j=-p}^{p} \tilde{u}_{kak}(x+2Lj,t), \qquad x \in [-L,L), \tag{9}$$

para $p \to \infty$; de hecho, cuando $x_0 = L/2$, y L es mayor que la anchura del *kink*, nuestra experiencia numérica indica que incluso para $p = 1$ se logra una solución periódica precisa, ya que las derivadas espaciales del *kink* y el *antikink* decrecen exponencialmente.

De forma similar a otras ecuaciones Klein–Gordon no lineales y no integrables [12], cuando se utiliza la ecuación (9) como condición inicial con una velocidad inicial dada para estudiar una colisión *kink–antikink*, el comportamiento a largo plazo de la solución depende de si esta velocidad inicial es menor o mayor que una velocidad crítica v_{cr} que es una función monótona creciente del parámetro geométrico b de la GSLeq. Por encima de la velocidad crítica el *kink* y el *antikink* tras su colisión inelástica, en la que emiten radiación perdiendo energía y velocidad, logran escapar hasta infinito. Sin embargo, por debajo de la velocidad crítica, el comportamiento genérico en una colisión es la formación de un estado oscilatorio, parecido a un *pseudo-breather*, con una amplitud que disminuye lentamente a medida que aumenta el tiempo.

Las simulaciones numéricas muestran una serie (que aparenta ser infinita numerable) de intervalos en velocidad en los que el *kink* y el *antikink* se acoplan en un estado oscilatorio transitorio caracterizado por un número creciente de rebotes (oscilaciones en la amplitud máxima desde un valor cercano a 2π hasta uno cercano a -2π, llamadas *bounces* en inglés) del que logran escapar hasta infinito; dicho estado ligado se interpreta como una resonancia entre el par *kink–antikink* y la radiación, por ello estos intervalos se denominan ventanas de resonancia y se caracterizan por su número de rebotes [12]. Se han observado ventanas con un número de rebotes igual o superior a dos. Conforme la velocidad se acerca a la velocidad crítica, las ventanas con dos rebotes reducen su anchura acumulándose por debajo de la velocidad crítica, que se comporta como un punto de acumulación; dentro de cada una de estas ventanas de dos rebotes, la amplitud máxima (cerca de 2π) o mínima (cerca de -2π) realiza cierto número de oscilaciones, de las que se pueden contar su número de picos (o crestas); el número de estos picos crece conforme la ventana se acerca a la velocidad crítica (hemos observado ventanas de dos rebotes con hasta cuarenta y cinco picos). Además, a ambos lados de cada ventana con dos rebotes se observa la acumulación de ventanas con tres rebotes de anchura decreciente conforme se acercan a ambos bordes de dicha ventana, que

actúan como velocidades críticas; excepto para la primera ventana con dos rebotes en la que solo se acumulan en su borde derecho. Esta estructura autosemejante se repite con las ventanas de cuatro rebotes, que rodean a las ventanas de tres rebotes, y así sucesivamente; en nuestras simulaciones hemos observado ventanas con gran número de rebotes. Gracias a ello hemos conjeturado una estructura fractal *ad infinitum* para las ventanas de resonancia, que hemos formalizado usando una nueva notación multiíndice para el número de rebotes, el número de picos de la oscilación y si la ventana con k rebotes se encuentra a la derecha o a la izquierda de una ventana con $k-1$ rebotes.

La estructura fractal observada en las colisiones *kink–antikink* de la GSLeq es similar a la que presenta la dsGeq, cuyas características generales se han estudiado usando la teoría del intercambio de energía resonante desarrollada por Campbell *et al.* [12, 13]. La aplicación de dicha teoría a la GSLeq permite estimar la posición central de las ventanas de resonancia con dos rebotes en función de su número de picos; para ello se estima la frecuencia de los modos de oscilación que dan lugar a dichos picos resolviendo un problema de valores propios para una ecuación de Schrödinger lineal con un potencial efectivo que depende del parámetro geométrico b de la GSLeq. Usando la frecuencia de oscilación del modo permite estimar también la duración del estado de resonancia asociado a cada ventana, que es una función lineal del número de picos dentro de dicha ventana. A diferencia de la dsGeq, los resultados con esta aproximación son mejores conforme el parámetro b crece y la frecuencia de resonancia disminuye de forma monótona.

Nuestros resultados muestran que la teoría del intercambio de energía resonante se ajusta mejor a las observaciones numéricas para la GSLeq que para la dsGeq [13]. Para esta última, en función del parámetro que combina sus dos senos, la velocidad crítica crece para luego decrecer; sin embargo, en la GSLeq a medida que aumenta el parámetro geométrico b de la GSLeq, la velocidad crítica crece de forma monótona acercándose de forma asintótica a un valor máximo (hasta donde hemos podido comprobar numéricamente). Nuestra conjetura es que esta podría ser la razón detrás de que el ajuste de la teoría del intercambio de energía resonante para la GSLeq mejore conforme b crece.

Búsqueda del *quasi-breather*

La GSLeq no tiene una solución tipo *breather* al ser una ecuación no integrable; sin embargo, se puede considerar como una modificación de la sGeq, que la tiene. La solución tipo *breather* de la sGeq se puede obtener mediante el método de separación de variables, pero dicho método no es aplicable a la GSLeq. En esta tesis se ha llevado a cabo una búsqueda numérica de soluciones de tipo *quasi-*

breather utilizando una nueva condición inicial basada en perturbar la solución nula de la GSLeq, en lugar de perturbar el *breather* de la sGeq (el método habitual en búsquedas previas). Como nuestro método numérico requiere dos condiciones iniciales, U_m^0 y U_m^{-1}, la nueva condición inicial es exacta para $U_m^0 = u(x_m,0) = 0$ y presenta un error relativo comparable al épsilon de la máquina para $U_m^{-1} = u(x_m,-\Delta t) + O\left(\Delta t^9\right)$.

La solución tipo *breather* de la sGeq viene dada por

$$u_{\rm br}(x,t) = 4\arctan(\operatorname{sech}(qx)\sin(\omega qt)/\omega), \qquad q = 1/\sqrt{1+\omega^2}, \tag{10}$$

donde el parámetro ω se denomina frecuencia, aunque la frecuencia de oscilación en tiempo del *breather* sea $\omega_{br}(\omega) = \omega/\sqrt{1+\omega^2}$. La solución (10) cumple que $u_{\rm br}(x,0) = 0$, y $u_{\rm br}(x,t) = 4q\operatorname{sech}(qx)t + O\left(t^3\right)$, por lo que sugiere para la solución correspondiente de la GSLeq el *ansatz* dado por

$$u_b(x,t) = 4q\operatorname{sech}(qx)t + u_3(x)t^3 + u_5(x)t^5 + u_7(x)t^7 + O\left(t^9\right),$$

que permite obtener la expansión asintótica regular

$$\begin{aligned} u_b(x,t) = {} & 4tq\operatorname{sech}(qx) - \frac{2t^3}{3}q\operatorname{sech}(qx)\left(1-q^2+2q^2\operatorname{sech}^2(qx)\right) \\ & + \frac{t^5}{30}\big(q(1-q^2)^2\operatorname{sech}(qx) + 4q^3(5+6b^2-5q^2)\operatorname{sech}^3(qx) \\ & \qquad + 24q^5\operatorname{sech}^5(qx)\big) \\ & + O\left(t^7\right), \end{aligned} \tag{11}$$

en la que es muy fácil determinar términos de mayor orden y que se puede utilizar como condición inicial $U_m^{-1} = u_b(x_m,-\Delta t)$. Nótese que para $\Delta t \leq 0.01$, $q < 1$ y $b \leq 1$ basta tomar el desarrollo hasta el término $O\left(t^9\right)$ para que el error sea mucho menor que el épsilon de la máquina; sin embargo, para $b \gg 1$ hay que añadir términos de mayor orden en la ecuación (11).

Las simulaciones numéricas muestran que la nueva condición inicial genera tres soluciones posibles dependiendo de la frecuencia ω, existiendo dos frecuencias críticas $\omega_{\rm cr}$ y $\omega_{\rm cr,br}$ que determinan el tipo de solución (no nos consta que la existencia de estas frecuencias críticas haya sido reportada en estudios previos de las soluciones de tipo *quasi-breather* en otras ecuaciones de Klein–Gordon). En concreto, se genera un par *kink–antikink* que escapan hacia infinito para $\omega < \omega_{\rm cr}$, un *pseudo-breather* para $\omega_{\rm cr} < \omega < \omega_{\rm cr,br}$, y una solución *quasi-breather* para $\omega > \omega_{\rm cr,br}$; donde hemos usado la nomenclatura de Malomed *et al.* [83], según la cual un *pseudo-breather* es una solución oscilatoria irregular que decae en radiación

tras un número pequeño de oscilaciones en tiempo, mientras un *quasi-breather* presenta oscilaciones regulares que se mantienen durante un largo tiempo.

Nuestras simulaciones muestran que la frecuencia crítica ω_{cr} crece de forma monótona con b, siendo nula para $b = 0$. Y que el *quasi-breather* para $\omega > \omega_{\mathrm{cr,br}}$ sobrevive más de mil períodos, mientras su amplitud y energía decrecen y su frecuencia se incrementa. Hemos caracterizado estos comportamientos ajustando la amplitud y la frecuencia con sendas leyes de potencia; aunque aún no disponemos de una explicación teórica para los exponentes observados que dependen del parámetro geométrico b. Además, hemos observado que la frecuencia de la primera oscilación del *quasi-breather* está por debajo de la frecuencia del *breather* ω_{br} de la sGeq, y decrece conforme b crece; la frecuencia de las sucesivas oscilaciones crece, pero manteniéndose siempre por debajo de ω_{br}. Como resultado, para b pequeño, el caso de más interés en las aplicaciones prácticas de la GSLeq, el *quasi-breather* de la GSLeq tiene una frecuencia muy constante y muy próxima a ω_{br}, presentando una robustez que lo asemeja a un *breather* verdadero. Gracias a ello esperamos que la búsqueda experimental de este *quasi-breather* en superredes de grafeno sea exitosa.

Conclusiones

Se han estudiado por primera vez usando métodos numéricos las soluciones de la GSLeq y sus interacciones, en concreto, las colisiones entre un *kink* y un *antikink* y la generación de soluciones de tipo *quasi-breather*. Para elegir el mejor método numérico para la GSLeq se han desarrollado diez esquemas numéricos de Padé que se han comparado entre sí para las soluciones kink–antikink y breather de la sGeq; cinco de ellos con y sin extrapolación de Richardson en tiempo. La comparación entre dichos métodos ha permitido seleccionar el método más eficiente para estudiar dichas soluciones en simulaciones de muy largo tiempo.

Se ha observado una estructura fractal en las colisiones *kink–antikink* para velocidades por debajo de una velocidad crítica que depende del parámetro geométrico de la GSLeq. En dicho caso la colisión da como resultado la formación de un estado oscilatorio, parecido a un *pseudo-breather*, que decae en radiación; además se observan una serie de ventanas donde el *kink* y el *antikink* logran escapar tras estar ligados de forma temporal en un estado resonante. La estructura fractal de estas ventanas se ha formalizado con una nueva notación multiíndice. La teoría del intercambio de energía resonante permite entender las características generales de estas colisiones, ajustándose mejor que para otras ecuaciones similares, como la dsGeq.

Se ha emprendido una búsqueda sistemática del *quasi-breather* de la GSLeq usando como condición inicial una perturbación de la solución nula que está caracte-

rizada por cierta frecuencia. Se han observado dos valores críticos de esta frecuencia que separan las soluciones que evolucionan a un par *kink–antikink*, a un *pseudo-breather* y a un *quasi-breather*. Para valores pequeños del parámetro geométrico de la GSLeq el *quasi-breather* se comporta de forma muy parecida al *breather* de la sGeq. Para valores mayores se observa que el *quasi-breather* sobrevive más de mil períodos, mientras su amplitud y energía decrecen y su frecuencia se incrementa.

Trabajo futuro

Hay múltiples líneas de investigación abiertas por el trabajo realizado en esta tesis. En cuanto al desarrollo y análisis de métodos numéricos para la GSLeq proponemos estudiar nuevas familias de métodos en espacio, como los pseudoespectrales, y en tiempo, como los métodos diagonalmente implícitos de Runge–Kutta–Nyström. También pretendemos estudiar los efectos numéricamente inducidos usando la técnica de ecuaciones modificadas.

Nuestra investigación ha mostrado la robustez de las soluciones estacionarias de tipo *quasi-breather* de la GSLeq. Pretendemos estudiar las colisiones mutuas entre *quasi-breathers* en movimiento y entre *quasi-breathers* y *kinks* y *antikinks*; esta investigación es muy prometedora desde el punto de vista de las aplicaciones potenciales de las superredes de grafeno. Además, como nuestros resultados apoyan la búsqueda experimental de *quasi-breathers* en superredes de grafeno, se hace necesario el estudio numérico de la generación de *kinks*, *antikinks* y *pseudo-breathers* a partir de diferentes condiciones iniciales.

Dado que la ecuación GSLeq se puede considerar una perturbación de la sGeq para valores pequeños del parámetro geométrico, proponemos la aplicación de técnicas perturbativas inspiradas en la transformada espectral inversa para la sGeq. Esperamos que dichas técnicas permitan aproximar de forma analítica las soluciones de tipo *kink–antikink* y *quasi-breather* de la GSLeq. Además, permitirán estudiar el efecto de términos disipativos, dispersivos y no lineales de alto orden en la GSLeq. Estos resultados analíticos serán validados con simulaciones numéricas específicas.

Para aplicaciones de las superredes de grafeno en el régimen de los terahercios, Kryuchkov, Kukhar', y Zavyalov [84] han derivado una ecuación integro-diferencial de tipo Klein–Gordon pero con una no linealidad no local descrita en forma integral. El desarrollo de métodos numéricos para dicha ecuación y el análisis de sus potenciales soluciones de tipo *kink*, *antikink* y *quasi-breather* es otra línea de investigación futura que pretendemos emprender.

Las superredes de grafeno están formadas por diferentes franjas de material dieléctrico donde se pueden propagar ondas de tipo plasmón-polaritón de superficie. En la derivación de la GSLeq de Kryuchkov y Kukhar' solo se considera una única franja; cuando no se desprecian los efectos de solape entre franjas se espera que dichas ondas sean modeladas por un conjunto de ecuaciones de tipo GSLeq acopladas entre sí. Su derivación y estudio numérico es otra línea de investigación que puede proporcionar resultados de gran impacto. Finalmente, parece muy interesante el estudio de versiones discretas de la GSLeq; en ellas se pueden propagar soluciones discretas de tipo *breather* (también llamados modos intrínsecos localizados). Nuestra intención es buscar dichas soluciones usando técnicas de deflación [85].

1 Introduction

1.1 Motivation

Graphene is an allotrope of carbon isolated in 2004 by the research group of Andre K. Geim and Konstantin S. Novoselov [1]; its discovery was awarded with the Nobel Prize in Physics 2010. This extraordinary material has remarkable mechanical, thermal, and electrical conduction properties, promising a relevant role in the future of the silicon electronics and optoelectronics. Current commercial devices are based on semiconductors, materials with a band gap, but graphene is gapless, a semi-metal. However, a band gap can be engineered into graphene by placing it on top of a suitable substrate [2], allowing the development of transistors and other optoelectronic devices.

In the terahertz (THz) regime, graphene superlattices are among the most promising graphene-based optoelectronic devices. This structure is formed by a sheet of graphene deposited on periodically alternating strips of a material that does not modify the graphene band structure and another one that introduces a band gap. Transversal electromagnetic irradiation on this device induces waves propagating in the strips of the dielectric that are coupled with the carriers (electrons and holes) in the graphene sheet; for intense irradiation the electrodynamic response of the device is described by a non-linear wave equation. This equation for the amplitude of the vector potential of the electromagnetic field is a nonlinear Klein–Gordon equation (KGeq), here referred to as the graphene superlattice equation (GSLeq); in fact, it depends on a geometrical parameter such that it can be interpreted as a perturbation of the sine–Gordon (sGeq). Hence, it is expected that the solutions of the GSLeq are similar to kink, kink-antikink, and breather solutions of the sGeq when this parameter is small enough; moreover, for larger values, the general features of these solutions should be similar to those of the double sine–Gordon equation (dsGeq).

Up to this author's knowledge, the detailed analysis of the solutions the GSLeq were not reported in the literature. In my opinion, such an analysis will be relevant for future optoelectronics applications of graphene superlattices, for example, for the high harmonic generation process that may be useful both in the detection and generation of THz signals.

1.2 Objectives

The research aim of this thesis is to gain understanding on the nonlinear behaviour of the solutions of the GSLeq in order to determine the regions of their parameter space were its behaviour is robust and predictable. In order to achieve such an aim, three objectives have been proposed. The first objective is the study of the inelastic scattering of kinks and antikinks of the GSLeq. The corresponding problem for the dsGeq shows a critical velocity below which a series of resonance windows with a fractal structure is observed. In these windows the kink and the antikink escape to infinity near elastically, resembling the solutions of the sGeq. The study of these solutions for the GSLeq is an open problem to be tackled here.

The second objective is the study of the generation of robust quasi-breather solutions of the GSLeq. Outside the resonance windows of the dsGeq, the kink-antikink interaction results in an oscillatory solution (a bion, oscillon, or pseudo-breather) that decays into radiation. Moreover, pseudo-breathers with a long lifetime of thousands of periods, referred to as quasi-breathers, have been observed for the dsGeq. The search for such robust quasi-breathers for the GSLeq is another open problem to be solved before claiming the use of graphene superlattices for future applications.

Finally, the third objective is a requirement in order to achieve the first two ones, the development of robust, fast, and efficient numerical methods for the long-time integration of the GSLeq. In order to fulfil such a task, a careful comparison of numerical schemes for the sGeq will be undertaken. Since the number of published numerical schemes for the sGeq is overwhelming, making a comprehensive and reliable comparison very time consuming. In order to limit the scope of our comparison, only Padé numerical methods inspired in the energy-conserving scheme by Strauss and Vázquez will be considered. These methods of high-order in space, but only second-order in time, almost conserve a discrete analogue of the energy of the GSLeq, so they are expected to be robust for long-time integrations. Moreover, in order to achieve high-order accuracy in time, Richardson's extrapolation can be implemented. We expect that, after our comparison, the best numerical method be competitive with other state-of-the art implementations.

1.3 Methodology

The methodology to be used in this thesis is the standard one for a computational research. Let us begin with the third objective, for which the standard methods to analyse the consistency, stability, and convergence of numerical schemes will be applied; specifically, their local truncation error will be calculated to check the consistency and the von Neumann analysis will be applied to determine the conditions for their linear stability. The existence of potential discrete analogues of the energy will be studied in order to ensure the nonlinear stability of the schemes. Extensive numerical simulations with exact solutions of the sGeq as initial conditions will be undertaken in order to numerically confirm the order of consistency in both space and time of the global error as a function of the meshgrid and the time-step. Specifically, the evolution in time of the discrete analogue of the energy will be used to ensure the good energy-conserving properties of the numerical methods in long-time integrations. Finally, the most cost-efficient method for long-time integrations of the sGeq, that will be used for the study of the solutions of the GSLeq, was selected in terms of the relation between the computational cost (estimated by the time of execution in seconds) and the maximum numerical error.

A combination of numerical and perturbative methods will be used to determine the initial condition for the computational study required by the first and second objectives. By using the kink solution of the sGeq as an *ansatz* an asymptotic approximation of the kink of the GSLeq for small geometrical parameter will be obtained; the accuracy of this solution will be assessed by comparison with the kink obtained by numerical integration; such kink solutions will be used to obtain the initial condition for the simulations of the collisions of kink and antikink required in the first objective. Instead of the standard asymptotic approximation of the quasi-breather solution of the GSLeq based on the breather solution of the sGeq as an *ansatz*, a new initial condition will be considered based on the perturbation of the null initial condition; it is expected that such new initial condition yields more robust quasi-breather solutions in the numerical simulations required in the second objective.

The standard methodology to study the fractal structure of the soliton scattering of nonlinear Klein–Gordon equations, like the dsGeq and the ϕ^4-model will be used to accomplish the first objective. Since for small values of the geometrical parameter of the GSLeq, its solution is expected to be a small perturbation of the corresponding sGeq solution, a large value of this parameter of the order of unity will be used (the value will be selected after an extensive set of numerical simulations). For such a parameter the main properties of the resonance windows, their self-similarity and their pre-fractal structure will be studied; our intention is to infer the fractal structure of the scattering of solitons and develop a new formalism to describe

it. Furthermore, the standard resonant energy exchange theory will be applied to understand this fractal structure and check whether its results for the GSLeq are as good as those for the dsGeq and the ϕ^4-model.

Finally, a perturbation of the null solution of the GSLeq will be used for the search of the quasi-breather solution. In the parameter region where quasi-breathers with long lifetime be observed, the standard methods for the characterisation of these solutions will be applied; specifically, the evolution in time of their amplitude and frequency will be determined. The existence of critical values for the frequency of the initial condition that separates the pseudo- and quasi-breather solutions will be searched. If they are found, a new methodology for its analysis will be developed.

1.4 Papers and contributions

Let us present the list of publications that have been directly derived from the development of this Ph.D. thesis. First, the papers in research journals that endorse to the quality of this work (most recent first). Second, a review paper published as a book chapter. And third, the works presented in international conferences. Along with the publication details, the available metrics of each publication are presented, i.e., the impact factor (ISI JCR), category, and ranking.

1.4.1 ISI JCR Indexed Journals

1. F. Martin-Vergara, F. Rus, F.R. Villatoro, "Numerical search for the stationary quasi-breather of the graphene superlattice equation," *Chaos, Solitons & Fractals* **162**: 112530 (2022). ISSN 0960-0779, doi:10.1016/j.chaos.2022.112530.

   - Impact factor: 9.922 (JCR 2021)
   - Categories:
     - Physics, Mathematical: Q1 (1/56)
     - Mathematics, Interdisciplinary Applications: Q1 (1/108)
     - Physics, Multidisciplinary: Q1 (7/85)

2. F. Martin-Vergara, F. Rus, F.R. Villatoro, "Fractal structure of the soliton scattering for the graphene superlattice equation," *Chaos, Solitons & Fractals* **151**: 111281 (2021). ISSN 0960-0779, doi:10.1016/j.chaos.2021.111281.

   - Impact factor: 9.922 (JCR 2021)
   - Categories:
     - Physics, Mathematical: Q1 (1/56)

  - Mathematics, Interdisciplinary Applications: Q1 (1/108)
  - Physics, Multidisciplinary: Q1 (7/85)

3. F. Martin-Vergara, F. Rus, F.R. Villatoro. "Padé schemes with Richardson's extrapolation for the sine–Gordon equation," *Communications in Nonlinear Science and Numerical Simulation* **85**: 105243 (2020). ISSN 1007-5704, doi:10.1016/j.cnsns.2020.105243.

   - Impact factor: 4.260 (JCR 2020)
   - Categories:
     - Physics, Mathematical: Q1 (3/55)
     - Physics, Fluids & Plasmas: Q1 (2/34)
     - Mathematics, Applied: Q1 (5/265)
     - Mathematics, Interdisciplinary Applications: Q1 (11/108)
     - Mechanics: Q1 (23/136)

4. F. Martin-Vergara, F. Rus, F.R. Villatoro, "Padé numerical schemes for the sine–Gordon equation," *Applied Mathematics and Computation* **358**: 232–243 (2019). ISSN 0096-3003, doi:10.1016/j.amc.2019.04.042.

   - Impact factor: 3.472 (JCR 2019)
   - Category:
     - Mathematics, Applied: Q1 (7/261)

1.4.2 Book chapter

1. F. Martin-Vergara, F. Rus, F.R. Villatoro, "Solitary waves on graphene superlattices," in J.F.R. Archilla, F. Palmero, M.C. Lemos, B. Sánchez-Rey, J. Casado-Pascual (eds), *Nonlinear Systems, Vol. 2. Nonlinear Phenomena in Biology, Optics and Condensed Matter*, Springer, Cham (Switzerland), 2018. ISSN 1860-0832; ISBN 978-3-319-72218-4. doi:10.1007/978-3-319-72218-4_4.

   - Scopus (Elsevier). CiteScore: 0.9 (2018)
     - Citations: 7
       * Engineering, Computational Mechanics (65/78)
       * Computer Science, Artificial Intelligence (240/269)
       * Computer Science, Software (374/398)
     - Field-Weighted citation impact: 2.67 (2018–2022)

  - Citation benchmarking: 91th percentile (2018–2022)

- Book Citation Index (Web of Science Core Collection)
  - Citations: 6
  - Research Areas:
    * Life Sciences & Biomedicine - Other Topics
    * Science & Technology - Other Topics
  - Categories: Biology Multidisciplinary Sciences
  - Citation Topics:
    * 2 Chemistry
    * 2.76 2D Materials
    * 2.76.39 Graphene

1.4.3 International conferences

1. F. Martin-Vergara, F. Rus, F.R. Villatoro, ”Quasi-breathers of the graphene superlattice equation,” Poster in RSME-UMA: II Encuentro de la Real Sociedad Matemática Española (RSME) y la Unión Matemática Argentina (UMA). Ronda, Málaga, Spain, 2022.

2. F. Martin-Vergara, F. Rus, F.R. Villatoro, ”Kink–antinkink collisions in the graphene superlattice equation,” Oral communication in NoLineal 20-21: International Conference on Nonlinear Mathematics and Physics. Madrid, Spain, 2021. ISBN: 978-84-09-31166-8.

3. F. Martin-Vergara. ”Solitary waves generated by graphene superlattices for tumours treatment,” Oral communication in VI International Conference of IMFAHE: International Mentoring Foundation For The Advancement Of Higher Education. Boston, USA, 2021.

4. F. Martin-Vergara, F. Rus, F.R. Villatoro. ”Padé numerical schemes for the sine–Gordon equation,” Oral communication in NoLineal 2018: International Conference on Nonlinear Mathematics and Physics. ISBN: 978-84-09-03289-1. Málaga, Spain, 2018.

5. F. Martin-Vergara, F. Rus, F.R. Villatoro. ”Numerical methods for graphene superlattice equation,” Poster in Graphene2018: 8th edition of the largest European Conference and Exhibition in Graphene and 2D Materials. Dresden, Germany, 2018.

6. F. Martin-Vergara, F. Rus, F.R. Villatoro. "Pseudospherical surfaces based on the graphene superlattice equation," Poster in EREP2017: Spanish-Portuguese Relativity Meeting. Málaga, Spain, 2017.

7. F. Martin-Vergara, F. Rus, F.R. Villatoro. "Solitary wave interactions in graphene superlattices," Poster in Graphene 2016: 6th edition of the largest European Conference and Exhibition in Graphene and 2D Materials. Genoa, Italy, 2016.

8. F. Martin-Vergara, F. Rus, F.R. Villatoro. "Kink-antikink collisions in the Kryuchkov–Kukhar' equation," Oral communication in NoLineal 2016: International Conference on Nonlinear Mathematics and Physics. Seville, Spain, 2016. ISBN: 978-84-09-05654-5.

1.5 Brief summary of the papers

Let us summarise the four journal papers and the book chapter in chronological order. Other publications, such as oral communications and posters presented at international conferences are not summarised because they contain preliminary or partial contributions included in these articles.

Paper 1. *Solitary waves on graphene superlattices* [3]. This review article summarises the derivation of the GSLeq and presents a first numerical analysis of its solutions. The electronic band structure of graphene is described and how it determines the electronic properties of the Ratnikov's graphene superlattice; specifically, the results obtained with two different methods, the matrix transfer method used by Ratnikov (2009) [4] and the one based on the Kronig–Penny model by Maksimova *et al.* (2012) [5]. Under the incidence of high-intensity electromagnetic waves, non-linear waves propagates in this device; they are governed by an equation for the transversal component of the potential vector derived by Kryuchkov and Kukhar' (2013) [6], here referred to as the graphene superlattice equation. The GSLeq is a modification of the sGeq that presents topological solitary waves (kinks and antikinks). The GSLeq is not integrable, but its solitons can be approximated analytically by using asymptotic methods; two approaches based on two *ansätze* are presented. The numerical method of Strauss–Vazquez that conserves a discrete analogue of the energy is used for a first study of their mutual interactions; results indicate that the kink-antikink collisions of the GSLeq are almost elastic when this equation is a small perturbation of the sGeq.

Paper 2. *Padé numerical schemes for the sine–Gordon equation* [8]. The sine–Gordon equation appears in multiple scientific and engineering problems; although it is integrable, in most practical applications its numerical simulation is required.

For this equation, five finite difference methods based on Padé approximations have been developed; in these methods the spatial derivative is substituted by a (q,s)-Padé operator, the quotient of a polynomial of degree q in the numerator and one of degree s in the denominator; the resulting scheme has a $(q+s)$-th order in space; all the methods are implicit, sharing the same treatment for nonlinearity and time integration. The first method is the one used in Paper 1 interpreted as a $(2,0)$-Padé scheme; this method has been compared with four novel $(4,0)$-, $(2,2)$-, $(4,2)$-, and $(4,4)$-Padé methods in terms of error, computational cost and energy conservation for both the kink-antikink and breather solutions of the sGeq. The linear stability analysis shows that these five methods are conditionally stable. The study of the minimum cost to attain a maximum error indicates that the most efficient method for small errors is the $(4,0)$-Padé method and for very small errors is the $(4,2)$-Padé method. Furthermore, the results in long-time integrations show that the spatial order of consistency is more important than energy conservation for the efficiency of the method.

Paper 3. *Padé schemes with Richardson's extrapolation for the sine–Gordon equation* [9]. For a more comprehensive comparison of numerical methods for the sGeq, another five implicit finite difference methods based on (q,s)-Padé operators have been developed, but with an integration in time based on the Guo, Pascual, Rodríguez, and Vázquez (GPRV) scheme [10], that preserves another discrete analogue of the energy. Specifically, the GPRV method is interpreted as a $(2,0)$-Padé method, and four new $(4,0)$-, $(2,2)$-, $(4,2)$- and $(4,4)$-Padé methods are developed. The linear stability of the GPRV methods is unconditional. To increase the order in time, Richardson's extrapolation has been used, giving rise to another five methods of fourth-order. These ten methods have also been compared in terms of global error, computational cost and energy conservation for both kink-antikink and breather solutions of the sGeq. The results show that, when it comes to reaching a certain level of maximum error, the methods with Richardson's extrapolation are more expensive than the methods without it. Among the latter, the most efficient method for small errors is the $(4,0)$-Padé method and for very small errors is the $(4,4)$-Padé one. The comparison between the fifteen methods studied in Papers 2 and 3 shows that the most efficient method for small errors is the $(4,0)$-Padé method from Paper 3, which will be used to simulate the GSLeq equation in the following papers.

Paper 4. *Fractal structure of the soliton scattering for the graphene superlattice equation* [11]. The graphene superlattice equation has a kink solution without an explicit analytic expression, so it is necessary to calculate it using numerical integration methods. The inelastic collision of a kink against an antikink, both with the same speed but in opposite directions, is studied for the first time. After their interaction, both escape to infinity when their common speed is greater than a

critical value; below it, they form a pseudo-breather that decays slowly as it radiates energy, except when they are within a series of intervals in velocity, referred to as resonance windows. In these windows the kink and the antikink are coupled in a resonant state from which they escape to infinity after a finite period of time. These resonance windows show a self-similar, pre-fractal structure; a new multi-index notation is developed that allows us to conjecture their fractal structure *ad infinitum*. The resonant energy exchange theory of Campbell *et al.* [12, 13] has been used to describe the main features of this fractal scattering; a good agreement is observed between the theoretical predictions and the numerical simulations. Our findings can be interpreted as new evidence supporting this theory in modified sine–Gordon equations.

Paper 5. *Numerical search for the stationary quasi-breather of the graphene superlattice equation* [14]. The kink-antikink collisions studied in Paper 4 suggest the possibility of a quasi-breather solution in the GSLeq. The numerical search of the static quasi-breather is carried out using a new initial condition derived from a regular perturbation of the null solution of the GSLeq characterised by a frequency. The results show a minimum critical frequency for the observation of an oscillatory solution; for values higher than but close to that frequency, this solution behaves like a pseudo-breather decaying into radiation after a finite number of irregular oscillations. However, there is a second critical frequency above which a robust quasi-breather surviving thousands of periods is observed. Since the GSLeq does not have a breather solution, as time passes, the amplitude and energy of the quasi-breather slowly decreases, while its frequency increases. The new robust quasi-breather, together with the contribution of Paper 4, supports the experimental search of nonlinear waves in graphene superlattice devices.

My contribution to the five articles has been the software development and implementation, the application of the methodology, the analysis of results, as well as the manuscripts' writing, edition and review. The other two authors, Francisco Rus and Francisco R. Villatoro, are responsible of the conceptualisation of the problem and the methodology, the analysis of results, as well as the manuscripts' writing, edition and review.

1.6 Thesis contents

The contents of this Ph.D. thesis are as follows. Chapter 2 is based in my review paper [3] and summarises the basic theoretical aspects of the propagation of nonlinear electromagnetic waves on the Ratnikov's graphene superlattice. It includes a literature review on solitary waves for the nonlinear Klein–Gordon equation and solitons for the sine-Gordon equation. The electronic band structure of graphene

and the Ratnikov's graphene superlattice are also presented. The derivation of the graphene superlattice equation for nonlinear waves in this device is reviewed and its solitary wave solutions are presented.

Chapter 3 is based on my papers [8] and [9], and compares fifteen numerical methods for the sine-Gordon equation in order to determine the best one for the graphene superlattice equation. After a literature review on numerical methods for the sine-Gordon, the formulation, analysis, and implementation of the fifteen Padé methods are described. The main results of the comparison among them for the kink-antikink and breather solutions of the sine-Gordon equation are presented. Moreover, the properties of the method selected for the GSLeq are emphasised and their selection properly justified.

Chapter 4 is based in my papers [11] and [14], and discusses the numerical results on the solutions for the graphene superlattice equation. It starts with the initial conditions used for the study of the kink–antikink collisions, and for the search of the quasi-breather solution. Then the fractal structure observed in the kink–antikink scattering is analysed in detail, and the main results on the numerical search for the quasi-breather of the GSLeq are summed up.

Chapter 5 summarises the main conclusions of this dissertation, highlighting its main contributions and launching future lines of research. Finally, the bibliography and five appendices with my papers are included.

2

Graphene superlattice equation

In this chapter my review paper [3] on the basic theoretical aspects of the propagation of nonlinear electromagnetic waves on a graphene superlattice is summarised. In Section 2.1 a short review on solitary waves in the nonlinear Klein–Gordon equation and solitons in the sine-Gordon equation is presented. In Section 2.2 graphene and the Ratnikov's graphene superlattice are introduced. In Section 2.3 the graphene superlattice equation for nonlinear waves in this device is derived. Finally, in Section 2.4 the solitary wave solutions of the GSLeq are presented.

2.1 Solitons in the nonlinear Klein–Gordon equation

Evolution equations with solitary waves are ideal models for the propagation of nonlinear waves in physical systems; under suitable conditions, when high-order dissipative, dispersive and nonlinear terms are incorporated, these equations describe some experimental observations. They can be either integrable or non-integrable. In the integrable case they present solitons, a term coined by Zabusky and Kruskal [15] for the Korteweg–de Vries equation [16]. Solitons are robust solitary waves that behave like particles maintaining their amplitude, shape and speed; additionally, their collisions are perfectly elastic, without emitting any radiation, although marked with a phase change at the point of collision. In the non-integrable case the solitary waves are not solitons, in the strict sense, because their interactions are inelastic, accompanied by the emission of radiation and other phenomena; however, the term soliton is also used to refer to such solutions in a broad sense.

Solitons have been found in multiple nonlinear evolution equations [17–20]. Thanks to this, its study covers all fields of applied mathematics and mathematical physics, from the study of waves in fluids, such as tsunamis [21], to waves in biological systems, such as DNA molecules [22] or the movement of living organism [23].

However, the most relevant applications of solitons are in one-dimensional media, such as optical fibers [24] and nonlinear transmission lines [25].

Among the soliton integrable equations, the most relevant for our research is the sine–Gordon equation [26] discovered in the study of surfaces of constant negative curvature by Bour in 1862. It was rediscovered as a continuous model for waves in a series of coupled pendulums for the study of dislocations in crystals by Frenkel and Kontorova in 1939. After the discovery of its integrability in the early 1970s, its applications multiplied, from the modelling of superconducting Josephson junctions to the propagation of ultrashort pulses in optical fibers, among others [26–28]. The sGeq is a Klein–Gordon equation, which means that it is a relativistic invariant equation with applications as a classical model in quantum field theory [29].

The solitons of the sGeq are called kinks and antikinks because they connect two different constant values at infinity, i.e., two vacua in a field theory; in the antikinks the constant values are interchanged with respect to the kinks. These solitons are called topological because they have a discrete charge. The integrability of the sGeq allows the writing of multisoliton solutions, exact solutions with multiple solitons in interaction; the simplest one is the solution with a kink and an antikink, in which they approach from infinity, collide elastically and separate towards infinity. Another exact solution is the breather, a solution localized in space and oscillating in time that corresponds to a bound state of a kink and an antikink characterised by a frequency; the breathers can be static or they can move at a constant speed (this solution is obtained by applying a Lorentz transformation to the static one).

The initial-value problem of the Klein–Gordon equation with periodic boundary conditions is given by

$$\frac{\partial^2 u}{\partial t^2} - \frac{\partial^2 u}{\partial x^2} + \frac{dF(u)}{du} = 0, \qquad x \in (-L/2, L/2] \quad t \in [0, \infty), \tag{2.1}$$

$$u(x,0) = u_0(x), \qquad \frac{\partial u}{\partial t}(x,0) = u_1(x), \tag{2.2}$$

$$u(x,t) = u(x+L,t), \qquad \frac{\partial u}{\partial x}(x,t) = \frac{\partial u}{\partial x}(x+L,t), \tag{2.3}$$

where $F(u)$ is a nonlinear potential, L is the spatial period, x is spatial coordinate, and t is time. This equation is Lorentz-invariant for the speed of light $c = 1$, hence its solitary wave solution with speed v can be calculated by applying a Lorentz boosting to a stationary solution $u(x)$, i.e. $u(x,t) = u((x - vt)/\sqrt{1 - v^2})$. The most

studied potentials for Eq. (2.1) corresponds to the ϕ^4-model [86],

$$F(u) = \frac{1}{4}(1-u^2)^2, \qquad \frac{dF(u)}{du} = -u+u^3,$$

the sine–Gordon equation [26],

$$F(u) = 1-\cos(u), \qquad \frac{dF(u)}{du}u = \sin(u),$$

and the double sine–Gordon equation [13],

$$F(u) = 1-\cos(u)-\frac{\lambda}{2},\cos(2u), \qquad \frac{dF(u)}{du} = \sin(u)+\lambda\,\sin(2u).$$

These three equations have kinks with known analytical expression.

Equation (2.1) has at least two invariants, the momentum

$$P(t) = -\int_{-\infty}^{\infty}\left(\frac{\partial u}{\partial t}\right)\left(\frac{\partial u}{\partial x}\right)dx = P(0), \tag{2.4}$$

and the energy

$$E(t) = \int_{-\infty}^{\infty}\left(\frac{1}{2}\left(\frac{\partial u}{\partial t}\right)^2+\frac{1}{2}\left(\frac{\partial u}{\partial x}\right)^2+F(u)\right)dx = E(0), \tag{2.5}$$

respectively. The sGeq is integrable in the sense of Liouville, hence it has an infinite set of invariants (and conservation laws), but only the momentum and energy will be used in this thesis.

The solitary wave solution of the sGeq is given by

$$u(x,t) = 4\arctan\left(\exp\left(\pm\frac{x-x_0-vt}{\sqrt{1-v^2}}\right)\right), \tag{2.6}$$

where $|v|<1$ is the speed, the positive sign corresponds to the kink and the negative one to the antikink [28]. The sGeq has multisoliton solutions, like the symmetrical kink-antikink solution

$$u_{ka}(x,t) = 4\arctan\left(\frac{1}{v}\frac{\sinh(vt/\sqrt{1-v^2}}{\cosh(x/\sqrt{1-v^2})}\right), \tag{2.7}$$

where v is the speed of the antikink and $-v$ of the kink, both at $t\to-\infty$, with the collision occurring at $t=0$. Another multisoliton solution is the stationary breather

solution

$$u(x,t) = 4 \arctan\left(\frac{\sqrt{1-\omega^2}}{\omega}\frac{\cos(\omega t)}{\cosh(x\sqrt{1-\omega^2})}\right), \tag{2.8}$$

where $\omega < 1$ is the frequency of the oscillation in time; this solution is periodic in time and spatially localized around $x = 0$, with an envelope whose amplitude decays exponentially as $|x| \to \infty$.

2.2 Ratnikov's graphene superlattice

Graphene is a flat hexagonal distribution of carbon atoms linked together by covalent bonds. The unit cell of the graphene honeycomb lattice consists of two identical carbon atoms. In the theory of solids, electrical conductivity is studied by using band theory. The maximum energy level occupied by electrons at absolute zero temperature is called Fermi level. Bands below the Fermi level are filled by electrons, the highest one being the valence band, and bands above it are empty, the lowest one being the conduction band. In metals and conductor materials, the valence and conduction bands overlap. However, in semiconductor and insulating materials, there is a forbidden band gap between the valence and conduction bands. In insulators, the band gap is so large that electrons cannot make the energy jump from the valence band to the conduction band; but in semiconductors, the small energy gap allows that an electron jumps into the conduction band so it can be move freely, generating a hole in the valence band that can also move freely. Graphene is a semimetal without a band gap because the valence and the conduction bands touch each other at a number of points, termed Dirac points (there are two in the momentum space associated with the two atoms of the unit cell). The bands at Dirac points are linear, called Dirac cones. This gives graphene extraordinary electronic properties, since the electrons that circulate through it behave as if they had no mass and move like a massless Dirac fermion [87].

In some applications it would be useful to provide graphene with a band gap; it can be engineered into graphene by placing it on top of a suitable substrate [2]. Actually, a spatial modulation of the band gap can be attained by placing a graphene sheet on a substrate fabricated from different layers, a graphene superlattice (GSL). There is a large number of proposed GSLs in the current literature, but this thesis only considers the GSL introduced by Pavel V. Ratnikov in 2009 [4]. The Ratnikov's GSL is made up of a single-layer graphene sheet on a superlattice made up of alternating strips of a material that does not alter the band structure of graphene, usually a dielectric such as silica, SiO_2, and another material that introduces a band

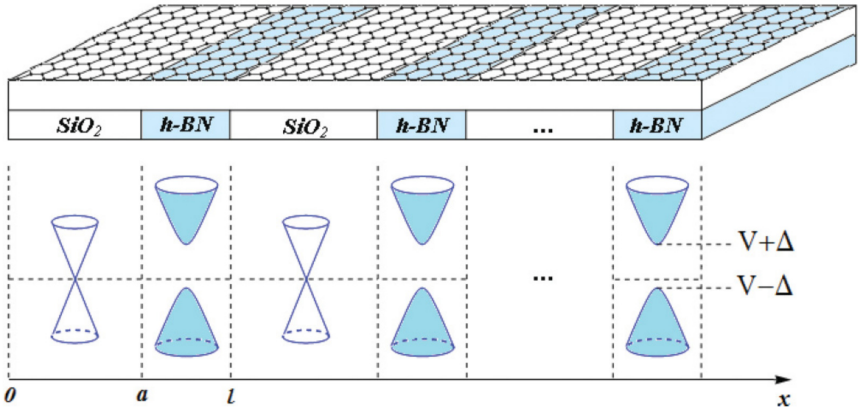

Figure 2.1: Graphene layer on the strip substrate composed of silicon dioxide and hexagonal boron nitride (top), and a schematic diagram showing the electronic energy spectrum in the GSL (bottom). Reproduced with permission of the American Physical Society [5].

gap, such as hexagonal boron nitride, h-BN, or silicon carbide, SiC. Figure 2.1 illustrates the Ratnikov's GSL with the axes used in this thesis. The periodic modulation of the band gap introduced in graphene affects the propagation of the carriers (electrons and holes) [4]. Moreover, the Fermi speed at which these carriers propagate is also modulated [30].

One of the most promising applications of the GSL is in optoelectronics, the propagation of electromagnetic waves in the transparent dielectric that can act as a waveguide and that of surface-plasmon polaritons in the interface between the dielectric and graphene [31]. Specifically, the GSL has been proposed for the detection, generation, and amplification of THz electromagnetic waves; for such an application graphene has been the subject of theoretical and experimental studies [88, 89]. In the context of this thesis, the most relevant potential applications are based on the nonlinear phenomena associated with the interaction between electromagnetic waves and massless Dirac fermion quasi-particles [90–94].

2.3 Graphene superlattice equation

Let us summarise the derivation of the graphene superlattice equation [3]. Figure 2.1 illustrates the gap modulation in graphene induced by the superlattice, where $\Delta(x)$ is the half-width of the band gap, $V(x)$ is the shift of the forbidden band centre in the gapped graphene with respect to the Dirac point in the gapless graphene,

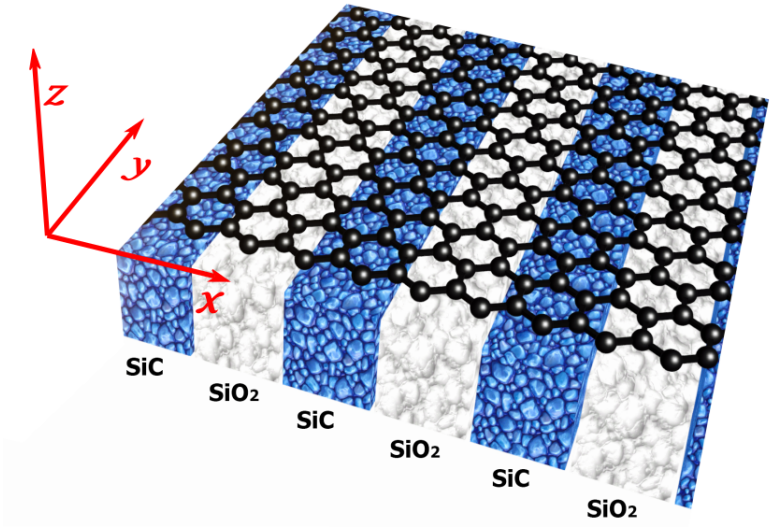

Figure 2.2: Graphene superlattice indicating the axes used in the main text.

and $\upsilon_F(x)$ is the Fermi speed of the massless Dirac fermions. These l-periodic functions can be approximated by piecewise constant expressions: $\Delta(x) = V(x) = 0$, and $\upsilon_F(x) = \upsilon_{F,0a}$ for $0 < x < a$, and $\Delta(x) = \Delta_0$, $V(x) = V_0$, and $\upsilon_F(x) = \upsilon_{F,al}$ for $a < x_0 < x < l$. The application of the matrix transfer method results in the energy dispersion relation for the graphene superlattice given by

$$\cos(kl) = 1 + \frac{a\bar{a}}{\hbar^2\,\upsilon_{F,0a}\,\upsilon_{F,al}}\left(E\,V_0 - E^2 - \upsilon_{F,0a}\,\upsilon_{F,al}\,(\hbar k_y)^2\right), \tag{2.9}$$

where $E(\mathbf{k})$ is the energy, $\mathbf{k} = (k, k_y, 0)$ is the wavenumber, $\hbar$ is the reduced Planck's constant, and $\bar{a} = l - a$; it should be notice that the following assumptions have been taken: $aE \ll \hbar\,\upsilon_{F,0a}$, and $\bar{a}E \ll \hbar\,\upsilon_{F,al}$. The solution of this quadratic equation for the energy results in

$$E(\mathbf{k}) = E_w \pm \sqrt{\Gamma^2 - \upsilon_{F,0a}\,\upsilon_{F,al}\,\hbar^2 k_y^2 + \Upsilon^2\,(1 - \cos(kl))}\,. \tag{2.10}$$

where

$$E_w = \frac{V_0}{2}\,, \qquad \Gamma^2 = \frac{V_0^2}{4}\,, \qquad \Upsilon^2 = \frac{\upsilon_{F,0a}\,\upsilon_{F,al}\,\hbar^2}{a\bar{a}}\,.$$

A graphene superlattice subjected to transversal electromagnetic radiation can propagate nonlinear electromagnetic waves in the dielectric when the radiation frequency is much greater than the plasma frequency, as shown by S.V. Kryuchkov

and E.I. Kukhar [6,32,34]. Let us consider that the incident EM wave has an electric field intensity $\mathbf{E} = (E_x, 0, 0)$ and a vector potential $\mathbf{A} = (0, A_y, 0)$, where E_x and A_y are sinusoidal functions of time, and the axes are illustrated in Fig. 2.2. The electron current density arising in the graphene is given by

$$j_x(\mathbf{p},t) = -e \sum_{\mathbf{p}} f(\mathbf{p},t)\, v_x(\mathbf{p}), \tag{2.11}$$

where e is the electron charge, the electron velocity $v_x(\mathbf{p}) = (1/\hbar)\,\partial E(\mathbf{k})/\partial k$ is calculated from Eq. (2.10), and $f(\mathbf{p},t)$ is the non-equilibrium distribution function that solves the kinetic Boltzmann equation with a term taking into account the EM field action. The collisionless regime is enough under the assumption that the characteristic scale of variation of the electromagnetic field is large in comparison with the de Broglie wavelength of the electron and with the period of the superlattice, and that the characteristic time of the variation of the EM field is much less than the free transit time of the electrons. In such a case, $f(\mathbf{p},t) = f_0(\mathbf{p})$, the equilibrium distribution function. Hence Eq. (2.11) reduces to

$$j_x = -e \sum_{\mathbf{p}} f_0 \left(\mathbf{p} - \frac{e}{c}\mathbf{A}\right) v_x(\mathbf{p}), \tag{2.12}$$

where the change of variables $\mathbf{p}' = \mathbf{p} - (e/c)\,\mathbf{A}$, results in

$$j_x = -e \sum_{\mathbf{p}'} f_0(\mathbf{p}')\, v_x \left(\mathbf{p}' + \frac{e}{c}\mathbf{A}\right). \tag{2.13}$$

Under the hypothesis that the electron gas is non-degenerate, the summation over the momentum in Eq. (2.13) yields

$$j_x = -\frac{e\,n_0}{w_0}\,\frac{\Upsilon^2\, l}{\hbar}\,\frac{\sin\alpha}{2\sqrt{\Gamma^2 + \Upsilon^2\,(1-\cos\alpha)}}, \tag{2.14}$$

where n_0 is the surface concentration of the charge carriers, w_0 is the width of the graphene sheet, and $\alpha = e\,l\,A_y/(\hbar c)$ is the dimensionless potential of the EM field. The typical values of the GSL parameters are $w_0 \approx 0.12$ nm, $n_0 = 10^{10}$ cm^{-2}, $\Gamma = 0.13$ eV $\approx \Upsilon$, and $\upsilon_F = 10^8$ cm/s, under *low* temperatures within the range $10\ \mathrm{K} \ll \theta \ll 10^3$ K [84].

The non-homogeneous wave equation for the vector potential $\mathbf{A}$ is written as

$$\frac{\partial^2 \mathbf{A}}{\partial t^2} - c^2\,\nabla^2\,\mathbf{A} = \frac{4\pi}{c}\,\mathbf{j}, \tag{2.15}$$

where c is the speed of light; after the substitution of Eq. (2.14) it yields a nonlinear Klein–Gordon equation for the normalized potential α given by

$$\frac{\partial^2\alpha}{\partial t^2} - c^2\frac{\partial^2\alpha}{\partial y^2} + \frac{\omega_{pl}^2 b^2 \sin\alpha}{\sqrt{1+b^2(1-\cos\alpha)}} = 0\,, \tag{2.16}$$

where $b = \Upsilon/\Gamma$ is a geometrical parameter of the order of unity, and ω_{pl} is the plasma frequency given by

$$\omega_{pl}^2 = \frac{2\pi n_0 e^2 l^2 \Gamma}{w_0 \hbar^2}\,.$$

In order to study the solutions of the Eq. (2.16) by using asymptotic and numerical methods, it is convenient to use a nondimensionalization. By making the change of variables $t' = \omega_{pl} b t$, $x' = \omega_{pl} b y/c$, and $u = \alpha$, to obtain the Klein–Gordon equation given by

$$\frac{\partial^2 u}{\partial t^2} - \frac{\partial^2 u}{\partial x^2} + \frac{dF(u)}{du} = 0, \tag{2.17}$$

where the primes have been dropped and

$$\frac{dF(u)}{du} = \frac{\sin u}{\sqrt{1+b^2(1-\cos u)}}, \qquad F(u) = \frac{2(1-\cos u)}{1+\sqrt{1+b^2(1-\cos u)}}, \tag{2.18}$$

where the constant of integration has been selected in order that it reduces to the potential of the sGeq, i.e. $F(u) = 1-\cos u$, for $b = 0$. Hereafter, Eq. (2.17) is referred to as graphene superlattice equation.

2.4 Solitary waves

Let us determine the soliton solutions of the GSLeq. A solitary wave solution of Eq. (2.17) with speed v is found by applying a Lorentz boost to the stationary solution $u(x)$, i.e. $u(x,t) = u((x-vt)/\sqrt{1-v^2})$, that solves

$$\frac{d^2u}{dx^2} = \frac{dF(u)}{du}, \qquad \frac{1}{2}\left(\frac{du}{dx}\right)^2 = F(u). \tag{2.19}$$

The periodic potential $F(u)$ has infinite zeroes at $u_n^* = 2n\pi$, for $n \in \mathbb{Z}$; hence the static solitary waves connect two consecutive zeroes, being a n-kink solution when connecting the asymptotic value u_n^*, and u_{n+1}^*, and a n-antikink when connecting

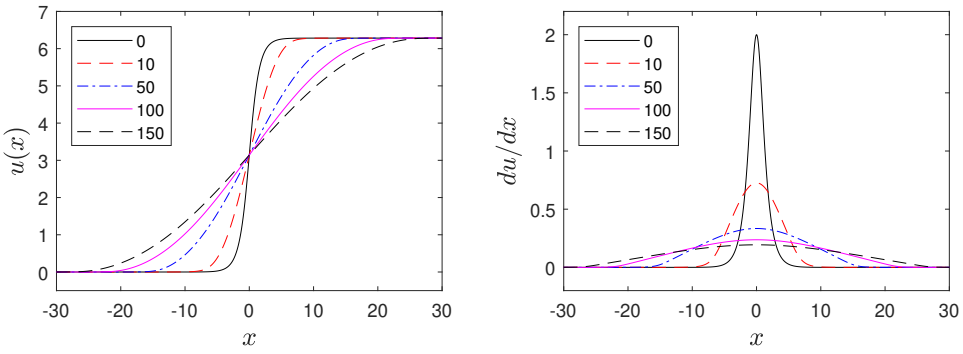

Figure 2.3: Kink solution (left plot) and its spatial derivative (right plot) numerically calculated by using the fast Fourier transform for $b = 0, 10, 50, 100$, and 150.

u^*_{n+1}, and u^*_n. In implicit form, the static 0-kink, $u_{k,0}(x)$, is given by

$$\int_{\pi}^{u_{k,0}} \frac{d\tilde{u}}{\sqrt{2F(\tilde{u})}} = \int_{x_0}^{x} d\tilde{x}, \qquad 0 < u_{k,0} < 2\pi, \tag{2.20}$$

where x_0 is the centre of the 0-kink, i.e., the position of the maximum of its spatial derivative. Hence, the n-kink can be written as $u_{k,n}(x) = 2\pi n + u_{k,0}(x)$, and the n-antikink as $u_{ak,n}(x) = 2\pi(n+1) - u_{k,0}(x)$. For the GSLeq, Eq. (2.20) for $u_{k,0}(x)$ reads as

$$\int_{\pi}^{u_{k,0}} \frac{\sqrt{1+\sqrt{1+b^2(1-\cos\tilde{u})}}}{2\sqrt{1-\cos\tilde{u}}}\, d\tilde{u} = x - x_0, \tag{2.21}$$

whose integration results in a complicated implicit expression written in terms of elliptic integrals. However, it is not possible to find an explicit analytic expression. Furthermore, as the implicit expression is cumbersome, so, in practise its numerical evaluation is preferred.

The application of a quadrature method to Eq. (2.21) has to take into account that the left-hand integrand is singular at $u_{k,0} = 2\pi$, and $u_{k,0} = 0$. In order to avoid such singularities, let us insert into Eq. (2.19) the *ansatz* $u_{k,0}(x) = 4\arctan(\exp(w_{k,0}(x)))$, resulting in

$$\frac{1}{\sqrt{2}} \int_0^{w_{k,0}} \sqrt{1+\sqrt{1+2b^2\,\mathrm{sech}^2(\tilde{w})}}\, d\tilde{w} = x - x_0, \tag{2.22}$$

where the identity

$$\cos(4\arctan(z)) = \frac{z^4 - 6z^2 + 1}{(z^2+1)^2},$$

has been used.

Figure 2.3 shows the kink solution (left plot) and its spatial derivative (right plot) for $b = 0$, 10, 50, 100, and 150. They have been numerically calculated by applying a Gauss–Konrod quadrature formula for the left-hand side of Eq. (2.22), and by using an inverse interpolation technique based on cubic splines for solving the nonlinear equation. The plots in Fig. 2.3 (right plot) show that the solution widens as the parameter b grows, starting with the sharpest one for $b = 0$, i.e., the kink of the sGeq.

3
Numerical schemes

Let us summarise the results for the fifteen finite difference schemes based on Padé approximations for the sGeq studied in my papers [8] and [9]. My objective is to select the best method for long-time integrations of kink-antikink collisions and quasi-breather of the GSLeq. Section 3.1 reviews the literature on numerical methods for the sGeq, with emphasis in finite difference and Padé methods. In Section 3.2 the formulation, analysis, and implementation of the fifteen Padé methods are described. Section 3.3 presents the results obtained after extensive numerical simulations of the fifteen methods. Finally, in Section 3.4 the selection of the best method for the GSLeq is justified.

3.1 Numerical schemes for the sine–Gordon equation

Let us summarise current literature on numerical methods for the sGeq. The first two numerical schemes for the sGeq were a method of characteristics and a leapfrog finite difference scheme developed by Perring and Skyrme (PS) [37]. Ablowitz, Kruskal, and Ladik (AKL) introduced a staggered-leapfrog scheme to stabilize the PS scheme [38]. Strauss and Vázquez (SV) introduced an energy-conserving, implicit, leapfrog finite difference scheme for the KGeq [7], used for the sine–Gordon equation in [39]. Guo, Pascual, Rodríguez y Vázquez (GPRV) [10] developed a variant of the SV method for the KGeq, which conserves another discrete analogue of the energy and which in their simulations is more robust in long-time integration simulations. Jiménez y Vázquez [40] compared four leapfrog numerical schemes, the PS, AKL, SV, and a new fully-explicit method shows that, for long-time integration, the best one is the SV scheme [40]. Several generalizations

of the SV method, also energy-conserving and second-order in both space and time, have been published in Refs. [41–44]; a general procedure for the development of energy-conserving methods based on the nonlinear treatment of the SV scheme [45] and starting from a discrete energy [46] have been introduced. However, the comparison among these methods shows that implicitness is the key property for long-time stability, instead of energy conservation [47].

Finite difference schemes with (q,s)-Padé approximants (a difference operator that is a quotient of polynomials of degree q for the numerator and s for the denominator), of order $(q+s)$ in space are Padé schemes also known as compact operator methods. Bratsos and Twizell in [48] used $(2,0)$-, $(1,1)$-, and $(2,1)$-Padé methods for the sGeq; Duncan [49] proposed a $(2,2)$-Padé scheme for the KGeq applied to the sGeq by Bratsos [50]; and Sari and Güarslan [51] used a $(4,2)$-Padé approximant. A comparison of some of the Padé methods with PS, AKL, and SV schemes shows that for high accuracy the high-order methods are more efficient [48,49]. Moreover, fourth-order Padé methods were also used for the 2D sGeq in Refs. [52–54].

Apart from finite difference methods, an extensive set of numerical schemes have been used for the sGeq. Pseudospectral methods like the split-step Fourier scheme [55–57], and spectral methods like an energy-conserving, Fourier scheme [58], a wavelet spectral method [59,60], a Legendre spectral element method [62], and a multiresolution analysis method based on Legendre wavelets [61]. Finite element methods based on a Petrov–Galerkin scheme [63], and a collocation scheme using Legendre–Gauss–Lobatto points [64] or cubic B-splines [65]. Multisymplectic methods [69,70], including a systematic method for discretizing Hamiltonian partial differential equations exactly preserving their energy [58, 71]. Even, meshless methods based on multiquadric quasi-interpolation [72, 73] and on radial basis functions [74, 75], exponentially-fitted and piecewise analytical methods [76], and numerical implementations of the inverse scattering transform [77, 78] have been developed for the sGeq. Finally, note that many of these methods have been extended to two and three dimensions [79].

In this thesis we have focused our attention on Padé methods for the sGeq with the treatments for the nonlinearity of SV and GPRV, since, up to this author's knowledge, all the Padé methods used for the sGeq use the nonlinearity treatment of the PS finite difference scheme. An exhaustive comparison of numerical methods for the sGeq, including pseudo-spectral, spectral, finite elements, multisymplectic, meshless and other ones, is outside the scope of this thesis, since our main goal is the study of the solutions of the GSLeq.

3.2 Padé schemes based on Strauss–Vázquez method

Let us consider ten numerical schemes for the solution of Eqs. (2.1)–(2.3) by using Padé approximants in space with the same central, second-order differences in time. They belong to two families of Padé methods, one based on the SV [7] method, given by

$$\mathscr{A}_i(\mathrm{E})\,\frac{U_m^{n+1}-2U_m^n+U_m^{n-1}}{\Delta t^2}-\mathscr{B}_i(\mathrm{E})\,U_m^n+\mathscr{A}_i(\mathrm{E})\,H(U_m^{n+1})=0, \tag{3.1}$$

with $i=1,2,\ldots,5$, and another one based on the GPRV method [10],

$$\mathscr{A}_i(\mathrm{E})\,\frac{U_m^{n+1}-2U_m^n+U_m^{n-1}}{\Delta t^2}-\mathscr{B}_i(\mathrm{E})\,\frac{(U_m^{n+1}+U_m^{n-1})}{2}+\mathscr{A}_i(\mathrm{E})\,H(U_m^{n+1})=0, \tag{3.2}$$

with $i=6,7,\ldots,10$, both using the same expression for the nonlinear term

$$H(U_m^{n+1})\equiv\frac{F(U_m^{n+1})-F(U_m^{n-1})}{U_m^{n+1}-U_m^{n-1}}, \tag{3.3}$$

where $U_m^n\approx u(x_m,t^n)=u_m^n$, E is the shift operator ($\mathrm{E}\,U_m^n=U_{m+1}^n$), $\mathscr{A}_i^{-1}(\mathrm{E})\,\mathscr{B}_i(\mathrm{E})\,u_m^n$ is a (q,s)-Padé approximant of $(q+s)$-order of accuracy for the second-order spatial derivative of $u(x_m,t^n)$, the grid size is $\Delta x=L/M$, $x_m=-L/2+m\Delta x$, with $m=1,2,\ldots,M$ (note that $u(x_0,t)\equiv u(x_M,t)$), the time-step $\Delta t=T/N$, and $t^n=n\Delta t$, with $n=0,1,\ldots,N$.

We have studied five methods from both families whose difference operators $\mathscr{A}_i$ and $\mathscr{B}_i$ are shown in Table 3.1; the five numerical methods (3.1) are called

i	Padé	$\mathscr{A}_i$	$\mathscr{B}_i$
1, 6	(2,0)-	$\mathscr{I}$	$\frac{E^{-1}-2+E^1}{\Delta x^2}$
2, 7	(4,0)-	$\mathscr{I}$	$\frac{-E^{-2}+16E^{-1}-30+16E^1-E^2}{12\Delta x^2}$
3, 8	(2,2)-	$\frac{E^{-1}+10+E^1}{12}$	$\frac{E^{-1}-2+E^1}{\Delta x^2}$
4, 9	(4,2)-	$\frac{2E^{-1}+11+2E^1}{3}$	$\frac{E^{-2}+16E^{-1}-34+16E^1+E^2}{4\Delta x^2}$
5,10	(4,4)-	$\frac{23E^{-2}+688E^{-1}+2358+688E^1+23E^2}{15}$	$\frac{31E^{-2}+128E^{-1}-318+128E^1+31E^2}{\Delta x^2}$

Table 3.1: Difference operators $\mathscr{A}_i$, $\mathscr{B}_i$ in the Padé methods (3.1) and (3.2). Symbol $\mathscr{I}$ is the identity operator.

Methods 1–5 and the other five ones (3.2) are Methods 6–10. Method 1 is the SV scheme [7], interpreted as a (2,0)-Padé numerical method of second-order in space. Method 2 is interpreted as a (4,0)-Padé method of fourth-order in space. Method 3 is a (2,2)-Padé method of fourth-order in space similar to those used in Refs. [49] and [50]. Methods 4 and 5 are sixth-order (4,2)- and eighth-order (4,4)-Padé schemes, respectively. Method 6 is the GPRV method [10] interpreted as a (2,0)-Padé method. Method 7 is a finite difference method interpreted as (4,0)-Padé method. And Methods 8, 9, and 10 are fourth-order (2,2)-, sixth-order (4,2)- and eighth-order (4,4)-Padé methods, respectively.

The local truncation error of all schemes can be calculated by using Taylor series expansion; the substitution of U_m^n by the exact solution $u(x_m,t^n)$ in Eqs. (3.1) and (3.2) results in

$$\mathscr{M}_i(u) \equiv \mathscr{G}(u) + \mathscr{L}_i(u) = 0, \tag{3.4}$$

where $\mathscr{G}(u)$ is the sGeq (2.1). The local truncation error $\mathscr{L}_i(u)$ can be written as

$$\mathscr{L}_i(u) = \mathscr{T}_i(u)\,\Delta t^2 + \mathscr{S}_i(u)\,\Delta x^{p_i} + \text{h.o.t.}, \tag{3.5}$$

where the exponent p_i is the spatial order of accuracy, and h.o.t. represents higher-order terms depending on u, and its spatial and temporal partial derivatives. The main temporal term in $\mathscr{L}_i(u)$ can be calculated as

$$\mathscr{T}_i(u) = -\frac{1}{6}\sin(u)\left(\frac{\partial u}{\partial t}\right)^2 + \frac{1}{2}\cos(u)\frac{\partial^2 u}{\partial t^2} + \frac{1}{12}\frac{\partial^4 u}{\partial t^4},$$

for $i = 1,2,\ldots,5$, and

$$\begin{aligned}\mathscr{T}_i(u) = &-\frac{1}{6}\sin(u)\left(\frac{\partial u}{\partial t}\right)^2 + \frac{1}{2}\cos(u)\frac{\partial^2 u}{\partial t^2} + \frac{1}{12}\frac{\partial^4 u}{\partial t^4} \\ &-\frac{1}{2}\sin(u)\left(\frac{\partial u}{\partial x}\right)^2 + \frac{1}{2}\cos(u)\frac{\partial^2 u}{\partial x^2} - \frac{1}{2}\frac{\partial^4 u}{\partial x^4},\end{aligned}$$

for $i = 6,7,\ldots,10$. The main spatial term in $\mathscr{L}_i(u)$ can be easily obtained resulting in

$$\mathscr{S}_1(u)\,\Delta x^{p_1} = \mathscr{S}_6(u)\,\Delta x^{p_6} = -\frac{\Delta x^2}{12}\frac{\partial^4 u}{\partial x^4}, \tag{3.6}$$

$$\mathscr{S}_2(u)\,\Delta x^{p_2} = \mathscr{S}_7(u)\,\Delta x^{p_7} = \frac{\Delta x^4}{90}\,\frac{\partial^6 u}{\partial x^6}, \tag{3.7}$$

$$\mathscr{S}_3(u), \Delta x^{p_3} = \mathscr{S}_8(u)\,\Delta x^{p_8} = \frac{\Delta x^4}{240}\,\frac{\partial^6 u}{\partial x^6}, \tag{3.8}$$

$$\mathscr{S}_4(u), \Delta x^{p_4} = \mathscr{S}_9(u)\,\Delta x^{p_9} = -\frac{23\,\Delta x^6}{75600}\,\frac{\partial^8 u}{\partial x^8}, \tag{3.9}$$

and

$$\mathscr{S}_5(u), \Delta x^{p_5} = \mathscr{S}_{10}(u)\,\Delta x^{p_{10}} = \frac{79\,\Delta x^8}{4762800}\,\frac{\partial^{10} u}{\partial x^{10}}. \tag{3.10}$$

Note that the $\mathbb{C}^\infty$ regularity of the solutions of the initial-boundary value problem for the sGeq when the initial condition is $\mathbb{C}^\infty$ ensures that all the truncation error terms for the ten schemes are properly defined.

i	A_i	B_i
1	1	$1-2\,r^2\sin^2\omega$
2	1	$1-\frac{8}{3}\,r^2\,\sin^2(\omega)+\frac{r^2}{6}\,\sin^2(2\,\omega)$
3	$1-\frac{1}{3}\,\sin^2(\omega)$	$A_3-2\,r^2\,\sin^2(\omega)$
4	$5-\frac{8}{3}\,\sin^2(\omega)$	$A_4-8\,r^2\,\sin^2(\omega)-\frac{1}{2}\,r^2\,\sin^2(2\,\omega)$
5	$252-\frac{2752}{15}\,\sin^2(\omega)-\frac{92}{15}\,\sin^2(2\,\omega)$	$A_5-504\,r^2\,\sin^2(\omega)+248\,r^2\,\sin^4(\omega)$
6	$1+2\,r^2\sin^2\omega$	1
7	$1+\frac{8}{3}\,r^2\,\sin^2(\omega)-\frac{1}{6}\,r^2\,\sin^2(2\,\omega)$	1
8	$B_8+2\,r^2\,\sin^2(\omega)$	$1-\frac{1}{3}\,\sin^2(\omega)$
9	$B_9+8\,r^2\,\sin^2(\omega)+\frac{1}{2}\,r^2\,\sin^2(2\,\omega)$	$5-\frac{8}{3}\,\sin^2(\omega)$
10	$B_{10}+256\,r^2\,\sin^2(\omega)+62\,r^2\,\sin^2(2\,\omega)$	$252-\frac{2752}{15}\,\sin^2(\omega)-\frac{92}{15}\,\sin^2(2\,\omega)$

Table 3.2: Coefficients A_i and B_i of the stability polynomial for the ten methods studied.

The linear stability of the ten schemes can be easily studied using the von Neumann analysis. The computational error $Z_m^n = U_m^n - U_m^{n*}$ of the solution with floating-point errors U_m^n with respect to a solution without them U_m^{n*} can be Fourier

expanded as $Z_m^n = e^{\mathrm{i}m\beta\Delta x}\xi^n$, where $\mathrm{i} = \sqrt{-1}$, β is the spatial frequency, and ξ is the amplification factor. After cancelling common factors in the corresponding equations for Z_m^n after the linearization of methods (3.1) and (3.2) the following polynomial equation for ξ is obtained

$$p_i(\xi) = A_i\,\xi^2 - 2\,B_i\,\xi + A_i = 0, \tag{3.11}$$

whose two roots ξ_1 and ξ_2 have modulus smaller than or equal to unity for every ξ if and only if $|B_i| \leq A_i$, i.e., $-A_i \leq B_i \leq A_i$. These two inequalities yield the necessary condition for linear stability on both Δx and Δt. For simplicity, let us use $r = \Delta t/\Delta x$, and $\omega = \beta\,\Delta x/2$. Table 3.2 contains A_i and B_i for the stability polynomials of all schemes studied. The stability condition is $r^2 \leq 1$, 3/4, 2/3, 7/12, and 257/480 for Methods 1, 2, ..., 5, respectively. Methods 6–10 are linearly, unconditionally stable since for all $B_i \geq 0$, and $A_i - B_i \geq 0$.

For a fair comparison of Methods 1–5 among them the discrete analogue of the energy exactly conserved by Method 1 (SV) is used, although none of Methods 2–5 exactly conserve it; it is given by

$$E_{\mathrm{SV}}^n = \Delta x \sum_m \left[\frac{1}{2} \left(\frac{U_m^{n+1} - U_m^n}{\Delta t} \right)^2 \left(\frac{U_{m+1}^{n+1} - U_m^{n+1}}{\Delta x} \right)^2 + \left(\frac{U_{m+1}^n - U_m^n}{\Delta x} \right)^2 \right] + \Delta x \sum_m \left[\frac{F(U_m^{n+1}) + F(U_m^n)}{2} \right]. \tag{3.12}$$

Similarly, for the comparison of Method 6–10 the discrete analogue of the energy exactly conserved by Method 6 (GPRV) is used

$$E_{\mathrm{GPRV}}^n = \Delta x \sum_m \left[\frac{1}{2} \left(\frac{U_m^{n+1} - U_m^n}{\Delta t} \right)^2 + \left(\frac{U_{m+1}^{n+1} - U_m^{n+1}}{2\,\Delta x} \right)^2 + \left(\frac{U_{m+1}^n - U_m^n}{2\,\Delta x} \right)^2 \right] + \Delta x \sum_m \left[\frac{F(U_m^{n+1}) + F(U_m^n)}{2} \right]. \tag{3.13}$$

Let us highlight that in order to numerically estimate the speed of kinks (antikinks) a discrete analogue of the analytical formula $v(t) = P(t)/E(t)$ can been used. For Methods 1–5, the discrete analogue of the momentum given by

$$P_{SV}^n = -\Delta x \sum_m \left[\left(\frac{U_m^{n+1} - U_m^{n-1}}{2\,\Delta t} \right) \left(\frac{U_{m+1}^n - U_{m-1}^n}{2\,\Delta x} \right) \right] \tag{3.14}$$

has been used [7], such that $v^n = P_{SV}^n/E_{SV}^n$. But for Methods 6–10, the alternative

discrete analogue

$$P^n_{GPRV} = -\Delta x \sum_m \left[\left(\frac{U^{n+1}_m - U^n_m}{\Delta t} \right) \left(\frac{U^n_{m+1} - U^n_{m-1}}{2\,\Delta x} \right) \right], \tag{3.15}$$

is preferred [10], so $v^n = P^n_{GPRV}/E^n_{GPRV}$ has been used.

A numerical method can be made more accurate by using Richardson's extrapolation (RE) [95]. This technique could be applied in both space and time [96,97]. In this thesis it is used to improve the accuracy in time of Methods 6–10 from second-order to fourth-order. To successfully apply RE, it is necessary to know the order of accuracy of the numerical scheme from its local truncation error. The best results have been obtained by applying only one level of extrapolation in time [98, 99]. Hence, only one level of Richardson's extrapolation is used, specifically

$$U^{n+1}_m = \frac{4\,U^{n+1,(\Delta t/2)}_m - U^{n+1,(\Delta t)}_m}{3}, \tag{3.16}$$

where $U^{n+1,(\Delta t/2)}_m$ and $U^{n+1,(\Delta t)}_m$ are the numerical approximations in time of second-order to $u(x_m, t^{n+1})$ calculated by using time-steps $\Delta t/2$ and Δt, respectively, and U^{n+1}_m is its fourth-order extrapolation in time.

Methods 1–10 are implicit, so a nonlinear equation should be solved in every time-step. Since the same iterative method is used for Eqs. (3.1) and (3.2), here only the one for Eq. (3.2) is presented; in such a case, Newton's iterative method can be written as

$$\begin{aligned} &\mathscr{A}_i(\mathrm{E}) \left(U^{(k+1)}_m - 2\,U^n_m + U^{n-1}_m \right) - \Delta t^2\, \mathscr{B}_i(\mathrm{E}) \frac{(U^{(k+1)}_m + U^{n-1}_m)}{2} \\ &\quad + \Delta t^2\, \mathscr{A}_i(\mathrm{E}) \left(H(U^{(k)}_m) + H_u(U^{(k)}_m)\,(U^{(k+1)}_m - U^{(k)}_m) \right) = 0, \end{aligned} \tag{3.17}$$

with

$$H_u(U^{(k)}_m) \equiv \frac{F_u(U^{(k)}_m)\,(U^{(k)}_m - U^{n-1}_m) - (F(U^{(k)}_m) - F(U^{n-1}_m))}{\left(U^{(k)}_m - U^{n-1}_m \right)^2}. \tag{3.18}$$

The stopping test for Newton's iteration convergence is based on the relative error by using the infinity norm,

$$\left\| U^{(k+1)}_m - U^{(k)}_m \right\|_\infty \leq \mathrm{Tol}_{\mathrm{rel}} \left\| U^{(k+1)}_m \right\|_\infty, \qquad \left\| U^{(k)}_m \right\|_\infty = \max_m \left| U^{(k)}_m \right|,$$

where $\mathrm{Tol}_{\mathrm{rel}} = 10^{-14}$ is a relative error tolerance.

In the numerical evaluation of Eqs. (3.3) and (3.18) there exists catastrophic cancellations when $|U_m^{n+1} - U_m^{n-1}| \ll 1$ and $|U_m^{(k)} - U_m^{n-1}| \ll 1$, respectively. For the sGeq, they can be avoided by rearranging the expression of $H(U)$ by means of the exact formula [43, 58, 71]

$$H(U) = \frac{\cos(U) - \cos(U_m^{n-1})}{U - U_m^{n-1}} = \frac{2\sin((U + U_m^{n-1})/2)\sin((U - U_m^{n-1})/2)}{U - U_m^{n-1}},$$

and that of $H_u(U)$ by means of

$$H_u(U) = \frac{\sin(U)}{U - U_m^{n-1}} - \frac{2\sin((U + U_m^{n-1})/2)\sin((U - U_m^{n-1})/2)}{\left(U - U_m^{n-1}\right)^2}.$$

It should be noticed that, although round-off errors are reduced after the application of these rearrangements, the discrete energy-conservation property of Methods 1 and 6 can be affected by its use.

3.3 Numerical results

The main results obtained for the behaviour in space of the schemes after an extensive set of simulations for both kink–antikink and breather solution for the sGeq are summarised. The methods are compared in terms of global error, energy conserving, computational cost, and behaviour in long-time integrations. Subsection 3.3.1 presents the kink-antikink and breather exact solutions of the sGeq used as initial conditions for the comparison of the numerical methods. In Subsection 3.3.2 the results obtained by the numerical methods without Richardson's extrapolation are summarised. Subsection 3.3.3 briefly reviews our results by using Richardson's extrapolation.

3.3.1 Kink–antikink and breather exact solutions

The comparison of the numerical schemes will be based on two exact solutions. First, the kink–antikink solution of the sGeq given by

$$u_{ka}(x,t) = 4\arctan\left(\frac{\sinh(v\,(t-10)/r_-)}{v\cosh(x/r_-)}\right), \tag{3.19}$$

where $r_- = \sqrt{1-v^2}$ and the collision occurs at $t = 10$; the left plot of Fig. 3.1 shows this solution with $v = 0.5$.

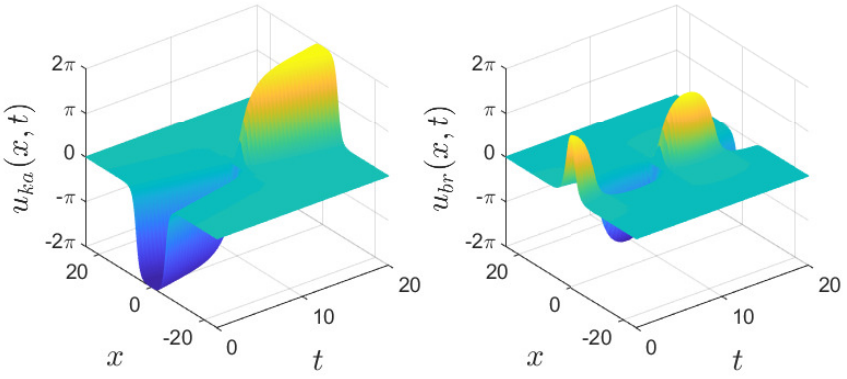

Figure 3.1: The kink–antikink with $v = 0.5$ (left plot) and the breather with $\omega = 0.5$ (right plot) for the sine–Gordon equation with $\Delta x = 0.01$, and $\Delta t = 0.001$.

Finally, the breather solution written as

$$u_{br}(x,t) = 4 \arctan\left(\frac{\sin(\omega\,(t-10)/r_+)}{\operatorname{sech}(x/r_+)/\omega}\right), \tag{3.20}$$

where $r_+ = \sqrt{1+\omega^2}$, and $\omega = 1/2$; the right plot of Fig. 3.1 shows this solution for $\omega = 0.5$.

Both exact solutions are used to evaluate the initial conditions (2.2) by $U_m^0 = u(x_m, 0)$, and $U_m^{-1} = u(x_m - \Delta t)$. Hence, there is no numerical error in the evaluation of these initial conditions.

3.3.2 Results without Richardson's extrapolation

Figure 3.2 (left plot) shows the numerical error for Methods 1–5 with $\Delta t = 0.001$ as a function of $\Delta x \in [0.001, 1]$. The spatial order of these methods can be validated by means of a linear fitting of the logarithm of the error versus the logarithm of the grid size when the error in time is smaller than the error in space (in this case, for $\Delta x > 0.2$); the resulting slopes are given by 2.8, 4.7, 5.0, 7.2, and 8.7, respectively, in agreement with their theoretical spatial order, cf. 2, 4, 4, 6, and 8, resp. Figure 3.2 (left plot) shows that for $\Delta x > 0.1$ the high-order methods are more accurate than the lower order ones; however, for $\Delta x \leq 0.03$ for Method 2, $\Delta x \leq 0.05$ for Method 3, and $\Delta x \leq 0.1$ for Methods 4 and 5, the error reaches a constant value $\approx 8.0 \times 10^{-7}$, due to the common error in time; such a plateau in the error that can be reduced by using values of $\Delta t < 0.001$. Figure 3.2 (right plot) shows the computational cost,

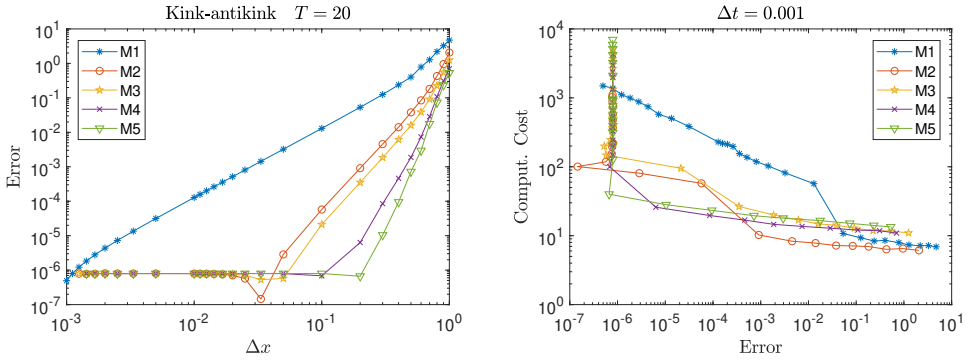

Figure 3.2: Numerical error (left plots) and computational cost (right plots) for the kink–antikink solution simulated with Methods 1–5 with $T = 20$ and $\Delta t = 1/1000$ as a function of $\Delta x \in \{1/1000, 1/900, ..., 1/10, 1/9, ..., 1\}$.

estimated by using the run-time in seconds, for Methods 1–5 with $\Delta t = 0.001$ as a function of the numerical error. Method 2 is the most efficient one for errors larger than 10^{-3}, with a cost similar in magnitude to that of the high-order methods. For errors smaller than 10^{-3}, Methods 4 and 5 are the most cost-efficient ones, being about tens of times more efficient than Method 1.

Figure 3.3 (left plot) shows the numerical error for Methods 1–5 for the breather solution with $\Delta t = 0.001$ and $\Delta x \in [0.001, 1]$. The estimation of the spatial order of the methods by means of linear fitting for $\Delta x \geq 0.3$, results in 2.0, 4.3, 4.8, 6.8, and 8.7, for Methods 1, 2, ..., 5, resp., values consistent with the theoretical order. Hence, for $\Delta x \geq 0.2$ the high-order methods are more accurate than the lower order ones; however, for $\Delta x \leq 0.03$ for Method 2, $\Delta x \leq 0.05$ for Method 3, $\Delta x \leq 0.1$ for Method 4, and $\Delta x \leq 0.2$ for Method 5, the error is dominated by error in time, reaching a constant value $\approx 7.0 \times 10^{-7}$; as expected, by using values of $\Delta t < 0.001$, the plateau error can be reduced. In the right plot of Fig. 3.3 the run-time (in seconds) for the five methods with $\Delta t = 0.001$ as a function of the numerical error is shown; Method 2 is the most efficient one for errors larger than 10^{-4}, but its cost is similar in magnitude to that of high-order methods; for errors smaller than 10^{-4}, Method 4 is the most efficient one, but Method 2 and Method 5 have similar cost.

Figure 3.4 (left plot) shows the numerical error for Methods 6–10 for the kink–antikink solution by using $\Delta t = 0.001$ and $\Delta x \in [1/800, 1]$; it should be noticed that $\Delta x < \Delta t$ in some cases, violating the CFL condition, thanks to the unconditional stability of these five methods. The error decreases as Δx does until the contribution of the time-step dominates that of the grid size; the error in time is about 2×10^{-6}. The numerical estimation of the spatial order of accuracy of Methods 6–10 are 2.06,

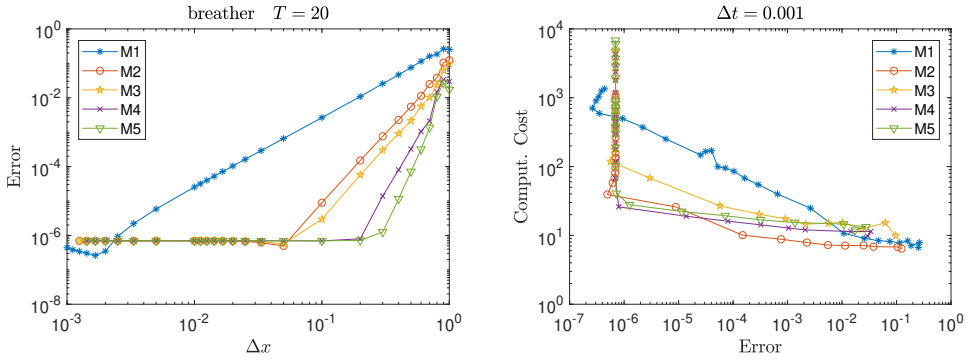

Figure 3.3: Numerical error (left plot) and computational cost (right plot) for the breather solution obtained with Methods 1–5 for $T = 20$ and $\Delta t = 1/1000$ as a function of $\Delta x \in \{1/1000, 1/900, ...1/10, 2/10, ...1\}$.

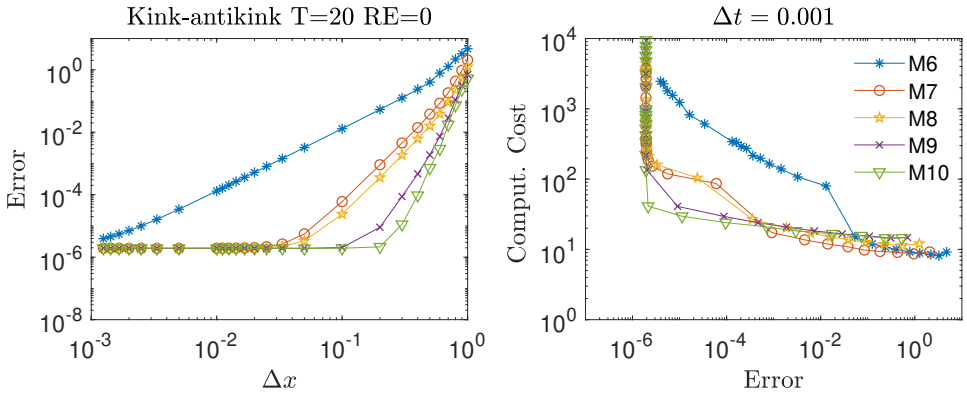

Figure 3.4: Numerical error (left plot) and computational cost (right plot) for the kink–antikink solution obtained for Methods 6–10 for $T = 20$ and $\Delta t = 0.001$ as a function of $\Delta x \in [1/800, 1]$.

3.98, 3.92, 5.83, and 8.14, resp., in good agreement with the theoretical calculation, cf., 2, 4, 4, 6, and 8, respectively. Figure 3.4 (right plot) shows the computational cost, estimated by using the run-time in seconds, for Methods 6–10 as a function of the numerical error attained. It is observed that Method 7 is the most efficient one for errors larger than 10^{-3}, but for error smaller than 10^{-3}, it is Method 10, whose cost is an order of magnitude smaller than that of the Method 7.

Figure 3.5 (left plot) shows the numerical error for Methods 6–10 as a function of $\Delta x \in [1/7000, 1]$ with $\Delta t = 0.001$ for the breather solution. The global error

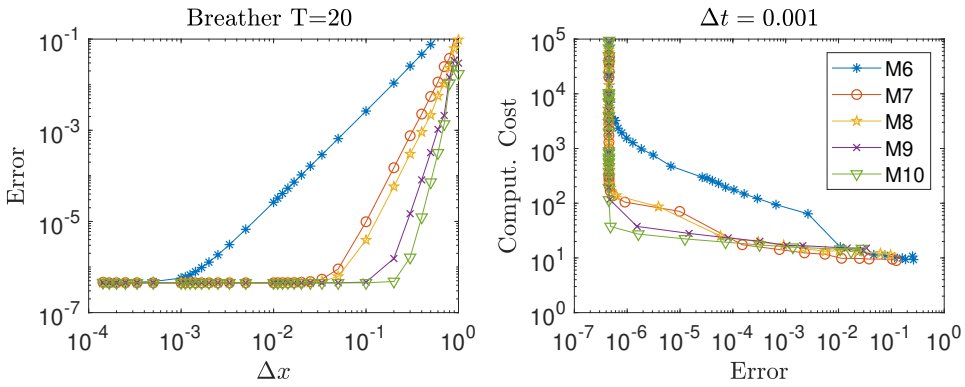

Figure 3.5: Numerical error (left plot) and computational cost (right plot) for the breather solution obtained for Methods 6–10 for $T = 20$ and $\Delta t = 0.001$ as a function of $\Delta x \in [1/7000, 1]$.

is dominated by error due to the discretization in time, reaching a constant value $\approx 4.5 \times 10^{-7}$ for $\Delta x \lesssim 0.001$ for Method 6, $\Delta x \lesssim 0.05$ for Methods 7 and 8, $\Delta x \lesssim 0.1$ for Method 9, and $\Delta x \lesssim 0.2$ for Method 10. Figure 3.5 (right plot) shows the run-time in seconds as a function of the numerical error; Method 7 is the most efficient one for errors larger than 10^{-4}, and the Method 10 otherwise.

3.3.3 Results with Richardson's extrapolation

Richardson's extrapolation in time was used with Methods 6–10, for both the kink–antikink and breather solutions. Figure 3.6 (left plot) shows the numerical error for Methods 6–10 with $\Delta t = 0.001$ and $\Delta x \in [1/800, 1]$. The error decreases as Δx does until the contribution of time-step dominates that of the grid size. Figure 3.6 (right plot) shows the computational cost for Methods 6–10 as a function of the numerical error; note that $\Delta x > \Delta t = 0.001$ is used in some cases. The trends of the error with RE are similar that those observed without RE (illustrated in Fig. 3.4). However, with RE the cost is higher, although the temporal error is smaller that without RE; specifically, the plateau band due to time integration is between 10^{-7} and 10^{-8} with RE instead of the 10^{-6} attainable without RE. This result suggest that Methods 6–10 are more efficient without RE than with RE.

The analysis of the results with RE for the breather solution (omitted here for brevity) [9] indicates that the behaviour is similar to that discussed for the kink-antikink solution. In all the cases the most efficient version of a method when the spatial error dominates the temporal error is that without RE, due to the increased cost of the RE.

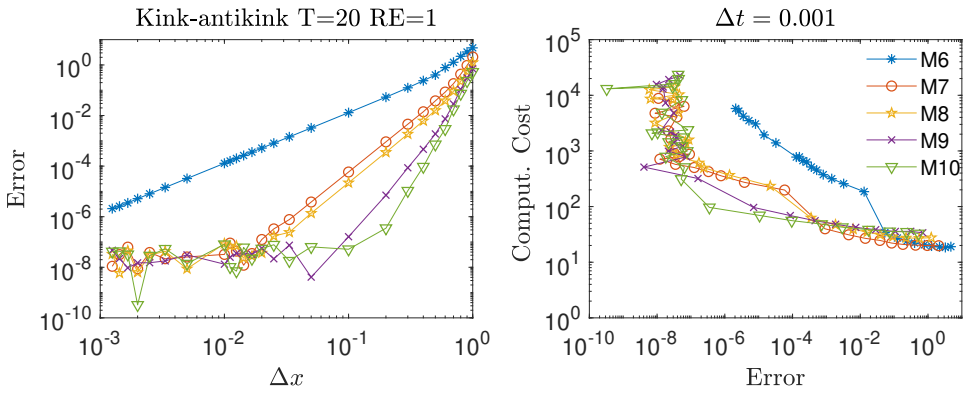

Figure 3.6: Numerical error (left plots) and computational cost (right plots) for the kink–antikink solution with $T = 20$ and $\Delta t = 1/1000$ as a function of $\Delta x \in 1/800, 1/700, ..., 1/10, 2/10, ..., 1$, for schemes developed with Eq. (3.2) with Richardson's extrapolation.

3.4 Selection of the method for the GSLeq

Let us summarise the main results of the analysis of Methods 1–10 with and without RE. First, the use of RE is not recommended due to its high cost in order to attain a given maximum error; unless that the cost is not a matter and the small error for fixed Δt and Δx is required, in such case, Method 10 with RE is the one that offers the least error. Second, the comparison of Methods 1–10 without RE shows that Methods 2 and 7 are the most efficient among Methods 1–5 and Methods 6–10, respectively, in terms of the relation between cost and error for long-time integration. Finally, Method 7 is better than Method 2 thanks to its robustness, unconditional stability and good energy conservation properties.

Therefore, the comparison of the fifteen Padé methods for the sGeq indicates that the best method for the GSLeq is Method 7. This second-order in time and fourth-order in space scheme will be used for the study of kink-antikink collisions and for searching the quasi-breather of the GSLeq.

4

Results for the graphene superlattice equation

This chapter summarises the numerical studies of the dynamics of GSLeq solutions of two types, the kink–antikink interaction published in my paper [11] and the generation of quasi-breathers in my paper [14]. In Section 4.1 the initial conditions used for the kink–antikink, and for the breather solutions are presented. In Section 4.2 the analysis of the kink–antikink scattering, including the resulting fractal structure, is analysed in detail. Finally, in Section 4.3 the quasi-breather of the GSLeq is numerically searched and characterised.

4.1 Initial conditions

The initial condition for the study of kink and antikink interaction is presented in Subsection 4.1.1, and for the searching of the quasi-breather is explained in Subsection 4.1.2.

4.1.1 Collision of a kink and an antikink

In order to study the collision between a kink and an antikink by means of a numerical method a *sum ansatz* will be used as initial condition given by

$$\tilde{u}_{kak}(x,t) = u_k\left(\frac{x+x_0-vt}{\sqrt{1-v^2}}\right) + u_{ak}\left(\frac{x-x_0+vt}{\sqrt{1-v^2}}\right), \tag{4.1}$$

where at $t=0$ the kink is located at x_0 and the antikink at $-x_0$, both with the same speed v. They can be calculated by means of a quadrature method presented in Section 2.4. In the numerical simulations, periodic boundary conditions are

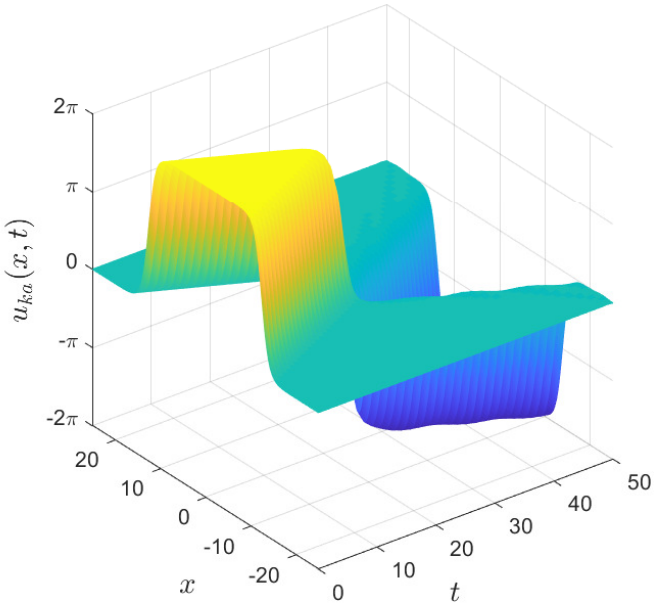

Figure 4.1: Plot of the kink–antikink collision for the GSLeq with $u(x,0;v) = u_{kak}(x,t)$ with $b = 1$, $v = 0.5$, $L = 50$, $x_0 = L/4$, $\Delta x = 0.01$, and $\Delta t = 0.001$.

used, but Eq. (4.1) is not a periodic solution of Eq. (2.17), having non-continuous derivatives at the boundaries. They introduce additional numerical errors. In order to solve this problem, an imbricated soliton series has be used [81,82]. The imbrication of a soliton solution is very easy, for $\tilde{u}_{kak}(x,t)$ it suffice with its replacement by the following sum:

$$u_{kak}(x,t) = \sum_{j=-p}^{p} \tilde{u}_{kak}(x+2Lj,t), \qquad x \in [-L,L), \tag{4.2}$$

for large enough p; in fact, when $x_0 = L/2$, and L is larger than the width of the kink, $p = 1$ is sufficient to obtain an accurate periodic solution since the spatial derivatives of the kink and the antikink are exponentially decaying.

Figure 4.1 illustrates the evolution of the collision between a kink and a antikink with the same but opposite speed $v = 0.5$ for the GSLeq with $b = 1$, numerically solved by Method 7 with initial condition (4.2). The kink is located at $x_0 = 12.5$ at $t = 0$ and the antikink at $x_0 = -12.5$, both with maximum amplitude of 2π. They

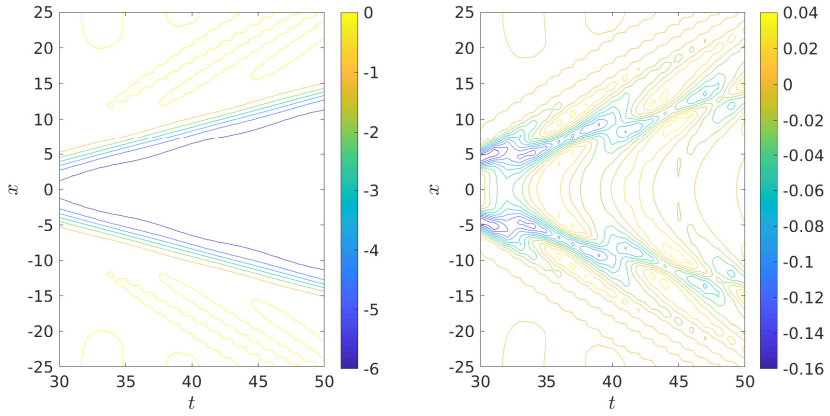

Figure 4.2: Contour plots of the radiation of the kink–antikink collision for the GSLeq shown in Fig. 4.1.

approach each other as time passes, colliding at $t = 20$, where the solution becomes nil. After this time, the kink and antikink reappear with negative amplitudes, but with a shape very similar to the original one at $t = 50$. The most noticeable feature is that they are accompanied by a background of radiation emitted during their inelastic collision since the GSLeq with $b = 1$ is non-integrable (it should be highlighted that for $b = 0.1$ this radiation is not visible in the corresponding plot, being the solution very similar to that of the sGeq). Figure 4.2 illustrates the radiation generated after the kink-antikink collision, from $t = 30$ until $t = 50$; the left contour plot shows the kink–antikink solution and the right contour one the radiation obtained by removing a kink and an antikink whose center positions are fitted to their positions in the numerical kink–antikink solution at $t = 50$. The radiation has an absolute amplitude smaller than 0.04, except near the collision (for $t < 35$) where it reaches 0.16.

4.1.2 Perturbation of the null solution

A proof of the non-existence of small-amplitude breathers in non-integrable, nonlinear Klein-Gordon equations was given by Segur and Kruskal in 1987 [100]; their asymptotic analysis was rigorously justified in Refs. [101, 102]. For a recent review of the current status of this proof the reader should consult Ref. [103].

The GSLeq does not have a breather solution. However, it can be considered as a perturbation of the sGeq, which has a breather solution obtained by means of the method of separation of variables (this method do not work for the GSLeq because it is not separable). A numerical search for quasi-breather solutions will be undertaken by using a new initial condition $U_m^{-1} = u(x_m, -\Delta t)$, and $U_m^0 = u(x_m, 0)$.

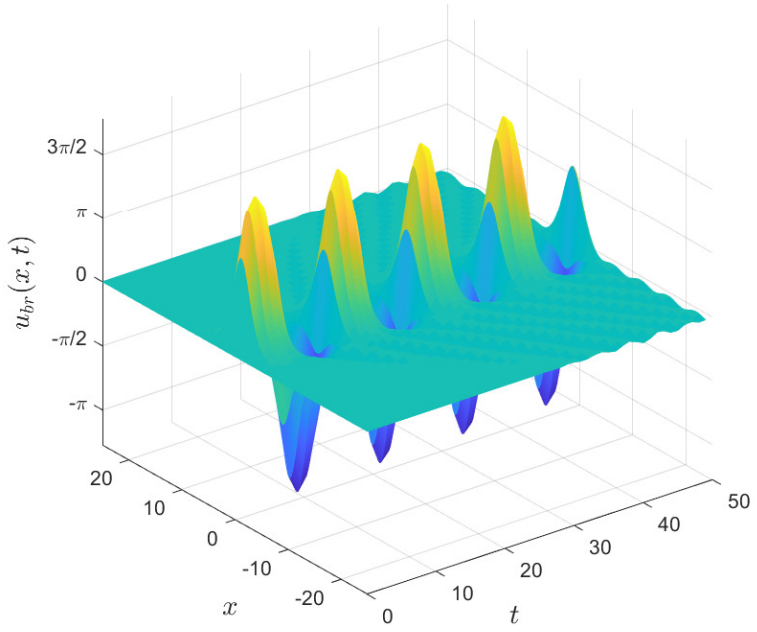

Figure 4.3: Plot of the breather solution for the GSLeq with $b = 1$, $\omega = 1.0$, $L = 100$, and $\Delta t = \Delta x = 0.01$.

The sine–Gordon breather can be written as

$$u_{\mathrm{br}}(x,t) = 4\arctan(\mathrm{sech}(qx)\sin(\omega qt)/\omega), \qquad q = 1/\sqrt{1+\omega^2}. \tag{4.3}$$

Here on, the parameter ω is referred to as frequency, although the breather frequency $\omega_{br} = \omega q = \omega/\sqrt{1+\omega^2}$. Equation (4.3) has the advantage that $u_{\mathrm{br}}(x,0) = 0$, so $U_m^0 = u_{\mathrm{br}}(x_m,0) = 0$ is an exact initial condition. Moreover, since $u_{\mathrm{br}}(x,t) = 4q\,\mathrm{sech}(qx)t + O(t^3)$, an asymptotic expansion in time can be used to obtain an accurate approximation $U_m^{-1} = u(x_m,-\Delta t)$ for the GSLeq.

The introduction of the *ansatz*

$$u_b(x,t) = 4q\,\mathrm{sech}(qx)t + u_3(x)t^3 + u_5(x)t^5 + u_7(x)t^7 + O(t^9), \tag{4.4}$$

into the GSLeq yields

$$(4\,\mathrm{sech}(qx)(q - q^3 + 2q^3\,\mathrm{sech}^2(qx)) + 6u_3(x))t = O(t^3), \tag{4.5}$$

where $u_3(x)$ can be trivially solved. The repetition of this procedure to higher orders in time yields the regular asymptotic expansion

$$\begin{aligned} u_b(x,t) = {} & 4t\,q\,\operatorname{sech}(qx) - \frac{2t^3}{3}\,q\,\operatorname{sech}(qx)\left(1-q^2+2q^2\,\operatorname{sech}^2(qx)\right) \\ & + \frac{t^5}{30}\left(q\,(1-q^2)^2\operatorname{sech}(qx) + 4q^3\,(5+6b^2-5q^2)\,\operatorname{sech}^3(qx)\right. \\ & \qquad \left. + 24q^5\,\operatorname{sech}^5(qx)\right) \\ & - \frac{t^7}{1260}\left(q\,(1-q^2)^3\,\operatorname{sech}(qx) + 2q^3\left(b^2\,(132-228q^2)\right.\right. \\ & \qquad \left. + 91\,(1-q^2)^2\right)\operatorname{sech}^3(qx) + 24q^5\left(8b^2\,(14+15b^2)\right. \\ & \qquad \left.\left. - 35\,(1-q^2)\right)\operatorname{sech}^5(qx) + 720q^7\,\operatorname{sech}^7(qx)\right) \\ & + O\left(t^9\right), \end{aligned} \tag{4.6}$$

which can be used for the initial condition $U_m^{-1} = u_b(x_m, -\Delta t)$. Note that for $\Delta t \leq 0.01$, $q < 1$, and $b \leq 1$, the $O\left(t^9\right)$ term in Eq. (4.6) is smaller than the epsilon of the machine (2.2×10^{-16}); however, for $b \gg 1$ high-order terms in Eq. (4.6) are required in order to obtain an accurate initial condition.

Figure 4.3 illustrates the evolution of a quasi-breather for the GSLeq with $b = 1$ propagating from the initial condition (4.6) with $\omega = 1$. It is clearly visible in the plot that the quasi-breather emits small-amplitude radiation that slowly increases over time. Moreover, this emission reduces the amplitude and energy of the quasi-breather, as time passes.

4.2 Kink–antikink interaction

Similarly to other non-integrable, nonlinear Klein–Gordon equations [12], when using Eq. (4.1) as initial conditions with a given initial velocity, the long-time behaviour of the solution depends on whether this initial velocity is smaller or larger than some critical velocity v_{cr} that is a function of the parameter b of the GSLeq.

Figure 4.4 shows a mesh plot of the kink–antikink collisions $u(x,t;v)$ for $b = 1.5$ with $v = 0.150$ (top left), 0.156 (top right), 0.162 (bottom left), and 0.164 (bottom right). Note that all these initial speeds are smaller than the corresponding critical velocity. The kink and the antikink can be trapped in an oscillatory bound state, resembling a pseudo-breather, with slowly diminishing amplitude as time increases, as shown in Fig. 4.4 (top left). This inelastic behaviour is not observed for all the initial speeds below the critical velocity, since there are a series of

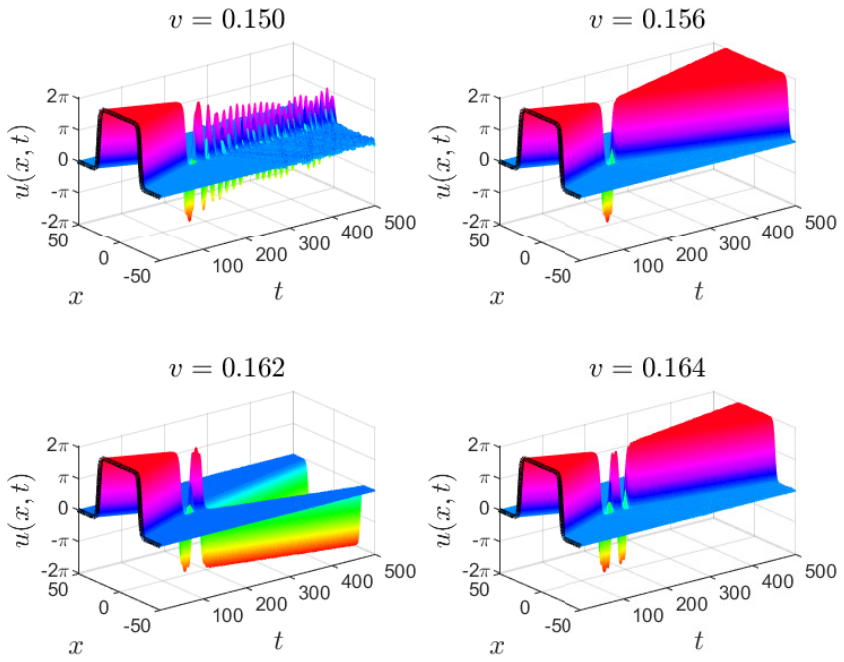

Figure 4.4: Mesh plots of the kink–antikink collision $u(x,t;v)$ for $v = 0.150$ (top left), 0.156 (top right), 0.162 (bottom left), and 0.164 (bottom right), with $b = 1.5$.

resonance windows in initial velocity, where after several bounces the kink and the antikink escape to infinity. Figure 4.4 (top right) shows an example of a two-bounce scattering, Fig. 4.4 (bottom left) of a three-bounce one, and Fig. 4.4 (bottom right) of four-bounce one. Further plots obtained after an extensive set of results show that the initial kink–antikink pair after an odd number of bounces escapes as an antikink–kink pair (they pass through each other), but after an even number of bounces escapes as a kink–antikink pair (they bounce off each other). Note that the multi-bounce scattering is a general prediction of the theory of chaotic scattering of solitons. Numerical simulations show an infinite numerable set of two-bounce windows of increasing initial speed $v < v_{cr}$ where the kink and antikink are temporally trapped in a resonance state before finally escaping from each other's influence, and also that the output velocity v_{out} of the kinks is always smaller than the input velocity v inside the two-bounce windows [104, 105].

Let us write the solution of the GSLeq as as $u(x,t;v)$ when the initial condition is given by Eq. (4.2) with speed v. Figure 4.5 shows contour plots of the solution

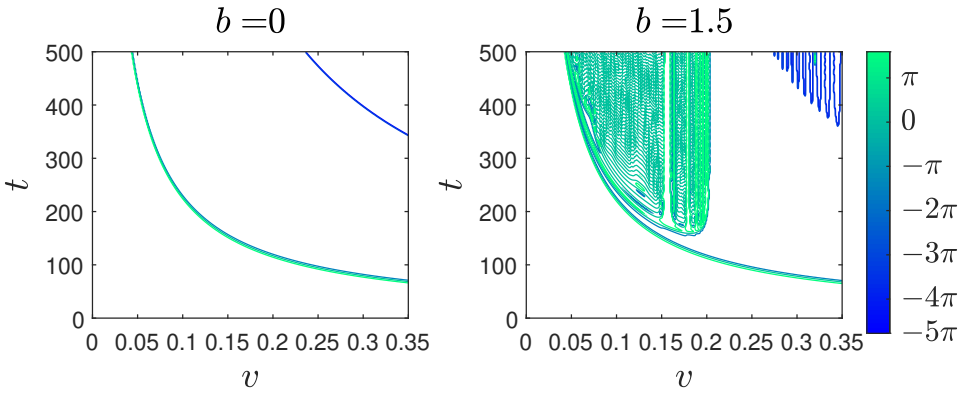

Figure 4.5: Contour plots of the kink–antikink collision $u(0,t;v)$ in the plane (v,t), with contour levels in $\{-15,-10,-5,0,5\}$, and $v \in [0,0.35]$ in velocity steps of $\Delta v = 10^{-3}$, for $b = 0$ and 1.5, with $x_0 = 25$, $\Delta t = \Delta x = 0.01$, $L = 100$, and $T = 500$.

$u(0,t;v)$ in the plane (v,t), with $v \in [0,0.35]$ in velocity steps of $\Delta v = 10^{-3}$, and contour levels at $\{-15,-10,-5,0,5\}$, for $b = 0$ (left plot) and 1.5 (right plot). For $b = 0$, the left plot shows two groups of contour curves for $u(0,t;v)$ with levels equal to $\{-5,0,5\}$ for the first kink–antikink collision (green color) of the sGeq under periodic boundary conditions and equal to $\{-15,-10\}$ for the second one (blue color). For $b = 1.5$, the right plot shows that the contour levels for the first collision coincide with those for $b = 0$, however they are shifted to a higher speed for the second collision; this is due to the appearance of a critical velocity, $v_{cr} = 0.204$ for $b = 1.5$; this behaviour is general for $b > 0$, but more noticeable for $b > 1$. The right plot also shows the multi-bounce scattering for $v < v_{cr}$ over the first group of contours, whose careful analysis requires a zoom.

Figure 4.6 (top) shows the contour plot of the kink–antikink collision $u(0,t;v)$ for $b = 1.5$ in the plane (v,t) with $v \in [0.04,0.22]$, and $t \in [100,500]$.This contour plot shows a series of white bands centred around $v_i = 0.156$, 0.179, 0.188, 0.193, ..., corresponding to the i-th two-bounce resonance window; note that only the first and second ones are noticeable in the right plot in Fig. 4.5. The width of the i-th two-bounce window, $W_i = 0.007$, 0.003, 0.002, 0.001, ..., decreases to zero as their centres approach v_{cr}; hence, the critical velocity as an accumulation point for these resonance windows.

The kink–antikink collisions in Fig. 4.6 (top) apparently shows a self-similar behaviour in the regions between the two-bounce resonance windows; note that it does not occur before the first one, i.e., for $v < 0.153$. In order to highlight this self-similarity, Fig. 4.6 (middle) shows a zoom of the contour plot of $u(0,t;v)$, and Fig. 4.6 (bottom) shows other three zooms to illustrate the resemblance. The

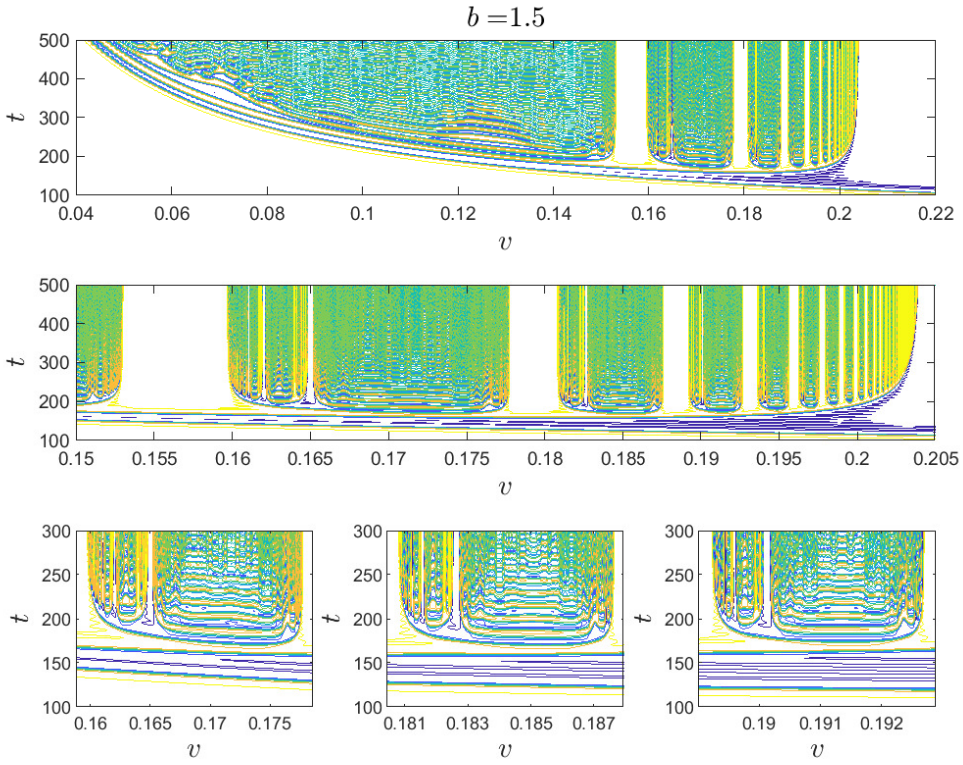

Figure 4.6: The top plot shows the kink–antikink collision $u(0,t;v)$ for $b = 1.5$ contour plotted in the plane (v,t) for $v \in [0.04, 0.22]$, with $\Delta v = 10^{-3}$ when $v \leq 0.15$ and $\Delta v = 10^{-4}$ otherwise, and $t \in [100, 500]$, by using simulations $\Delta t = \Delta x = 0.01$. The middle plot shows a zoom of the contour plot $u(0,t;v)$ for $v \in [0.150, 0.205]$, with $\Delta v = 10^{-5}$, and $t \in [100, 500]$, using simulations with $\Delta x = 0.1$ and $\Delta t = 0.01$. And the bottom plots show zooms of $u(0,t;v)$ with $t \in [100, 300]$, for $v \in [0.15880, 0.17858]$ (bottom left), $v \in [0.18044, 0.18797]$ (bottom centre), and $v \in [0.18901, 0.19289]$ (bottom right), using simulations with $\Delta x = 0.1$ and $\Delta t = 0.01$. In all the simulations $x_0 = 25$, $L = 100$, and $T = 500$.

comparison of the region between the first and second two-bounce windows, Fig. 4.6 (bottom left), with that between the second and third windows, Fig. 4.6 (bottom centre), or with that between the third and fourth windows, Fig. 4.6 (bottom right), clearly confirms the self-similarity.

In every two-bounce window, the function $u(0,t;v)$ shows an oscillatory waveform with an integer number of oscillation peaks; it is determined by counting

the number of local maxima of $|u(0,t;v)|$ for t such that $|u(0,t;v)| > 6$ inside the two-bounce window. The number of oscillations peaks is referred to as the index of the window in Ref. [12], where the ϕ^4 model was studied; here on the two-bounce window with index i is referred to as an (i)-window, for $i \geq 1$. The oscillation in the (1)-window corresponds to the double line around $t \approx 150$ for $v \approx 0.16$ in Fig. 4.6 bottom left plot; the two oscillations in the (2)-window to the two double lines around $t \approx 140$–150 for $v \approx 0.180$ in Fig. 4.6 bottom middle plot and for $v \approx 0.181$ in Fig. 4.6 bottom centre plot; the three oscillations in the (3)-window to the three double lines around $t \approx 130$–150 for $v \approx 0.188$ in Fig. 4.6 bottom centre plot and for $v \approx 0.189$ in Fig. 4.6 bottom right plot; and successively.

In order to describe the self-similar structure of the multi-bounce windows, let us introduce a multi-index notation that generalises the index introduced in Ref. [12]. Let us anticipate that, for the GSLeq, there can be p-bounce windows around both sides of the 2-bounce windows. Hence, the $(i_{1L}, i_2, \ldots, i_{p-1})$- and $(i_{1R}, i_2, \ldots, i_{p-1})$-windows, with $i_q \in \mathbb{N}$, are p-bounce windows with i_q oscillations in each q-th bounce, which are located at the left and right sides, respectively, of the (i_1)-window; in order to shorten the multi-index notation, the non-oscillation peaks are represented by $i_q = 0$. Each $(i_{1L|R}, i_2, \ldots, i_{p-1})$-window is characterised by its central velocity, denoted as $v_{(i_{1L|R}, i_2, \ldots, i_{p-1})}$, its left boundary velocity, indicated as $v^L_{(i_{1L|R}, i_2, \ldots, i_{p-1})}$, and its right boundary velocity, as $v^R_{(i_{1L|R}, i_2, \ldots, i_{p-1})}$.

Figure 4.7 (a) shows the absolute value of the output velocity $|v_{out}|$ of the kink after the kink–antikink collision as a function of its initial velocity $v \in [0.15, 0.21]$ for $b = 1.5$. In the horizontal axis for $v \in [0.15000, 0.21000]$, a $\Delta v = 10^{-5}$ was generally used. Note that $v_{out} > 0$ ($v_{out} < 0$) for the even-bounce (odd-bounce) windows, and that the 2-, 3-, 4-, 5-, 6-, and 7- windows are marked by circle, asterisk, triangle, filled-circle, square, and star symbols.

The continuous blue curves marked with a blue circle symbol in the plots in Fig. 4.7 are (i_1)-windows with $i_1 \geq 1$, corresponding to the white bands shown in Fig. 4.6 (middle); the dot-dashed red curves marked with a red asterisk symbol in the plots in Fig. 4.7 are $(i_{1L|R}, i_2)$-windows with $i_1 \geq 1$ and $i_2 \geq 0$; the blue triangle symbols in Fig. 4.7 correspond to the $(i_{1L|R}, i_2, i_3)$-windows with $i_1 \geq 1$ and $i_2, i_3 \geq 0$. In addition, the plots in Fig. 4.7 show brown filled-circle symbols corresponding to $(i_{1L|R}, \ldots, i_4)$-windows, yellow square symbols for $(i_{1L|R}, \ldots, i_5)$-windows, and a green star symbols for $(i_{1L|R}, \ldots, i_6)$-windows. Let us notice that by using a $\Delta v < 10^{-6}$ multi-bounce windows with more than seven bounces will appear, but the main fractal-like features of the corresponding plot remain.

Figure 4.7 (b) shows a zoom of the multi-bounce windows located after the (1)-window for $v > v^R_{(1)}$, calculated with $\Delta v = 10^{-6}$; it has numerically checked that there are no multi-bounce windows with $v < v^L_{(1)}$. The red dot-dashed lines

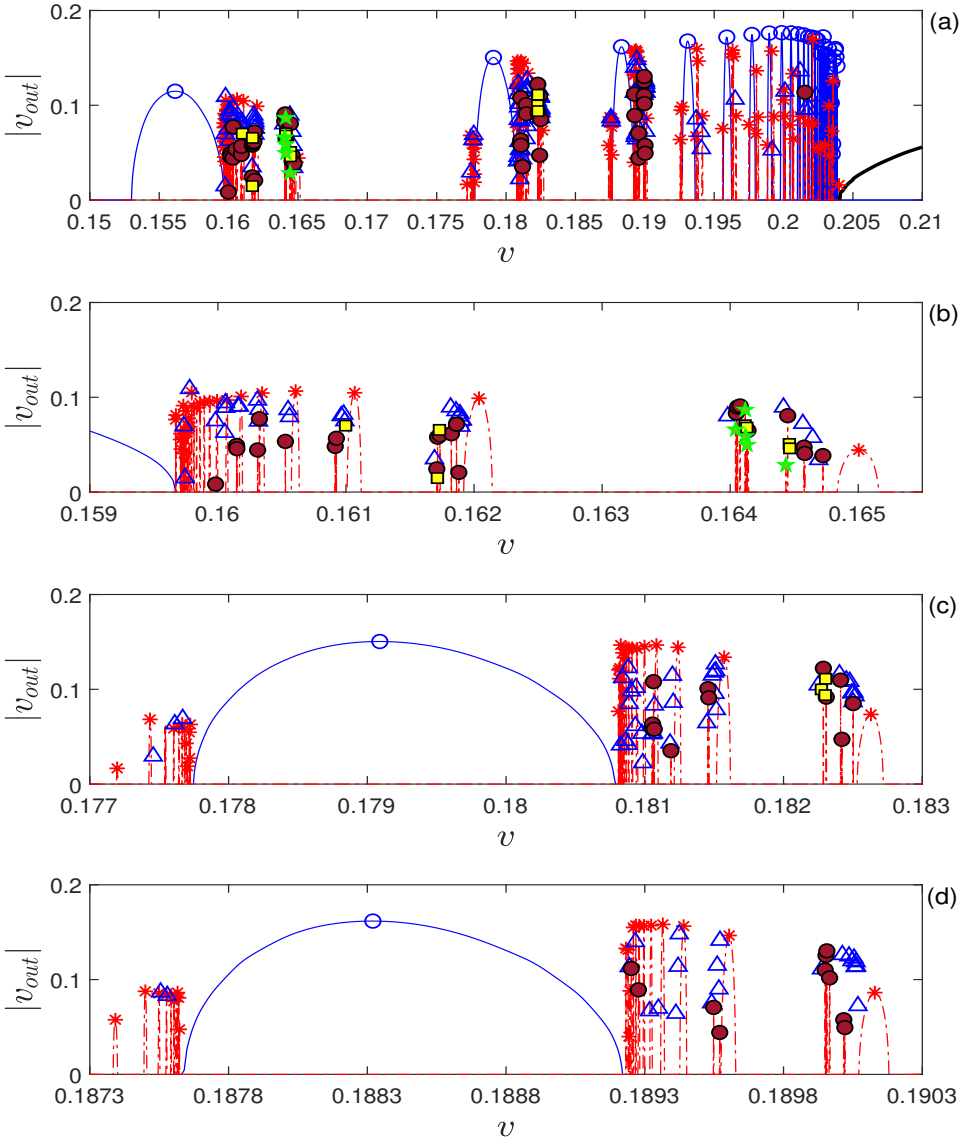

Figure 4.7: The absolute value of the output velocity $|v_{out}|$ of the kink after the kink–antikink interaction as a function of its initial velocity v for $b = 1.5$ (a), and zooms in the intervals $v \in [0.155, 0.166]$ (b), $v \in [0.177, 0.183]$ (c), and $v \in [0.1873, 0.1903]$ (d). See the main text for a detailed explanation of this figure. All the simulations use $\Delta x = 0.1$, $\Delta t = 0.01$, $x_0 = 25$, $L = 100$, and $T = 500$.

marked with a red asterisk symbol in this plot correspond to 3_R-bounce windows, concretely $(1_R, i_2)$-windows with $i_2 = 0, 1, \ldots 94$; they clearly suggest that $\lim_{i_2\to\infty} v_{(1_R,i_2)} = v^R_{(1)} = 0.159667$, for $i_2 \geq 0$, where a one-sided limit approaching from the right has been used, and will be used hereafter, for limits towards right boundary velocities. The 4_R-bounce windows marked with a blue triangle symbol in Fig. 4.7 (b) correspond to twenty $(1_R, i_2, i_3)$-windows with $i_2, i_3 \geq 0$ and suggest that $\lim_{i_3\to\infty} v_{(1_R,0,i_3)} = v^L_{(1_R,0)} = 0.164834$, for $i_3 \geq 0$, where a one-sided limit approaching from the left is used, and will be used hereafter, for limits towards left boundary velocities, and $\lim_{i_3\to\infty} v_{(1_R,1,i_3)} = v^L_{(1_R,1)} = 0.161920$, for $i_3 \geq 0$; moreover, they could be generalised to $\lim_{i_3\to\infty} v_{(1_R,i_2,i_3)} = v^L_{(1_R,i_2)}$, for all $i_2, i_3 \geq 0$. The 5_R-bounce windows marked with a brown filled circle symbol in Fig. 4.7 (b) correspond to the $(1_R, i_2, i_3, i_4)$-windows with $i_2, i_3, i_4 \geq 0$, and suggest that $\lim_{i_4\to\infty} v_{(1_R,0,0,i_4)} \to v^R_{(1_R,0,0)} = 0.164027$, and, apparently, $\lim_{i_4\to\infty} v_{(1_R,i_2,i_3,i_4)} = v^R_{(1_R,i_2,i_3)}$, both limits for $i_2, i_3, i_4 \geq 0$. Finally, further results shown in Fig. 4.7 (b) could be generalised to $\lim_{i_{p-1}\to\infty} v_{(1_R,i_2,\ldots,i_{p-1})} = v^R_{(1_R,i_2,\ldots,i_{p-2})}$, for odd p, and $\lim_{i_{p-1}\to\infty} v_{(1_R,i_2,\ldots,i_{p-1})} = v^L_{(1_R,i_2,\ldots,i_{p-2})}$, for even p, in both cases for all $i_2, \ldots, i_{p-2} \geq 0$.

Figure 4.7 (c) shows the distribution of multi-bounce windows at both sides of the (2)-window, for $v \in [0.1770, 0.1830]$; the plot shows p-bounce windows with $p = 3_L$, and 4_L for $v < v^L_{(2)} = 0.177747$, and with $p = 3_R$, 4_R, 5_R, and 6_R for $v > v^R_{(2)} = 0.180780$. On the left side of the (2)-window in this plot, the red dot-dashed lines marked with a red asterisk symbol for $v < v^L_{(2)}$ correspond to the 3_L-bounce windows and velocities; they clearly suggest that $\lim_{i_2\to\infty} v_{(2_L,i_2)} = v^R_{(2)}$, for $i_2 \geq 1$; note that the numerical results do not show a $(2_L, 0)$-window. The scarce results for the 4_L-bounce windows, marked with a blue triangle in this figure, show that $v_{(2_L,2,1)} = 0.177457 > v^R_{(2_L,2)} = 0.177443$, $v_{(2_L,4,1)} = 0.177612 > v^R_{(2_L,4)} = 0.177607$, and $v_{(2_L,6,1)} = 0.177669 > v^R_{(2_L,6)} = 0.177667$; these results suggest that $\lim_{i_3\to\infty} v_{(2_L,i_2,i_3)} = v^R_{(2_L,i_2)}$, for $i_2 \geq 1$, and $i_3 \geq 0$. On the right side of the (2)-window in this plot, the red dot-dashed lines marked with a red asterisk symbol for $v > v^R_{(2)}$ in Figure 4.7 (c) correspond to the 3_R-bounce windows; the velocities of the $(2_R, 17)$-, …, $(2_R, 1)$-, $(2_R, 0)$-windows clearly suggest that $\lim_{i_2\to\infty} v_{(2_R,i_2)} = v^R_{(2)}$, for $i_2 \geq 0$. The 4_R-bounce windows marked with a blue triangle and the corresponding values for $p = 4_R$ suggest that $\lim_{i_3\to\infty} v_{(2_R,i_2,i_3)} = v^L_{(2_R,i_2)}$, for $i_2, i_3 \geq 0$. The 5_R-bounce windows marked with a brown filled circle in the plot suggest that $\lim_{i_4\to\infty} v_{(2_R,i_2,i_3,i_4)} = v^R_{(2_R,i_2,i_3)}$, for $i_2, i_3, i_4 \geq 0$. The scarce results for the 6_R-bounce windows, marked with a yellow square, show that $v_{(2_R,0,0,0,0)} = 0.182300 < v_{(2_R,0,0,0,1)} = 0.182303 < v^L_{(2_R,0,0,0)} = 0.182306$, suggesting that $\lim_{i_5\to\infty} v_{(2_R,i_2,i_3,i_4,i_5)} = v^L_{(2_R,i_2,i_3,i_4)}$, for $i_2, i_3, i_4, i_5 \geq 0$.

Figure 4.7 (d) shows the distribution of p-bounce windows at both sides of

the (3)-window, for $v \in [0.1873, 0.1903]$; the plot show multi-bounce windows with $p = 3_L$ and 4_L for $v < v^L_{(3)} = 0.187640$, and with $p = 3_R$, 4_R, and 5_R for $v > v^R_{(3)} = 0.189220$. On the left side of the (3)-window in this plot, 3_L-bounce windows for $v < v^L_{(3)}$ are shown in the red dot-dashed lines marked with a red asterisk symbol, clearly suggest that $\lim_{i_2\to\infty} v_{(3_L,i_2)} = v^L_{(3)}$, for $i_2 \geq 1$; note that we have numerically searched for a $(3_L, 0)$-window in the results but we have found no one. The results for the 4_L-bounce windows, marked with a blue triangle, show that $v_{(3_L,3,1)} = 0.187555 > v^L_{(3_L,3)} = 0.187549$, and $v_{(3_L,4,2)} = 0.187579 > v^L_{(3_L,4)} = 0.187576$; these results suggest that $\lim_{i_3\to\infty} v_{(3_L,i_2,i_3)} = v^L_{(3_L,i_2)}$, for $i_2 \geq 1$, and $i_3 \geq 0$. On the right side of the (3)-window in this plot, the $(3_R, 29)$-, $\ldots$, $(3_R, 1)$-, $(3_R, 0)$-windows for $v > v^R_{(3)}$ are shown in the red dot-dashed lines marked with a red asterisk symbol in Figure 4.7 (d); they suggest that $\lim_{i_2\to\infty} v_{(3_R,i_2)} = v^R_{(3)}$, for $i_2 \geq 0$. The 4_R-bounce windows marked with a blue triangle suggest that $\lim_{i_3\to\infty} v_{(3_R,i_2,i_3)} = v^L_{(3_R,i_2)}$, for $i_2, i_3 \geq 0$. Finally, the 5_R-bounce windows marked with a brown filled circle in the plot, suggest that $\lim_{i_4\to\infty} v_{(3_R,i_2,i_3,i_4)} = v^R_{(3_R,i_2,i_3)}$, for $i_2, i_3, i_4 \geq 0$.

The self-similar structure of the fractal scattering of kink–antikink solutions observed for $b = 1.5$, shown in Figure 4.7, is similar to that for $b = 2.5$ and 3.5; the corresponding figures are omitted here for the sake of brevity [11]. The general features observed in the numerical experiments suggest the following conjecture about the self-similar pattern of the multi-bounce windows for the GSLeq with $b > 0$. The velocity of the two-bounce windows accumulates at the critical velocity such as

$$\lim_{i_1\to\infty} v_{(i_1)} = v^L_{cr} \equiv v_{cr}, \qquad i_1 \geq 1;$$

and the velocity of the p-bounce windows with even $p \geq 2$ at the right side of a 2-bounce window are

$$\lim_{i_{p-1}\to\infty} v_{(i_{1R},i_2,\ldots,i_{p-1})} = v^L_{(i_{1R},i_2,\ldots,i_{p-2})}, \qquad i_1 \geq 1,\ i_2,\ldots,i_{p-1} \geq 0,$$

with even $p > 2$ at the left side are as

$$\lim_{i_{p-1}\to\infty} v_{(i_{1L},i_2,\ldots,i_{p-1})} = v^R_{(i_{1L},i_2,\ldots,i_{p-2})}, \qquad i_1 \geq 2,\ i_2 \geq 1,\ i_3,\ldots,i_{p-2} \geq 0,$$

with odd $p > 1$ at the right side of a 2-bounce window are

$$\lim_{i_{p-1}\to\infty} v_{(i_{1R},i_2,\ldots,i_{p-1})} = v^R_{(i_{1R},i_2,\ldots,i_{p-2})}, \qquad i_1 \geq 1,\ i_2,\ldots,i_{p-2} \geq 0,$$

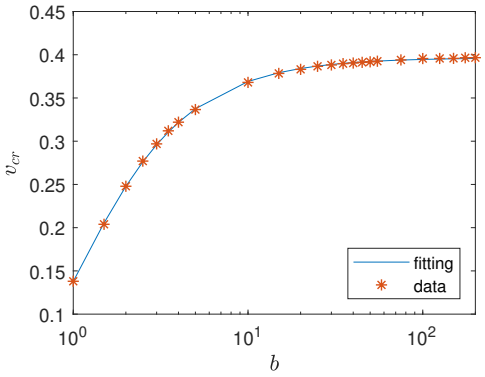

Figure 4.8: The plot shows the critical velocity v_{cr} as function of b estimated from numerical calculations and fitted by Eq. (4.7), by using $x_0 = 25$ for $b < 25$, and $x_0 = 50$ for $25 \leq b \leq 200$; in all the simulations $\Delta t = \Delta x = 0.01$, $L = 100$, and $T = 500$.

and odd $p > 1$ at the left side are as

$$\lim_{i_{p-1}\to\infty} v_{(i_{1L},i_2,\ldots,i_{p-1})} = v^L_{(i_{1L},i_2,\ldots,i_{p-2})}, \qquad i_1 \geq 2,\ i_2 \geq 1,\ i_3,\ldots,i_{p-2} \geq 0.$$

These results for $b = 1.5$ are representative of those obtained for other values of b. They can be understood by applying the resonant energy exchange theory developed by Campbell *et al.* [12, 106]. The critical velocity for the two-bounce windows depend on the parameter b; Figure 4.8 shows its values numerically calculated from the simulations for $b \in [1, 200]$. It monotonically grows as a function of b apparently reaching a constant asymptotic value near 0.4; let us guess the following *ansatz*

$$v_{cr}(b) = \gamma \exp(-\alpha\,(1 + 1/b^{\beta})), \tag{4.7}$$

whose numerical fitting results in $\alpha = 1.056 \pm 0.010$, $\beta = 1.169 \pm 0.013$, and $\gamma = 1.14 \pm 0.011$ at the 95% confidence level. Note that $v_{cr}(b) \to 0$, for $b \to 0$, as expected for the sGeq, and that the asymptotic value of the critical velocity fitted by Eq. (4.7) is $v_{cr}(\infty) = 0.3965$. The good accuracy of this fitting is illustrated by the blue curve shown in Fig. 4.8; quantitatively, the relative error is smaller than 1% for $b \in [1, 200]$. The analytical estimation of the critical velocity by means of using a singular perturbation theory with $\varepsilon = b$ as small parameter is outside the scope of this thesis; however, let us remark that such an approach usually results in errors for $\varepsilon = 1$ within 6% [107, 108].

The resonant energy exchange theory [12, 106] explains the 2-bounce windows

in the interaction of the kink and the antikink as the result of the excitation of internal modes during the collision. Assuming a single internal mode with frequency ω_B, the time between the first and second bounces $T(v_{(n)})$ satisfy the resonance condition

$$\omega_B T(v_{(n)}) = 2\pi n + \delta, \tag{4.8}$$

for the (n)-window, where $\delta \in [0, 2\pi)$ is an offset phase. Moreover, assuming that the energy "stored" in the internal mode is roughly conserved, it predicts that

$$T(v_{(n)}) = \frac{\beta}{\sqrt{v_{cr}^2 - v_{(n)}^2}}, \tag{4.9}$$

where β is an empirically determined constant. Combining Eqs. (4.8) and (4.9), the central velocity of the (n)-window can be estimated as

$$v_{(n)} \approx \sqrt{v_{cr}^2 - \frac{\beta^2 \omega_B^2}{(2\pi n + \delta)^2}}. \tag{4.10}$$

Campbell *et al.* [13] presents a theoretical estimation β_{th} of the empirical parameter β given by

$$\beta_{th} = \frac{\pi}{\omega_0 \sqrt{\alpha}}, \tag{4.11}$$

where $\omega_0^2 = d^2G(u_0)/du^2 = 1$, for $dG(u_0)/du = 0$ (note that u_0 depends on b, but ω_0 is independent of b for the GSLeq), and α is another empirical parameter determined by fitting $v_{out}^2 = \alpha\,(v^2 - v_{cr}^2)$, for $v > v_{cr}$, i.e., the black curve at the left part of the plot in Fig. 4.7 (a).

Our results show that the resonant energy exchange theory fits the numerical observations better for the GSLeq than for the dsGeq [13]. For the dsGeq, depending on the parameter that combines its two sines, the critical velocity increases and then decreases; however, in the GSLeq as the geometric parameter b of the GSLeq increases, the critical velocity increases monotonically, approaching a maximum value asymptotically (as far as we have been able to verify numerically). Our conjecture is that this could be the reason why the fit of the resonant energy exchange theory for the GSLeq improves as b grows.

4.3 Quasi-breather search

The numerical solution of the sine–Gordon equation, i.e., the GSLeq with $b = 0$, with the initial condition (4.6) results in a good approximation to its exact breather

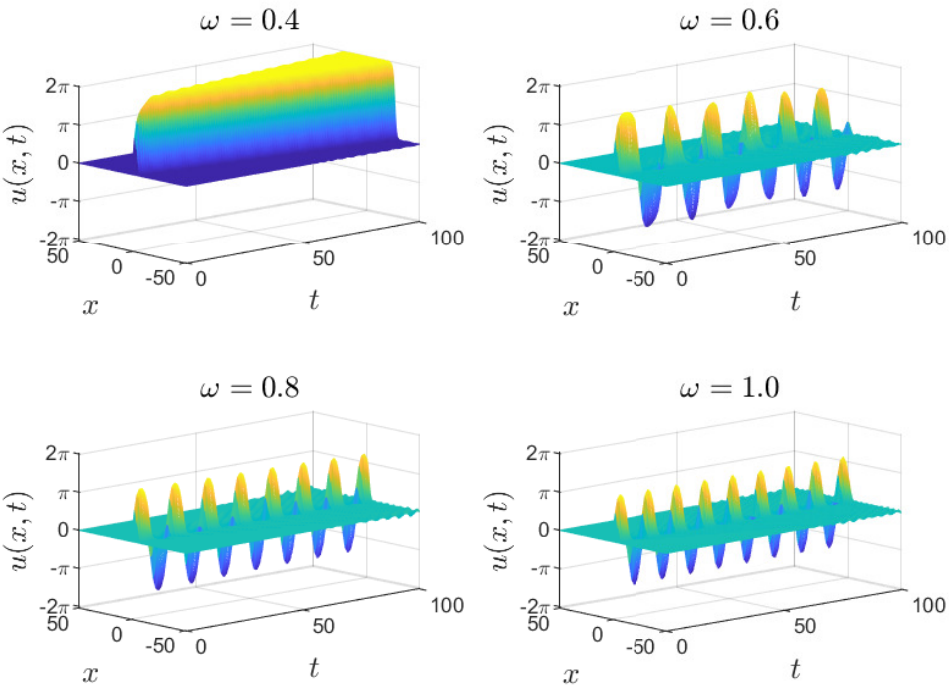

Figure 4.9: Three-dimensional mesh plot of the solution of the GSLeq with $b = 1$ and the initial condition (4.6) for $\omega = 0.4$, 0.6, 0.8, and 1.0, by using $\Delta t = \Delta x = 0.01$, $x \in [-50, 50)$, and $t \in [0, 100]$.

solution for every value of the frequency ω. However, for the GSLeq with $b > 0$ numerical simulations show that there is a critical minimum frequency ω_{cr}, such that the solution evolves into a kink–antikink solution for $\omega < \omega_{\text{cr}}$ and into a quasi-breather for $\omega > \omega_{\text{cr}}$. This result is illustrated in Fig. 4.9, where the GSLeq with $b = 1$ is solved with initial condition (4.6) for $\omega = 0.4$ (top left plot), 0.6 (top right plot), 0.8 (bottom left plot), and 1.0 (bottom right plot). Because the radiation reenters the domain due to the periodic boundary conditions, the four plots denotes solutions emitting small-amplitude radiation with a small amplitude that slowly increases over time.

Figure 4.10 shows plots of $u(0,t)$ for the solutions shown in Fig. 4.9 in order to illustrate the profile of the corresponding kink–antikink and quasi-breather solutions. The top left plot ($\omega = 0.4$) shows that the amplitude in the centre of the kink–antikink solution increases from 0 to 2π, with a small ripple whose amplitude decreases in time. The top right plot ($\omega = 0.6$) shows the central profile of the pseudo-breather, whose profile in every period changes appreciably both in amplitude and frequency.

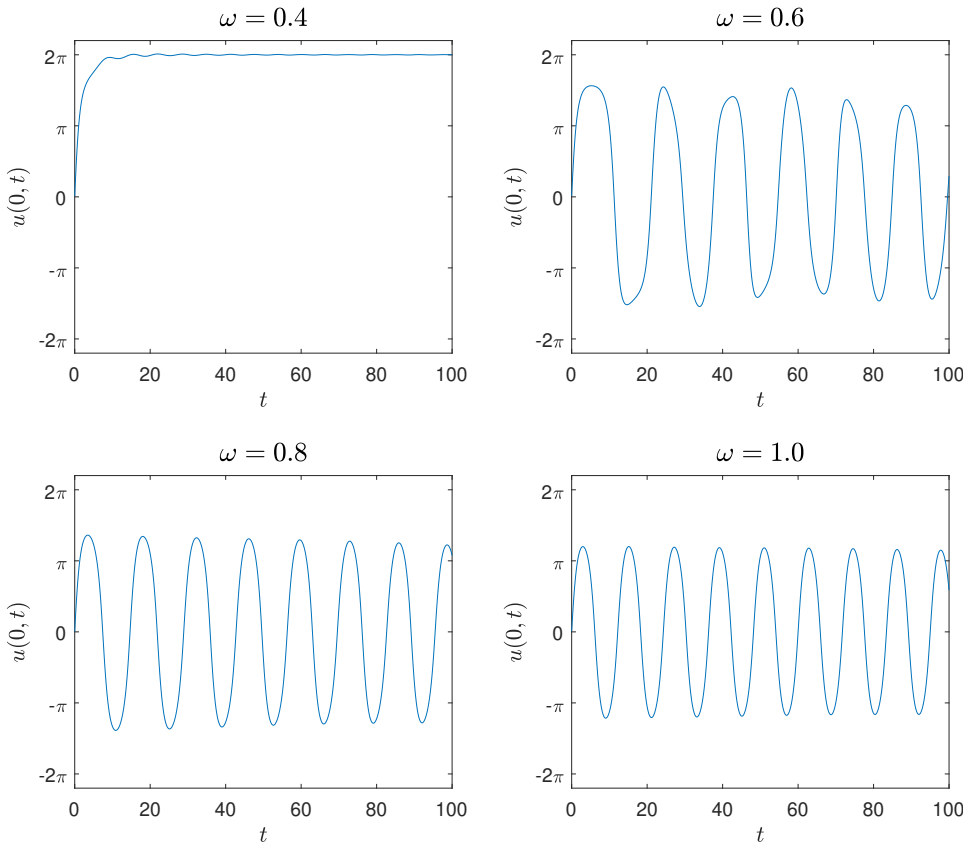

Figure 4.10: The centre $u(0,t)$ of the numerical solutions of the GSLeq with $b = 1$ shown in Fig. 4.9.

The bottom left plot ($\omega = 0.8$, $q = 5/\sqrt{41}$) and the bottom right plot ($\omega = 1.0$, $q = 1/\sqrt{2}$) show the central profile of quasi-breather solutions with nearly constant amplitude and frequency; in fact, a careful analysis concludes that the amplitude (frequency) decreases (increases) in an small amount as time passes due to the slow emission of radiation (not noticeable in these plots).

Figure 4.11 shows contour plots of the solution $u(0,t)$ in the plane (ω,t), with $\omega \in [0,1]$ in steps of $\Delta\omega = 10^{-3}$, for the numerical solution of Eq. (2.17) with $b = 0$, 0.2, 0.4, 0.6, 0.8, and 1. The top left plot for $b = 0$ shows the analytical breather solution, Eq. (3.20), of the sGeq; it clearly shows that the frequency of the breather increases as ω does, as expected from $\omega_{\rm br} = \omega/\sqrt{1+\omega^2}$. The other five plots for $b > 0$ in Fig. 4.11 clearly show the existence of two critical frequencies, $\omega_{\rm cr}$, such that the solution evolves into a kink–antikink solution for $\omega < \omega_{\rm cr}$ and $\omega_{\rm cr,br}$, such

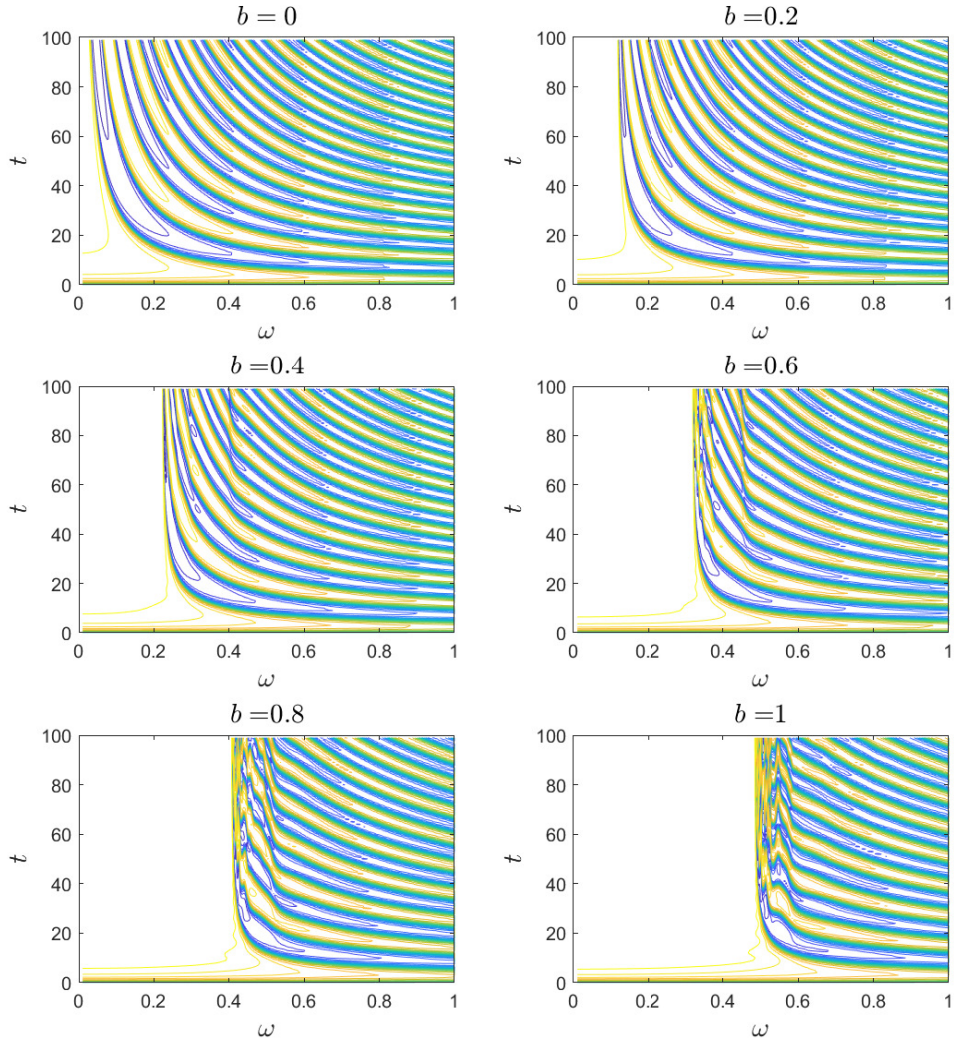

Figure 4.11: Contour plots of the quasi-breather solution $u(0,t)$ in the plane (ω,t) with $\omega \in [0,1]$ in steps of $\Delta\omega = 10^{-3}$, for $b = 0$, 0.2, 0.4, 0.6, 0.8, and 1, with $\Delta t = \Delta x = 0.01$, $x \in [-50,50)$, and $t \in [0,100]$.

that the solution is a quasi-breather for $\omega > \omega_{\mathrm{cr,br}}$, but an irregular solution for $\omega_{\mathrm{cr}} < \omega < \omega_{\mathrm{cr,br}}$, as illustrated for $b = 1$ in the three-dimensional mesh plots in Fig. 4.9; the values of ω_{cr} and $\omega_{\mathrm{cr,br}}$ for $b = 0, 0.2, \ldots, 1$, are shown in Table 4.2. The top right plot for $b = 0.2$ shows that the contour plot of the numerical quasi-breather for $\omega > \omega_{\mathrm{cr}}$ is very similar to that of the breather for $\omega > 0$ (top left plot); however,

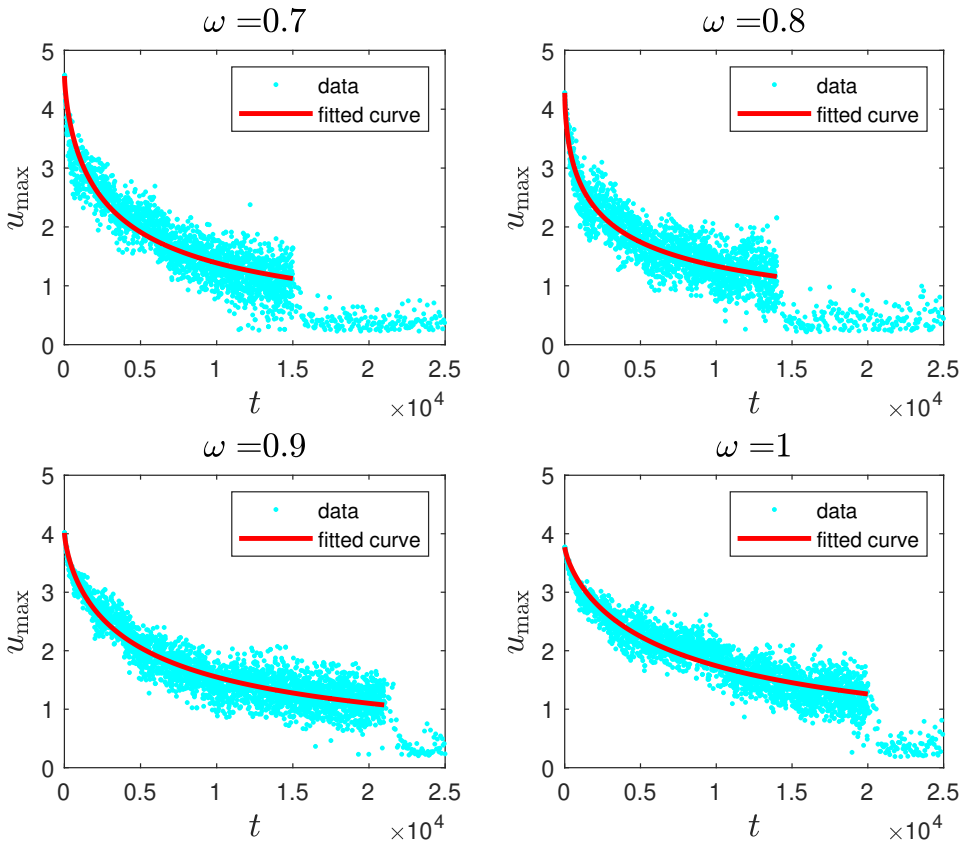

Figure 4.12: Plots of the quasi-breather amplitude maxima $u_{\max}(t_i)$ (cyan points) and its fitting (red line) by Eq. (4.12) for $\omega = 0.7$ (top left), 0.8 (top right), 0.9 (bottom left plot), and 1 (bottom right), with $b = 1$, $\Delta t = \Delta x = 0.01$, $x \in [-50, 50)$, and $t \in [0, 25000]$.

the slope of the contours for $\omega \gtrsim \omega_{\rm cr}$ for $b = 0.2$ is larger than for $\omega \gtrsim 0$ for $b = 0$. The middle left plot for $b = 0.4$ shows a new feature in the contour plot with respect to that for $b = 0.2$ (top right plot), a change of the contours' slope around $\omega_{\rm cr,br}$; such a feature is also shown in the middle right plot ($b = 0.6$). The bottom left plot for $b = 0.8$ and the bottom right plot for $b = 1$ show, for $\omega_{\rm cr} < \omega < \omega_{\rm cr,br}$, an irregular behaviour in both amplitude and frequency of the oscillatory solution, including several slope changes in the contour plots, here on referred to as a pseudo-breather.

The maximum amplitude $u_{\max}(t_i)$, $i = 1, 2, \ldots$, of the oscillatory profile $u(0,t)$ of the quasi-breather decreases as time marches due to the emission of radiation, until the quasi-breather loses its identity decaying into small-amplitude radiation

at a time $t = T_{\max}$. Figure 4.12 shows $u_{\max}(t_i)$ of the quasi-breather of the GSLeq with $b = 1$ for $\omega = 0.7$, 0.8, 0.9, and 1, from a long-time numerical integration until $t = 25000$. This figure shows a sharp transition between a decaying quasi-breather and a small-amplitude radiation solution at time $t \approx T_{\max}$. The values of $u_{\max}(t_i)$, $i = 1, 2, \ldots, N$, with $t_N \leq T_{\max}$ have been fitted by the expression

$$u_{\max}(t) = \frac{u_{\max}(t_1)}{1 + \alpha\,(t - t_1)^{\gamma}}, \tag{4.12}$$

where the first data point $(t_1, u_{\max}(t_1))$ has been fixed in order to enforce that Eq. (4.12) exactly holds for such a point. Table 4.1 shows the values of the fixed parameters t_1, $u_{\max}(t_1)$, and $T_{\max}$, and the fitted parameters α and γ with 95% confidence intervals for $\omega = 0.7$, 0.8, 0.9, and 1. Figure 4.12 and Table 4.1 show that t_1 and $u_{\max}(t_1)$ decrease as ω grows; the behaviour of $T_{\max}$ is irregular, although the general trend is to increase as ω does. Table 4.1 shows that the fitted coefficient α decreases and γ increases as ω grows, except for $\omega = 0.8$.

Figure 4.13 (left plot) shows the critical frequency $\omega_{\rm cr}$ as function of b, showing that it is monotonically increasing. The data points can be fitted by an exponential function

$$\omega_{\rm cr}(b) = \tilde{\alpha}\,(1 - \exp(-\tilde{\beta}\,b)), \tag{4.13}$$

resulting in

$$\tilde{\alpha} = 1.19^{+0.09}_{-0.08}, \qquad \tilde{\beta} = 0.52^{+0.05}_{-0.04}, \tag{4.14}$$

both with 95% confidence intervals and a coefficient of determination $R^2 = 0.9999$.

Table 4.1: The parameters of Eq. (4.12) for the local maxima of the quasi-breather shown in the plots of Fig. 4.12; α and γ are fitted from data in $t \in [0, T_{\max}]$, showing 95% confidence intervals, but $T_{\max}$ and t_1 are fixed from the data.

ω	t_1	$u_{\max}(t_1)$	$T_{\max}$	α	γ
0.7	3.94	4.5640	15000	0.0030 ± 0.0004	0.72 ± 0.02
0.8	3.47	4.2775	14000	0.0089 ± 0.0013	0.60 ± 0.02
0.9	3.19	4.0146	21000	0.0018 ± 0.0002	0.73 ± 0.01
1.0	2.98	3.7694	20000	0.0009 ± 0.0001	0.77 ± 0.01

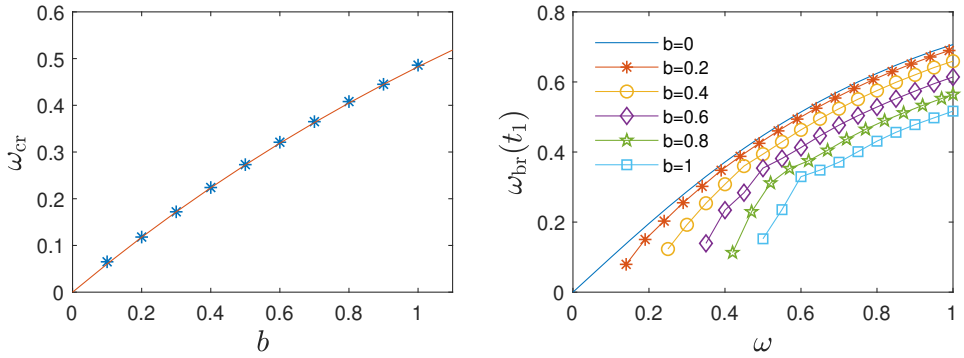

Figure 4.13: The left plot shows the critical frequency $\omega_{\rm cr}$ as function of b estimated from numerical calculations and its fitting by Eq. (4.13). The right plot shows the first quasi-breather frequency $\omega_{\rm br}(t_1)$ for $b = 0.2$, 0.4, 0.6, 0.8, and 1 as a function of ω, and the breather frequency $\omega_{\rm br}(\omega)$ for the sGeq (continuous line). All the simulations use $\Delta t = \Delta x = 0.01$, $x \in [-50, 50)$, and $t \in [0, 100]$.

Figure 4.13 (right plot) shows the breather frequency $\omega_{\rm br}(\omega)$ for the sGeq $b = 0$ (continuous line), and the first quasi-breather frequency $\omega_{\rm br}(t_1)$ for $b = 0.2$, 0.4, 0.6, 0.8, and 1 as a function of ω; this plot shows the first quasi-breather frequency $\omega_{\rm br}(t_1)$ as a function of ω for $b = 0, 0.2, \ldots, 1$. The values of $\omega_{\rm br}(t_1)$ increase as ω does and decrease as b increases, but always being smaller than the frequency of the sG breather ($\omega/\sqrt{1+\omega^2}$).

The numerical simulations show that the new initial condition generates three possible solutions depending on the frequency ω, there being two critical frequencies $\omega_{\rm cr}$ and $\omega_{\rm cr,br}$ that determine the type of solution (we are not aware that the existence of these critical frequencies has been reported in previous studies of quasi-breather type solutions in other Klein–Gordon equations). Specifically, an infinitely escaping kink–antikink pair is generated for $\omega < \omega_{\rm cr}$, a pseudo-breather for $\omega_{\rm cr} < \omega < \omega_{\rm cr,br}$, and a *quasi-breather* solution for $\omega > \omega_{\rm cr,br}$; where we have used the Malomed

Table 4.2: Critical frequencies $\omega_{\rm cr}$ and $\omega_{\rm cr,br}$ for $b = 0, 0.2, \ldots, 1$, determined from the simulations plotted in Fig. 4.11.

b	0	0.2	0.4	0.6	0.8	1.0
$\omega_{\rm cr}$	0	0.118	0.224	0.321	0.408	0.486
$\omega_{\rm cr,br}$	0	0.118	0.40	0.46	0.53	0.59

et al. [83] nomenclature, according to which a pseudo-breather is an irregular oscillating solution that decays into radiation after a small number of oscillations in time, while a quasi-breather presents regular oscillations that are maintained for a long time.

Let us briefly summarise our main results on the search of the quasi-breather solution. Our simulations show that the critical frequency ω_{cr} increases monotonically with b, being zero for $b = 0$; and that the quasi-breather for $\omega > \omega_{\mathrm{cr,br}}$ survives more than a thousand periods, while its amplitude and energy decrease and its frequency increases. We have characterised these behaviours by fitting the amplitude and frequency with respective power laws; although we do not yet have a theoretical explanation for the observed exponents that depend on the geometric parameter b. Furthermore, we have observed that the frequency of the first oscillation of the quasi-breather is below the frequency of the breather ω_{br} of the sGeq, and decreases as b increases; the frequency of the successive oscillations grows, but always staying below ω_{br}. Finally, let us highlight that, for small b, the case of most interest in practical applications of the GSL, the quasi-breather of the GSLeq has a very constant frequency which is very close to ω_{br}, presenting a robustness that resembles a breather. Thanks to this, we hope that the experimental search for this quasi-breather in graphene superlattices will be successful.

5 Conclusions

The propagation of nonlinear waves in the Ratnikov's graphene superlattice modelled by the GSLeq has been studied by means of a numerical method. A significant understanding on their behaviour has been gained, and the regions of the parameter space were their behaviour is robust and predictable have been determined. Section 5.1 summarises the concluding remarks of this dissertation, and Section 5.2 proposes a few directions in which this work can be extended.

5.1 Concluding remarks

A robust, fast, and efficient numerical method for the long-time integration of the GSLeq has been developed. For such a task fifteen numerical Padé schemes for the sGeq have been compared by using their kink–antikink and breather solutions; five of them with Richardson's extrapolation in time. The comparison between these methods has allowed to select the most efficient one to study these solutions in very long time simulations. All these methods use the same implicit, second-order scheme for the integration in time and the same approximation to the nonlinearity, with a proper rearrangement to avoid catastrophic cancellations in its numerical evaluation.

Two families of Padé methods for the sGeq have been compared; Methods 1–5 are based on the SV method, and Methods 6–10 on the GPRV scheme. Methods 1 and 6 are interpreted as (2,0)-Padé schemes of second-order in space. Methods 2 and 7 use a (4,0)-Padé approximant of fourth-order in space, and Methods 3 and 8 a (2,2)-Padé formula of the same order. Methods 4 and 9 are sixth-order (4,2)-Padé schemes, and Methods 5 and 10 are eight-order (4,4)-Padé methods. Their linear stability has been studied by using the von Neumann analysis; the stability condition for Methods 1–5 has been determined, and the unconditional stability of

Methods 6–10 has been proved. Moreover, Methods 1 and 6 exactly conserve two discrete analogues of the energy for the sGeq, so they are nonlinearly stable. A version of Methods 6–10 with one level of Richardson's extrapolation in time to obtain fourth-order accuracy has also been developed.

The fifteen methods have been compared for the kink-antikink and breather solutions of the sGeq. The study of the computational cost required in order to ensure that the global error is smaller than a given threshold shows that methods without Richardson's extrapolation should be preferred; among them, Methods 2 and 7 are the most efficient ones for small error, and Methods 5 and 10 for very small error. In long-time integrations Methods 7 and 10 are more robust than Methods 2 and 5, therefore, Method 7 has been selected for the numerical simulation of the solutions of the GSLeq.

Our first objective has been accomplished by the study of the inelastic scattering of kinks and antikinks of the GSLeq. A fractal structure has been observed in kink–antikink collisions for speeds below a critical velocity that depends on the geometric parameter of the GSLeq. In such a case the collision results in the formation of an oscillatory state, similar to a pseudo-breather which decays into radiation; in addition, a series of windows are observed where the kink and the antikink escape after being temporarily bounded in a resonant state with multiple bounces. The fractal structure of these windows has been formalised with a new multi-index notation, that allows the formulation of a conjecture for this structure *ad infinitum*.

The resonant energy exchange theory has been applied to understand the general characteristics of the multi-bounce windows observed in the kink-antikink collisions below the critical velocity. The interval in time between the first and second bounces inside the two-bounce windows has been fitted in order to determine its central velocity with a good accuracy. The frequency of the resonance mode responsible for the trapping of the kink and the antikink inside the two-bounce windows has been estimated by solving an eigenvalue problem for a linear Schrödinger equation with an effective potential; this estimation is better as the geometrical parameter of the graphene superlattice equation increases, the effective potential widens, and the frequency monotonically decreases. Our results validate the application of the resonant energy exchange theory for the GSLeq; in fact, they are better than those obtained for similar equations like the dsGeq.

Our second objective has been fulfilled by a quasi-breather search based on a regular perturbation of the null solution depending on a frequency parameter ω as initial condition. The advantage of such an initial condition is that it is very accurate for small enough time-steps, so the initial emission of radiation during the quasi-breather development is reduced; another advantage is that the total energy of the solution can be calculated exactly. The new initial condition evolves into three possible solutions depending on ω, a kink–antikink solution, a

pseudo-breather, and a quasi-breather solution, separated by two critical frequencies. The pseudo-breather shows irregular oscillations and decays into radiation after a low number of oscillations; however, the quasi-breather survives in long-time simulations for more than one thousand periods, although its amplitude and energy decrease, and its frequency increases. The robustness of the quasi-breather solution has been analysed by using a new contour plot inspired by the corresponding plot used to study the fractal structure of the kink–antikink collisions. This new plot highlights the existence of critical frequencies that separate the three possible solutions observed.

The evolution in time of the properties of the quasi-breather solution of the GSLeq has been determined. The maximum amplitude of its oscillatory profile decreases as time marches due to the emission of radiation. The evolution has been fitted by using a power law whose parameters depend on ω. The quasi-breather frequency has also been fitted by another power law that increases as ω does, but always remain smaller than the frequency of the breather solution of the sG equation for the same ω. Moreover, the critical frequency separating the pseudo- and quasi-breather solutions monotonically increases. These results suggest that the quasi-breather of the GSLeq can be interpreted as a perturbation of the sGeq, at least for small geometrical parameter. The existence of robust, high-frequency quasi-breathers suggests that their experimental search in graphene superlattices may be successful.

5.2 Future research

There are multiple lines of research opened by the work carried out in this thesis. Regarding the development and analysis of numerical methods for the GSLeq, we propose the study of new families of methods in space, such as the pseudospectral ones, and in time, such as the diagonally implicit Runge–Kutta–Nyström methods. We also intend to study numerically induced effects using the method of modified equation technique.

Our research has shown the robustness of stationary quasi-breather solutions for the GSLeq. We will study the collisions between moving quasi-breathers, and between quasi-breathers and kinks or antikinks. As our results support the experimental search for quasi-breathers in graphene superlattices, the numerical study of the generation of kinks, antikinks and pseudo-breathers from different initial conditions is necessary.

Since the GSLeq equation can be considered a perturbation of the sGeq for small values of the geometric parameter, we propose the application of perturbative techniques inspired by the inverse spectral transform for the sGeq. We hope that

these techniques allow us to analytically approximate the kink-antikink and quasi-breather solutions of the GSLeq. In addition, they will allow studying the effect of high-order dissipative, dispersive, and non-linear terms on the GSLeq. These analytical results will be validated with specific numerical simulations.

For applications of graphene superlattices in the terahertz regime, Kryuchkov, Kukhar', and Zavyalov [84] have derived an integro-differential equation of the Klein-Gordon type with a nonlocal nonlinearity. The development of numerical methods for this equation and the analysis of its potential kink, antikink and quasi-breather solutions is another promising line of future research.

Graphene superlattices are formed by different strips of dielectric material where surface plasmon-polariton waves can propagate. In the derivation of GSLeq by the Kryuchkov and Kukhar' only a single strip is considered; when the overlapping effects between strips are not neglected, it is expected that these waves are modelled by a set of coupled equations similar to GSLeq. Its derivation and numerical study will be considered in the future. In this line, the study of discrete versions of the GSLeq with localised discrete modes (also called discrete breathers) seems very interesting. The search for such solutions can be undertaken using deflation techniques [85].

Bibliography

[1] K.S. Novoselov, A.K. Geim, S.V. Morozov, D. Jiang, Y. Zhang, S.V. Dubonos, I.V. Grigorieva, and A.A. Firsov. Electric field effect in atomically thin carbon films. *Science*, 306(5696):666–669, 2004.

[2] S. Y. Zhou, G.-H. Gweon, A. V. Fedorov, P. N. First, W. A. de Heer, D.-H. Lee1, F. Guinea, A. H. Castro Neto, and A. Lanzara. Substrate-induced bandgap opening in epitaxial graphene. *Nature Materials*, 6:770–775, 2007.

[3] Francisca Martin-Vergara, Francisco Rus, and Francisco R. Villatoro. Solitary waves on graphene superlattices. In Juan F. R. Archilla, Faustino Palmero, M. Carmen Lemos, Bernardo Sánchez-Rey, and Jesús Casado-Pascual, editors, *Nonlinear Systems, Vol. 2. Nonlinear Phenomena in Biology, Optics and Condensed Matter*, pages 85–110. Springer, Berlin, 2018.

[4] P. V. Ratnikov. Superlattice based on graphene on a strip substrate. *JETP Letters*, 90:469–474, 2009.

[5] G. M. Maksimova, E. S. Azarova, A. V. Telezhnikov, and Burdov V. A. Graphene superlattice with periodically modulated Dirac gap. *Physical Review B*, 86:205422, 2012.

[6] S. V. Kryuchkov and E. I. Kukhar'. The solitary electromagnetic waves in the graphene superlattice. *Physica B: Condensed Matter*, 408:188–192, 2013.

[7] W. Strauss and L. Vázquez. Numerical solution of a nonlinear klein-gordon equation. *J. Comput. Phys.*, 28:271–278, 1978.

[8] Francisca Martin-Vergara, Francisco Rus, and Francisco R. Villatoro. Padé numerical schemes for the sine-Gordon equation. *App. Math. Comput.*, 358:232–243, 2019.

[9] F. Martin-Vergara, F. Rus, and F.R. Villatoro. Padé schemes with Richardson extrapolation for the sine-Gordon equation. *Commun. Nonlinear Sci. Numer. Simul.*, 85:105243, 2020.

[10] Guo Ben-Yu, Pedro J. Pascual, María J. Rodriguez, and Luis Vázquez. Numerical solution of the sine-gordon equation. *Appl. Math. Comput.*, 18(1):1–14, 1986.

[11] F. Martin-Vergara, F. Rus, and F.R. Villatoro. Fractal structure of the soliton scattering for the graphene superlattice equation. *Chaos, Solitons & Fractals*, 151:111281, 2021.

[12] David K. Campbell, Jonathan F. Schonfeld, and Charles A. Wingate. Resonance structure in kink-antikink interactions in ϕ^4 theory. *Physica D: Nonlinear Phenomena*, 9(1):1–32, 1983.

[13] David K. Campbell, Michel Peyrard, and Pasquale Sodano. Kink-antikink interactions in the double sine-Gordon equation. *Physica D: Nonlinear Phenomena*, 19(2):165 – 205, 1986.

[14] F. Martin-Vergara, F. Rus, and F.R. Villatoro. Numerical search for the stationary quasi-breather of the graphene superlattice equation. *Chaos, Solitons & Fractals*, 162:112530, 2022.

[15] N.J. Zabusky and M.D. Kruskal. Interaction of "solitons" in a collisionless plasma and the recurrence of initial states. *Phys. Rev. Lett.*, 15(6):240–243, 1965.

[16] D.J. Korteweg and G. de Vries. On the change of form of long waves advancing in a rectangular canal, and on a new type of long stationary waves. *Philos. Mag.*, 39(5):422–443, 1895.

[17] Mark J. Ablowitz and Harvey Segur. *Solitons and the inverse scattering transform*. SIAM studies in applied mathematics, vol. 4. Society for Industrial and Applied Mathematics, Philadelphia, 1981.

[18] Alan C. Newell. *Solitons in mathematics and physics*. SIAM, 1985.

[19] P. G. Drazin and R. S. Johnson. *Solitons: An Introduction*. Cambridge Texts in Applied Mathematics. Cambridge University Press, 2 edition, 1989.

[20] Mark J. Ablowitz and Peter A. Clarkson. *Solitons, nonlinear evolution equations and inverse scattering*. London Mathematical Society Lecture Note Series vol. 149. Cambridge University Press, Cambridge, 1991.

[21] Anjan Kundu. *Tsunami and Nonlinear Waves*. Earth and Environmental Science vol. 1. Springer Berlin, Heidelberg, 2007.

[22] A. S. Davydov. *Solitons in Molecular Systems*. Mathematics and its Applications. Springer Dordrecht, 1985.

[23] S.V. Petoukhov. *Biosolitons - One Secret of Living Matter. The Bases of Solitonic Biology*. Mechanical Engineering Research Institute, Russian Academy of Sciences, Russia, 1999.

[24] A. Hasegawa and Y. Kodama. *Solitons in optical communications*. Oxford series in optical and imaging sciences. Clarendon Press, 1995.

[25] Michel Remoissenet. *Waves Called Solitons*. Springer Berlin, Heidelberg, 1994.

[26] Jesús Cuevas-Maraver, Panayotis G. Kevrekidis, and Floyd Williams. *The sine-Gordon model and its applications*. Nonlinear Systems and Complexity vol. 10. Springer, Berlin, 2014.

[27] A. Barone, F. Esposito, C. J. Magee, and A. C. Scott. Theory and applications of the sine-Gordon equation. *Riv. Nuovo Cimento*, 1:227–267, 1971.

[28] Alwyn C. Scott, Flora Y. F. Chu, and David W. McLaughlin. The soliton: A new concept in applied science. *Proc. IEEE*, 61(10):1443–1483, 1973.

[29] Nicholas Manton and Paul Sutcliffe. *Topological solitons*. Cambridge Monographs on Mathematical Physics. Cambridge University Press, 2004.

[30] P. V. Ratnikov and Silin A. P. Novel type of superlattices based on gapless graphene with the alternating Fermi velocity. *JETP Letters*, 100:311–318, 2014.

[31] P. A. D. Gonçalves and N. M. R. Peres. *An Introduction to Graphene Plasmonics*. World Scientific, 2016.

[32] S. V. Kryuchkov and E. I. Kukhar'. Influence of the constant electric field on the mutual rectification of the electromagnetic waves in graphene superlattice. *Physica E*, 46:25–29, 2012.

[33] S. V. Kryuchkov and E. I. Kukhar'. Solitary electromagnetic waves in a graphene superlattice under influence of high-frequency electric field. *Superlattices and Microstructures*, 70:70–81, 2014.

[34] S. V. Kryuchkov and E. I. Kukhar'. Alternating current-driven graphene superlattices: Kinks, dissipative solitons, dynamic chaotization. *Chaos*, 25:073116, 2015.

[35] Peter A. Clarkson, J. Bryce McLeod, Peter J. Olver, and Alfred Ramani. Integrability of klein–gordon equations. *SIAM Journal on Mathematical Analysis*, 17(4):798–802, 1986.

[36] D. V. Zav'yalov, V. I. Konchenkov, and S. V. Kryuchkov. May kink solution to the nonlinear Klein–Gordon equation be classified as a soliton? *Technical Physics*, 64(10):1391–1394, 2019.

[37] J. K. Perring and T. H. R. Skyrme. A Model unified field equation. *Nucl. Phys.*, 31:550–555, 1962.

[38] M.J. Ablowitz, M.D. Kruskal, and J.F. Ladik. Solitary wave collisions. *SIAM J. Appl. Math.*, 36(3):428–443, 1979.

[39] P. J. Pascual and L. Vázquez. Sine-Gordon solitons underweak stochastic perturbations. *Phys. Rev. B*, 32(12):8305–8311, 1985.

[40] Salvador Jiménez and Luis Vázquez. Analysis of four numerical schemes for a nonlinear Klein-Gordon equation. *App. Math. Comput.*, 35(1):61–94, 1990.

[41] Zhang Fei and Luis Vázquez. Two energy conserving numerical schemes for the sine-Gordon equation. *App. Math. Comput.*, 45(1):17–30, 1991.

[42] Loc Vu-Quoc and Shaofan Li. Invariant-conserving finite difference algorithms for the nonlinear Klein-Gordon equation. *Comput. Meth. Appl. Mech. Eng.*, 107(3):341–391, 1993.

[43] Loc Vu-Quoc and Shaofan Li. Finite difference calculus invariant structure of a class of algorithms for the nonlinear Klein-Gordon equation. *SIAM J. Numer. Anal.*, 32(6):1839–1875, 1995.

[44] Chaolong Jiang, Wenjun Cai, and Yushun Wang. A linear-implicit and local energy-preserving scheme for the sine-Gordon equation based on the invariant energy quadratization approach. *arXiv e-prints*, page arXiv:1808.06854, August 2018.

[45] Salvador Jiménez. Derivation of the discrete conservation laws for a family of finite difference schemes. *Appl. Math. Comput.*, 64(1):13–45, 1994.

[46] Daisuke Furihata. Finite-difference schemes for nonlinear wave equation that inherit energy conservation property. *J. Comput. Appl. Math.*, 134(1):37–57, 2001.

[47] Mark A. M. Lynch. Large amplitude instability in finite difference approximations to the Klein-Gordon equation. *Appl. Numer. Math.*, 31(2):173–182, 1999.

[48] A. G. Bratsos and E. H. Twizell. The solution of the sine-Gordon equation using the method of lines. *Int. J. Comput. Math.*, 61(3–4):271–292, 1996.

[49] D. Duncan. Sympletic finite difference approximations of the nonlinear Klein-Gordon equation. *SIAM J. Numer. Anal.*, 34(5):1742–1760, 1997.

[50] A. G. Bratsos. A fourth order numerical scheme for the one-dimensional sine-Gordon equation. *Int. J. Comput. Math.*, 85(7):1083–1095, 2008.

[51] Murat Sari and Gürhan Gürarslan. A sixth-order compact finite difference method for the one-dimensional sine-Gordon equation. *Int. J. Numer. Meth. Biomed. Eng.*, 27(7):1126–1138, 2011.

[52] A. G. Bratsos. A third order numerical scheme for the two-dimensional sine-Gordon equation. *Math. Comput. Simul.*, 76(4):271–282, 2007.

[53] A. G. Bratsos. The solution of the two-dimensional sine-Gordon equation using the method of lines. *J. Comput. Appl. Math.*, 206(1):251–277, 2007.

[54] Yuesheng Luo, Xiaole Li, and Cui Guo. Fourth-order compact and energy conservative scheme for solving nonlinear Klein-Gordon equation. *Numer. Meth. Part Differ. Equ.*, 33(4):1283–1304, 2016.

[55] C. Wingate. Numerical search for a ϕ^4 breather mode. *SIAM J. Appl. Math.*, 43(1):120–140, 1983.

[56] Mark J. Ablowitz, B. M. Herbst, and Constance M. Schober. Numerical simulation of quasi-periodic solutions of the sine-Gordon equation. *Physica D*, 87(1):37–47, 1995.

[57] Mark J. Ablowitz, B. M. Herbst, and Constance M. Schober. On the numerical solution of the sine-Gordon equation. *J. Comput. Phys.*, 131(2):354–367, 1997.

[58] E. Celledoni, V. Grimm, R. I. McLachlan, D. I. McLaren, D. O'Neale, B. Owren, and G. R. W. Quispel. Preserving energy resp. dissipation in numerical PDEs using the "Average Vector Field" method. *J. Comput. Phys.*, 231(20):6770–6789, 2012.

[59] G. W. Wei, D. S. Zhang, D. J. Kouri, and D. K. Hoffman. Lagrange distributed approximating functionals. *Phys. Rev. Lett.*, 79:775–779, 1997.

[60] G. W. Wei. Discrete singular convolution for the sine-Gordon equation. *Physica D*, 137(3):247–259, 2000.

[61] Behzad Nemati Saray, Mehrdad Lakestani, and Carlo Cattani. Evaluation of mixed Crank-Nicolson scheme and Tau method for the solution of Klein-Gordon equation. *App. Math. Comput.*, 331:169–181, 2018.

[62] A. S. Vasudeva Murthy Ameya D. Jagtap. Higher order scheme for two-dimensional inhomogeneous sine-Gordon equation with impulsive forcing. *Commun. Nonlinear Sci. Numer. Simul.*, 64:178–197, 2018.

[63] J. Argyris and M. Haase. An engineer's guide to soliton phenomena: Application of the finite element method. *Comput. Meth. Appl. Mech. Eng.*, 61(1):71–122, 1987.

[64] Yingying Shan, Wenjie Liu, and Boying Wu. Space-time Legendre-Gauss-Lobatto collocation method for two-dimensional generalized sine-Gordon equation. *Appl. Numer. Math.*, 122:92–107, 2017.

[65] H. S. Shukla, Mohammad Tamsir, and Vineet K. Srivastava. Numerical simulation of two dimensional sine-Gordon solitons using modified cubic B-spline differential quadrature method. *AIP Adv.*, 5(1):017121, 2015.

[66] Mahboub Baccouch. Optimal energy-conserving local discontinuous Galerkin method for the one-dimensional sine-Gordon equation. *Int. J. Comput. Math.*, 94(2):316–344, 2017.

[67] Mahboub Baccouch. Superconvergence of the local discontinuous Galerkin method for the sine-Gordon equation in one space dimension. *J. Comput. Appl. Math.*, 333:292–313, 2018.

[68] Mehdi Dehghan and Davoud Mirzaei. The dual reciprocity boundary element method (DRBEM) for two-dimensional sine-Gordon equation. *Comput. Meth. Appl. Mech. Eng.*, 197(6):476–486, 2008.

[69] Jerrold E. Marsden, George W. Patrick, and Steve Shkoller. Multisymplectic geometry, variational integrators, and nonlinear PDEs. *Commun. Math. Phys.*, 1999(2):351–395, 1998.

[70] Sebastian Reich. Multi-symplectic Runge-Kutta collocation methods for Hamiltonian wave equations. *J. Comput. Phys.*, 157(2):473–499, 2000.

[71] Chaolong Jiang, Jianqiang Sun, Haochen Li, and Yifan Wang. A fourth-order AVF method for the numerical integration of sine-Gordon equation. *App. Math. Comput.*, 313:144–158, 2017.

[72] Ma Li-Min and Wu Zong-Min. A numerical method for one-dimensional nonlinear sine-Gordon equation using multiquadric quasi-interpolation. *Chin. Phys. B*, 18(8):3099–3103, 2009.

[73] Zi-Wu Jiang and Ren-Hong Wang. Numerical solution of one-dimensional Sine-Gordon equation using high accuracy multiquadric quasi-interpolation. *App. Math. Comput.*, 218(15):7711–7716, 2012.

[74] Mehdi Dehghan and Ali Shokri. A numerical method for solution of the two-dimensional sine-Gordon equation using the radial basis functions. *Math. Comput. Simul.*, 79(3):700–715, 2008.

[75] Arshad Hussain, Sirajul Haq, and Marjan Uddin. Numerical solution of Klein-Gordon and sine-Gordon equations by meshless method of lines. *Eng. Anal. Bound. Elem.*, 37(11):1351–1366, 2013.

[76] J. I. Ramos. The sine-Gordon equation in the finite line. *App. Math. Comput.*, 124(1):45–93, 2001.

[77] Randy Flesch, M. Gregory Forest, and Amarendra Sinha. Numerical inverse spectral transform for the periodic sine-Gordon equation: Theta function solutions and their linearized stability. *Physica D*, 48(1):169–231, 1991.

[78] Bernard Deconinck, Thomas Trogdon, and Xin Yang. Numerical inverse scattering for the sine-gordon equation. *Physica D: Nonlinear Phenomena*, 399:159–172, 2019.

[79] Lu Trong Khiem Nguyen. A numerical scheme and some theoretical aspects for the cylindrically and spherically symmetric sine-Gordon equations. *Commun. Nonlinear Sci. Numer. Simul.*, 36:402–418, 2016.

[80] Ivan C. Christov, Robert J. Decker, A. Demirkaya, Vakhid A. Gani, P. G. Kevrekidis, and R. V. Radomskiy. Long-range interactions of kinks. *Phys. Rev. D*, 99:016010–016010, Jan 2019.

[81] John P. Boyd. Solitons from sine waves: Analytical and numerical methods for non-integrable solitary and cnoidal waves. *Physica D: Nonlinear Phenomena*, 21(2):227–246, 1986.

[82] John P. Boyd. New directions in solitons and nonlinear periodic waves: Polycnoidal waves, imbricated solitons, weakly nonlocal solitary waves, and numerical boundary value algorithms. In John W. Hutchinson and Theodore Y. Wu, editors, *Advances in Applied Mechanics*, volume 27, pages 1–82. Elsevier, 1989.

[83] B. A. Malomed, N. N. Rosanov, and S. V. Fedorov. Dynamics of nonlinear Schrödinger breathers in a potential trap. *Phys. Rev. E*, 97:052204, May 2018.

[84] S. V. Kryuchkov, E. I. Kukhar', and D. Zav'yalov. Charge dynamics in graphene and graphene superlattices under a high-frequency electric field: A semiclassical approach. *Laser Physics*, 23(6):065902, apr 2013.

[85] P. E. Farrell, Á. Birkisson, and S. W. Funke. Deflation techniques for finding distinct solutions of nonlinear partial differential equations. *SIAM Journal on Scientific Computing*, 37(4):A2026–A2045, 2015.

[86] Panayotis G. Kevrekidis and Jesús Cuevas-Maraver. *A Dynamical Perspective on the ϕ^4 Model*. Nonlinear Systems and Complexity vol. 26. Springer, Berlin, 2019.

[87] A.H. Castro Neto, F. Guinea, N.M.R. Peres, Kostya S. Novoselov, and Andre K. Geim. The electronic properties of graphene. *Rev. Mod. Phys.*, 81(1):109, 2009.

[88] Farhan Rana. Graphene terahertz plasmon oscillators. *IEEE Transactions on Nanotechnology*, 7(1):91–99, 2008.

[89] A.R. Wright, G.X. Wang, W. Xu, Z. Zeng, and C. Zhang. The spin–orbit interaction enhanced terahertz absorption in graphene around the K point. *Microelectronics Journal*, 40(4):857–859, 2009.

[90] L.A. Falkovsky. Optical properties of graphene and iv - vi semiconductors. *Physics-Uspekhi*, 51(9):887–897, 2008.

[91] S.A. Mikhailov. Non-linear electromagnetic response of graphene. *EPL—Europhysics Letters*, 79(2):27002, 2007.

[92] S.A. Mikhailov and K. Ziegler. Nonlinear electromagnetic response of graphene: Frequency multiplication and the self-consistent-field effects. *J. Phys. Condens. Matter*, 20(38):469–474, 2008.

[93] J. Parashar and H. Sharma. Optical rectification in a carbon nanotube array and terahertz radiation generation. *Physica*, 44(10):2069–2071, 2012.

[94] E. McCann and M. Koshino. The electronic properties of bilayer graphene. *Rep. Prog. Phys.*, 76(5), 2013.

[95] Clarence Burg and Taylor Erwin. Application of Richardson extrapolation to the numerical solution of partial differential equations. *Numer. Meth. Part Differ. Equ.*, 25(4):810–832, 2009.

[96] K. Djidjeli, W. G. Price, and E. H. Twizell. Numerical solutions of a damped sine-Gordon equation in two space variables. *J. Eng. Math.*, 29(4):347–369, 1995.

[97] Shane A. Richards. Completed Richardson extrapolation in space and time. *Commun. Numer. Methods Eng.*, 13(7):573–582, 1997.

[98] Dingwen Deng and Chengjian Zhang. A new fourth-order numerical algorithm for a class of nonlinear wave equations. *Appl. Numer. Math.*, 62(12):1864–1879, 2012.

[99] Hamid Moghaderi and Mehdi Dehghan. A multigrid compact finite difference method for solving the one-dimensional nonlinear sine-Gordon equation. *Math. Meth. Appl. Sci.*, 38(17):3901–3922, 2014.

[100] Harvey Segur and Martin D. Kruskal. Nonexistence of small-amplitude breather solutions in phi^4 theory. *Phys. Rev. Lett.*, 58:747–750, Feb 1987.

[101] Jochen Denzler. Nonpersistence of breather families for the perturbed sine gordon equation. *Communications in Mathematical Physics*, 158(2):397–430, 1993.

[102] Björn Birnir, Henry P. McKean, and Alan Weinstein. The rigidity of sine-gordon breathers. *Communications on Pure and Applied Mathematics*, 47(8):1043–1051, 1994.

[103] Otávio M. L. Gomide, Marcel Guardia, Tere M. Seara, and Chongchun Zeng. On small breathers of nonlinear klein-gordon equations via exponentially small homoclinic splitting, 2021.

[104] Roy H. Goodman and Richard Haberman. Chaotic scattering and the *n*-bounce resonance in solitary-wave interactions. *Physical Review Letters*, 98:104103, Mar 2007.

[105] Roy H. Goodman. Chaotic scattering in solitary wave interactions: A singular iterated-map description. *Chaos: An Interdisciplinary Journal of Nonlinear Science*, 18(2):023113, 2008.

[106] M. Peyrard and D. K. Campbell. Kink-antikink interactions in a modified sine-Gordon model. *Physica D: Nonlinear Phenomena*, 9(1):33–51, 1983.

[107] Roy H. Goodman and Richard Haberman. Interaction of sine-Gordon kinks with defects: the two-bounce resonance. *Physica D: Nonlinear Phenomena*, 195(3):303 – 323, 2004.

[108] Roy H. Goodman and Richard. Haberman. Kink-antikink collisions in the ϕ^4 equation: The n-bounce resonance and the separatrix map. *SIAM J. App. Dyn. Sys.*, 4(4):1195–1228, 2005.

Appendices

A

Solitary waves on graphene superlattices

This Appendix is a copy of the book chapter [3]:

Martin-Vergara, F., Rus, F., Villatoro, F.R. (2018). *Solitary Waves on Graphene Superlattices*. In: Archilla, J., Palmero, F., Lemos, M., Sánchez-Rey, B., Casado-Pascual, J. (eds) Nonlinear Systems, Vol. 2. Understanding Complex Systems. Springer, Cham. https://doi.org/10.1007/978-3-319-72218-4_4. ISBN 978-3-319-66765-2.

Abstract

This chapter reviews the basic theoretical aspects of the propagation of solitary electromagnetic waves in graphene superlattices, a one atom thick sheet of graphene deposited on a superlattice, made by several periodically alternating layers of SiO_2 and h-BN. The electronic band structure of graphene and the techniques of band gap engineering are briefly presented. The analysis of the electronic properties of graphene superlattices by using both the transfer matrix method and the Kronig–Penny model are summarized. The nonlinear wave equation for the vector potential of the electromagnetic wave field is derived. This graphene superlattice equation (GSLeq) generalizes the sine-Gordon equation (sGeq). Hence, it also has kink and antikink solutions propagating at a constant speed. There is no closed-form expression for their shape. A straightforward asymptotic method is applied in order to analytically approximate its shape. The interactions of kinks and antikinks is studied by using a numerical method, the Strauss–Vázquez, which is a conservative, finite difference scheme. This numerical method is second-order accurate in both space and time, and nonlinearly stable, exactly conserving a discrete energy. Extensive numerical results for the kink–antikink interactions are presented as a function of a asymptotic parameter. For small values of this parameter, the interaction is apparently elastic, without noticeable radiation, being very similar to that expected for the sGeq. For large values of the asymptotic parameter, the

inelasticity of the interaction results in the emission of wavepackets of radiation. In summary, the whole set of results suggest that the GSLeq behaves as a nearly integrable perturbation of the sGeq. Consequently, graphene superlattices can be used to study nonlinear wave phenomena with electromagnetic waves in the THz scale.

B

Padé numerical schemes for the sine-Gordon equation

This Appendix is a copy of the paper [8]:

F. Martin-Vergara, F. Rus, F.R. Villatoro. *Padé numerical schemes for the sine-Gordon equation*. Applied Mathematics and Computation, Volume 358, 2019, Pages 232-243,doi:10.1016/j.amc.2019.04.042.

Abstract

The sine-Gordon equation turn up in several problems in science and engineering. Although it is integrable, in practical applications, its numerical solution is powerful and versatile. Four novel implicit finite difference methods based on (q,s) Padé approximations with $(q+s)$-th order in space have been developed and analyzed for this equation; all share the same treatment for the nonlinearity and integration in time. Concretely, $(0,4)$, $(2,2)$, $(2,4)$, and $(4,4)$ Padé methods; additionally, the energy conserving, Strauss–Vázquez scheme has been considered in a $(0,2)$ Padé implementation. These methods have been compared among them for both the kink–antikink and breather solutions in terms of global error, computational cost and energy conservation. The $(0,4)$ and $(2,4)$ Padé methods are the most cost-effective ones for small and large global error, respectively. Our results indicate that spatial order of accuracy is more relevant to effectiveness of a method than energy conservation even in very long time integrations.

C

Padé schemes with Richardson extrapolation for the sine-Gordon equation

This Appendix is a copy of the paper [9]:

F. Martin-Vergara, F. Rus, F.R. Villatoro. *Padé schemes with Richardson extrapolation for the sine-Gordon equation*. Commun.Nonlinear Sci.Numer.Simul. Volumen 85, Pages 105243, Jun, 2020. doi:10.1016/j.cnsns.2020.105243.

Abstract

Four novel implicit finite difference methods with $(q+s)$-th order in space based on (q,s)-Padé approximations have been analyzed and developed for the sine-Gordon equation. Specifically, $(4,0)$-, $(2,2)$-, $(4,2)$-, and $(4,4)$-Padé methods. All of them share the treatment for the nonlinearity and integration in time, specifically, the one that results in an energy-conserving $(2,0)$-Padé scheme. The five methods have been developed with and without Richardson extrapolation in time. All the methods are linearly, unconditionally stable. A comparison among them for both the kink–antikink and breather solutions in terms of global error, computational cost and energy conservation is presented. Our results indicate that the $(4,0)$- and $(4,4)$-Padé methods without Richardson extrapolation are the most cost-effective ones for small and large global error, respectively; and the $(4,4)$-Padé methods in all the cases when Richardson extrapolation is used.

D

Fractal structure of the soliton scattering for the graphene superlattice equation

This Appendix is a copy of the paper [11]:

F. Martin-Vergara, F. Rus, F.R. Villatoro. Fractal structure of the soliton scattering for the graphene superlattice equation. Chaos, Solitons & Fractals. Volume 151, 2021. 111281. ISSN 0960-0779, doi:10.1016/j.chaos.2021.111281.

Abstract

The graphene superlattice equation, a modified sine-Gordon equation, governs the propagation of solitary electromagnetic waves in a graphene superlattice. This equation has kink solutions without explicit analytical expression, requiring the use of quadrature methods. The inelastic collision of kinks and antikinks with the same but opposite speed is studied numerically for the first time; after their interaction they escape to infinity when its speed is either larger than a critical value or it is inside a series of resonance windows; otherwise, they form a breather-like state that slowly decays by radiating energy. Here, the fractal structure of these resonance windows is characterized by using a multi-index notation and their main features are compared with the predictions of the resonant energy exchange theory showing good agreement. Our results can be interpreted as new evidence in favour of this theory.

E

Numerical search for the stationary quasi-breather of the graphene superlattice equation

This Appendix is a copy of the paper [14]:

F. Martin-Vergara, F. Rus, F.R. Villatoro. Numerical search for the stationary quasi-breather of the graphene superlattice equation. Chaos, Solitons & Fractals. Volume 162, 2022, 112530. ISSN 0960-0779, doi:10.1016/j.chaos.2022.112530.

Abstract

The propagation of electromagnetic solitons in a graphene superlattice device is governed by a modified sine-Gordon equation, referred to as the graphene superlattice equation. Kink-antikink collisions suggest the existence of a quasi-breather solution. Here, a numerical search for static quasi-breathers is undertaken by using a new initial condition obtained by a regular perturbation of the null solution. Our results show that the frequency of the initial condition has a minimum critical value for the appearance of a robust quasi-breather able to survive during more than one thousand periods. The amplitude and energy of the quasi-breather solution decrease, but its frequency increases, as time grows. The robustness of the new quasi-breather supports its experimental search in real graphene superlattice devices.